Analysis of the Implementation of Fluid Viscous Dampers in a Steel Special Moment Frame

By:
Brad Weber

SENIOR PROJECT REPORT

Submitted in partial fulfillment of the requirements for the degree of Bachelor of Science in Architectural Engineering at California Polytechnic State University

San Luis Obispo, California

Senior Project Advisor:
Cole McDaniel, PhD, PE

June 2021

ABSTRACT

This report examines the effects of adding fluid viscous dampers to a steel special moment frame through a series of analysis methods. Simple analysis procedures are first carried out and described, including a linear static procedure and a linear dynamic procedure. Then further analysis is carried out using a nonlinear dynamic analysis procedure. Multiple parameters are modified throughout the analysis processes to determine the impact on results and the data from all the analysis methods are compiled and used to demonstrate the overall impact of the use of fluid viscous dampers in a steel special moment frame.

TABLE OF CONTENTS

LIST OF FIGURES

LIST OF TABLES

1. INTRODUCTION

Based on the current building codes used to design buildings today, structures are both allowed and expected to experience damage during a seismic event. Typically, the preferred response is ductile yielding, since it provides indicators of failure before it happens and it is gradual, unlike brittle failures which can happen very suddenly. For this type of response to happen in a structure, the members must yield and go beyond the elastic region to the point where permanent deformation takes place.

While this type of response may meet code requirements for life safety in the case of a seismic event, it often leads to extensive damage in the structural, and nonstructural elements of the building. This damage can often be very costly to repair and can take a significant amount of time. This makes the building unoccupiable which negatively impacts anyone who uses the building. By limiting or even eliminating this damage, the time after a seismic event before a building can once again be occupiable can be decreased significantly.

The use of fluid viscous dampers allows for some of the force from the earthquake to be diverted into the dampers so that the actual structure has to resist less force. This can cause the necessary yielding of the structural members to be very minimal if not nonexistent, and therefore the structure experiences less damage. Since the dampers are not integrally a part of the lateral force resisting system, if they become damaged after a seismic event it is much easier to remove and replace them, leading to a much shorter recovery period before the building is occupiable again.

In order to ensure that the additional cost of adding fluid viscous dampers is less than the amount saved in the reduced recovery and repair time, it is necessary to know specifically what the effects of the added dampers are, and how the dampers should be implemented in the structure to get the desired outcome. This report investigates such affects by examining the many variables that impact the performance of fluid viscous dampers when added to a steel special moment frame.

2. BACKGROUND

Fluid viscous dampers (FVDs) are devices that are designed to dissipate energy through heat. An FVD is made up of a piston inside of a cylindrical container that is filled with a viscous fluid. When the FVD experiences loading, one end of the damper moves relative to the other, causing the piston to move through the viscous fluid, which pushes it through multiple orifices [7]. The work done by the piston converts the kinetic energy from the movement of the structure into heat which is given off into the environment. When applied in building structures, FVDs are used as a tool to divert energy from a seismic event away from the structure of the building. FVDs are velocity dependent devices since they rely on the movement of the ends of the damper. The relationship between the force in the damper and velocity is shown in equation 1 below. The physical properties of the damper such as its size determine the coefficient, C and the relationship between the velocity and the force can either be nonlinear or linear, depending on what value is chosen for the damping coefficient α. Since FVDs are velocity dependent and not frequency dependent, they do not have to be tuned to a specific frequency. FVDs also do not add any additional stiffness to the structure which means that the use of FVDs does not change the fundamental building period.

Taylor Devices Inc. is one of the industry leaders in the creation of FVDs. The company began in 1955 with the mission to create high quality products and to provide systems analysis, product development, and manufacturing and testing capabilities to their customers [3]. Fluid viscous dampers were originally made for NASA in the 1960s and then were later adopted into use for structural engineering [4]. The first structures that FVDs were used in were for the military such as missile launch structures, and then they were eventually sold commercially to be used in any buildings [5]. The technology of FVDs continued to develop throughout the 1980s and 1990s and after the Northridge earthquake in 1994, there was increased interest in the use of FVDs to protect buildings during seismic events. The fluid viscous dampers created by Taylor Devices can increase structural damping levels to as much as 50% of critical. The dampers they create are designed and tested to meet the necessary requirements of the customer.

FVDs connect to the structure through a Clevis on either end and to allow for additional movement there is typically a spherical bearing inside the Clevis [7]. Taylor Devices dampers are rated for forces up to 1800 kips and they are analyzed for strength using finite element analysis [7]. Since FVDs only provide resistance to force when the structure causes them to move, they do not carry any static load in the structure. As a structure moves to its farthest point velocity goes to zero, and when it moves back to the point where it started the velocity increases to a maximum. This means the damper force is largest when the structure is not deflecting and it is at zero when the structure is at peak deflection which means the FVD is out of phase with the movement of the structure, and it increases the building's ability to withstand earthquakes.

$$F = C * V^{\alpha} \qquad \text{(Eq-1)}$$

A diagram of a typical fluid viscous damper is shown in Figure 1, and Figures 2 through 4 show images of fluid viscous dampers after they have been installed in buildings.

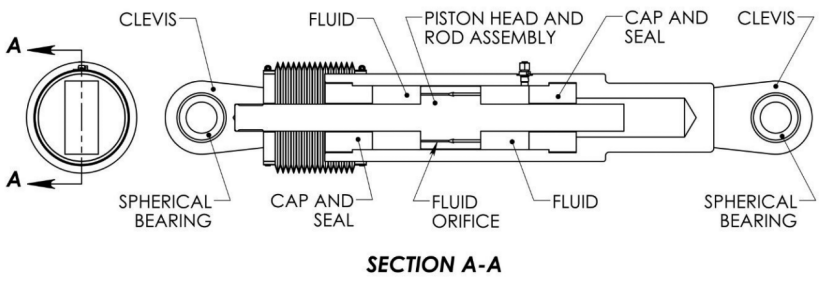

Figure 1: Diagram of a Fluid Viscous Damper [7]

Figure 2: Photo of Damper - Cal Poly Pomona Library, Pomona, CA [7]

Figure 3: Photo of Damper - 999 Sepulveda, El Segundo, CA [7]

Figure 4: Close Up of Fluid Viscous Damper [6]

3. ANALYSIS PROCEDURES

3.1 Linear Static Analysis

3.1.1 Structural System

The structural system is a steel special moment frame that would be used as the lateral force resisting system in a typical steel building built in a high seismic area. The Frame is 3 stories tall and 3 bays wide. Each bay is 30 ft long, the height from the ground to the first level is 16 ft, and the height from the first level to the second level, and from the second level to the third level is 14 ft. All columns in the frame are W14x93 sections. The beams at the first level are W24x84 sections, the beams at the second level are W18x76 sections, and the beams at the third level are W16x26 sections. An elevation of the frame and member sections is shown in fig 5.

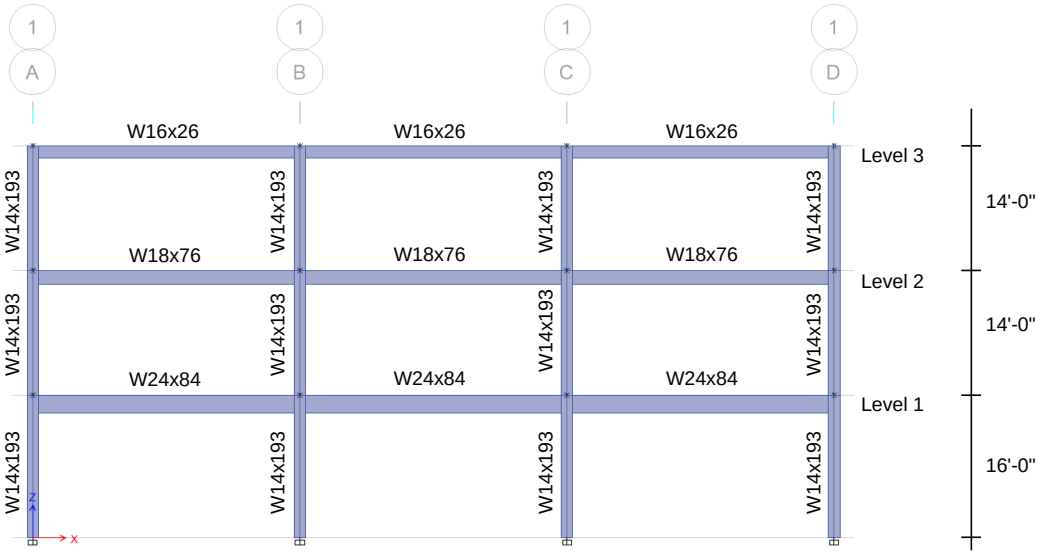

Figure 5: Frame Elevation

3.1.2 Mass of Frame

The desired period for the frame is .7 which is the period of the building from which this frame came from and is roughly .2 seconds per story. To get an initial estimation for the mass of the building based on a period of .7, the following equation is used:

$$T = 2\pi * \sqrt{\frac{m}{k}} \longrightarrow m = \left(\frac{T}{2\pi}\right)^2 k$$

To find the stiffness of the structure the assumptions below are used:

for the first level: $k = \frac{6EI}{H^3}$

for all other levels: $k = \frac{3EI}{H^3}$

for W14x193 columns, the moment of inertia is $I = 2400\ in^4$ and for steel the modulus of elasticity is $E = 29000\ ksi$.

Column stiffnesses on the same level are in parallel so their stiffness values will be added, while the stiffnesses from each level are in series so the inverse of their stiffnesses will be added together.

$$k_1 = \frac{6 * 29000\ ksi * 24000\ in^4}{(16\,ft\ * 12\,in/ft)^3} = 59\ k/in$$

Since there are 4 columns on one level: $4 * 59\ k/in\ = 236\ k/in$

$$k_2 = \frac{3 * 29000\ ksi * 24000\ in^4}{(14\,ft\ * 12\,in/ft)^3} = 44\ k/in$$

Since there are 4 columns on one level: $4 * 44\ k/in\ = 176\ k/in$

To find the total stiffness for the building:

$$\frac{1}{k_{total}} = \frac{1}{236\ k/in} + \frac{1}{176\ k/in} + \frac{1}{176\ k/in} \longrightarrow k_{total} = 64.1\ k/in$$

Using the equation for mass previously determined:

$$m = \left(\frac{.7}{2\pi}\right)^2 (64.1\,k/in) = .796\ ks^2/in$$

To determine the distribution of mass in the frame, the total mass is divided by 2.9 to get the mass at each floor and that value is multiplied by .9 to get the mass at the roof.

floor mass: $.796\ ks^2/in/2.9 = .2745\ ks^2/in\ * (1000\ lb/k) * (12\ in/ft) = 3292\ lb-s^2/ft$
roof mass: $.2745\ ks^2/in * .9 = .2470\ ks^2/in\ * (1000\ lb/k) * (12\ in/ft) = 2963\ lb-s^2/ft$

The portal method is used to distribute the mass between the columns at each level, where the interior columns receive twice the mass as the exterior columns:

interior floor column mass: $3292\ lb-s^2/ft\ /3 = 1097\ lb-s^2/ft$
exterior floor column mass: $3292\ lb-s^2/ft\ /6 = 548.7\ lb-s^2/ft$
interior roof column mass: $2963\ lb-s^2/ft\ /3 = 987.7\ lb-s^2/ft$
exterior roof column mass: $2963\ lb-s^2/ft\ /6 = 493.8\ lb-s^2/ft$

The frame is modeled in Etabs and the mass is applied in the x direction to the joints where the columns and beams intersect at every level. The frame is analyzed with modal analysis and the period with the initial assumption for mass determined above is .6091 seconds. To increase the period so that it is closer to .7 seconds, the mass is increased by approximately 40%. The new mass values are:

interior floor column mass: 1553 $lb-s^2/ft$
exterior floor column mass: 776.5 $lb-s^2/ft$
interior roof column mass: 1398 $lb-s^2/ft$
exterior roof column mass: 699.2 $lb-s^2/ft$

An elevation of the frame with the masses applied is shown in Figure 6 below.

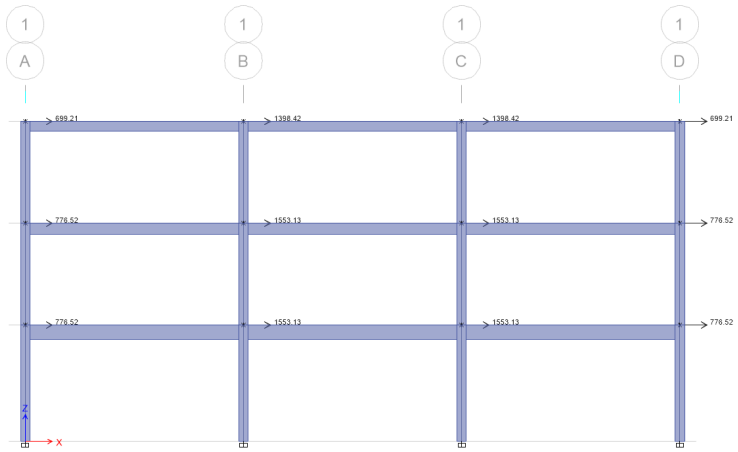

Figure 6: Frame Model with Applied Mass

With these new masses, the period increases to .7142 seconds, which is determined to be close enough to .7 to be acceptable.

3.1.3 Equivalent Lateral Force Procedure

The seismic base shear, V is calculated for the frame based on the equivalent lateral force procedure presented in ASCE 7-16. The site class is assumed to be site class D - Stiff Soil, and the risk category selected for a typical building that this frame would be a part of is category II. The location used to determine the spectral acceleration values is located in a high seismic region of the Bay Area. The coordinates are: latitude 37.87319797, longitude -122.01933144. Using the SEAOC Seismic Maps Tool, the spectral accelerations are determined to be $S_S = 2.142$ and $S_1 = .716$. The site coefficient modification factors are found in tables 11.4-1 and 11.4-2 in ASCE 7-16: $F_a = 1.0$ and $F_v = 1.7$. The modified and design spectral response accelerations are found as shown below:

$$S_{MS} = F_a S_S = 1.0 * 2.142 = 2.142 \quad \text{[ASCE 7-16 Eq. 11.4-1]}$$

$$S_{M1} = F_v S_1 = 1.7 * .716 = 1.217 \quad \text{[ASCE 7-16 Eq. 11.4-2]}$$

$$S_{DS} = \frac{2}{3} S_{MS} = \frac{2}{3} * 2.142 = 1.428 \quad \text{[ASCE 7-16 Eq. 11.4-3]}$$

$$S_{D1} = \frac{2}{3} S_{M1} = \frac{2}{3} * 1.217 = .8115 \quad \text{[ASCE 7-16 Eq. 11.4-4]}$$

The seismic response coefficient is determined using the S_{DS} and S_{D1} values previously calculated. The period, T is .7 as assumed above. From ASCE 7-16 Table 12.2-1, the response modification factor, R for a steel special moment frame is found to be 8. For a risk category II building, the importance factor, I_e is equal to 1.0 . Assuming that the period is less than T_L, the seismic response coefficient, C_S will be the lesser value from the two equations below:

$$C_S = \frac{S_{DS}}{\frac{R}{I_e}} = \frac{1.428}{\left(\frac{8}{1}\right)} = .1785 \quad \text{[ASCE 7-16 Eq. 12.8-2]}$$

$$C_S = \frac{S_{D1}}{T * \left(\frac{R}{I_e}\right)} = \frac{.8115}{.7 * \left(\frac{8}{1}\right)} = .1449 \quad \text{[ASCE 7-16 Eq. 12.8-3]}$$

C_S also cannot be less than: $.044 S_{DS} I_e \geq 0.01 = .0444 * 1.428 * 1 = .0628 \geq 0.01$

For an S_1 value larger than .6g, C_S shall not be less than: $\frac{0.5 S_1}{\left(\frac{R}{I_e}\right)} = \frac{.5 * .716}{\left(\frac{8}{1}\right)} = .0448$

Based on all the requirements from ASCE 7-16, $C_S = .1449$
The seismic base shear is calculated with the following equation:

$$V = C_S W \quad \text{[ASCE 7-16 Eq. 12.8-1]}$$

The seismic weight, W is found by multiplying the frame mass found previously by gravity:

$$W = (.796\ ks^2/in) * (386.4\ in/s^2) = 307.6\ k$$

Seismic base shear, $V = .1449 * 307.6 = 44.57\ k$

The seismic base shear is distributed vertically to each level with the following equation:

$$F_x = C_{vx} V \qquad \text{where } C_{vx} = \frac{w_x h_x^k}{\Sigma w_i h_i^k}$$

w_x and w_i are the portions of the seismic weight at level x or i
h_x and h_i are the heights from the base to level x or i
the exponent k is related to the period, and for a period of .7142 (between .5 and 2.5 s), k is determined through linear interpolation between 1 and 2:

$$k = 1 + \left[\left(\frac{2-1}{2.5-.5}\right) * (.7142 - .5)\right] = 1.1$$

the table below shows the distribution of forces to each level:

level x	h_x	h_x^k	w_x	$w_x h_x^k$	C_{vx}	F_x
3	44	64.24	95.45	6132	.4775	21.281
2	30	42.15	106.1	4471	.3481	15.516
1	16	21.11	106.1	2239	.1744	7.7711
totals			307.6	12842	1.00	44.57

Table 1: Vertical Distribution of Base Shear

The distributed forces in the table are applied to the frame model in Etabs to determine the story displacements at each level

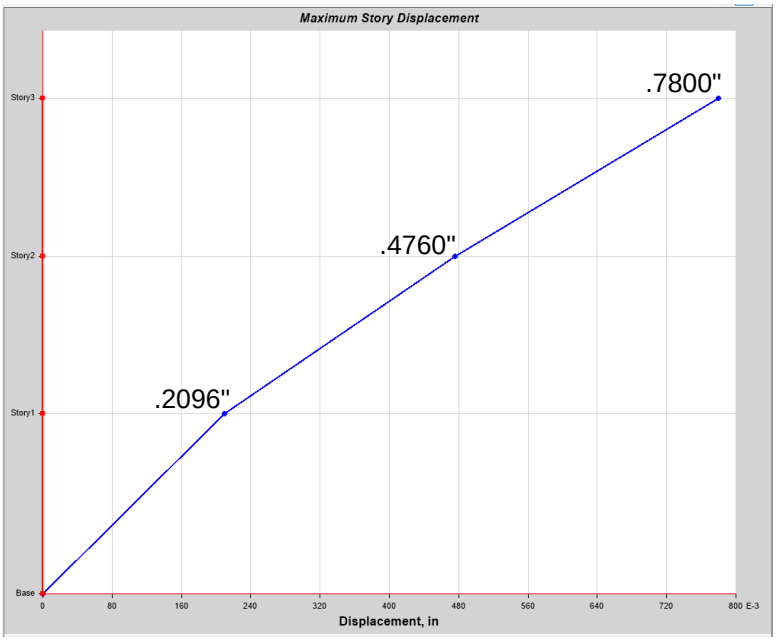

Figure 7: Plot of Story Displacements

The elastic displacements from Etabs are used in the following equation to determine the deflection used to calculate the story drift:

$$\delta_x = \frac{C_d \delta_{xe}}{I_e} \qquad \text{[ASCE 7-16 Eq. 12.8-15]}$$

C_d is the deflection amplification factor and it is found in ASCE 7-16 table 12.2-1
For a steel special moment frame $C_d = 5.5$

$$\text{for level 3: } \delta_x = \frac{5.5 * .7800}{1} = 4.29\ in$$

$$\text{for level 2: } \delta_x = \frac{5.5 * .4760}{1} = 2.62\ in$$

$$\text{for level 1: } \delta_x = \frac{5.5 * .2096}{1} = 1.15\ in$$

The story drift, Δ is equal to the change in displacement between the 2 adjacent stories:

$$\text{for level 3: } \Delta_3 = 4.29\ in - 2.62\ in = 1.67\ in$$

$$\text{for level 2: } \Delta_2 = 2.62\ in - 1.15\ in = 1.47\ in$$

$$\text{for level 1: } \Delta_1 = 1.15\ in - 0\ in = 1.15\ in$$

Through this initial simple analysis procedure, a general idea of the story drift in the frame is determined. To ensure the reliability of the Etabs model, the base shear is compared to the value found by hand:

V (by hand) $= 44.5684\ k$
V (Etabs) $= 44.5682\ k$

$$\text{percent difference: } \left(\frac{44.5684 - 44.5682}{44.5684}\right) * 100 = .00045\%$$

3.2 Linear Dynamic Analysis

3.2.1 Response Spectrum Analysis

To determine the maximum performance of the structure, Response Spectrum Analysis is carried out to determine how the frame deflects for each mode. The analysis is done both by hand and in Etabs to ensure that the results from the computer model are reliable.

The calculations for the response spectrum analysis by hand were done in python and the code can be found in Appendix B. For the hand calculations, double bending was assumed for stiffness, and it was assumed that the bottom level of columns would have greater stiffness than the upper levels. Eigen analysis was used to determine the mode shapes and squared frequency values (Φ and Ω^2). The

response spectrum was created based on the equations found in section 11.4 in ASCE 7-16 and the same values from the Equivalent Lateral Force Procedure were used for S_s and S_1. The plotted response spectrum can be seen in Figure 8. The period for each mode was calculated using Ω^2 and for each period the associated acceleration from the response spectrum was determined, which was then used to determine the displacement for each mode. This, along with the modal participation factor, allowed for the calculation of the max q values which were then converted back into u (displacement) values. Once the max displacements from each mode were found, they were combined using the square root of the sum of squares (SRSS) method to determine the max displacement at each degree of freedom (DOF).

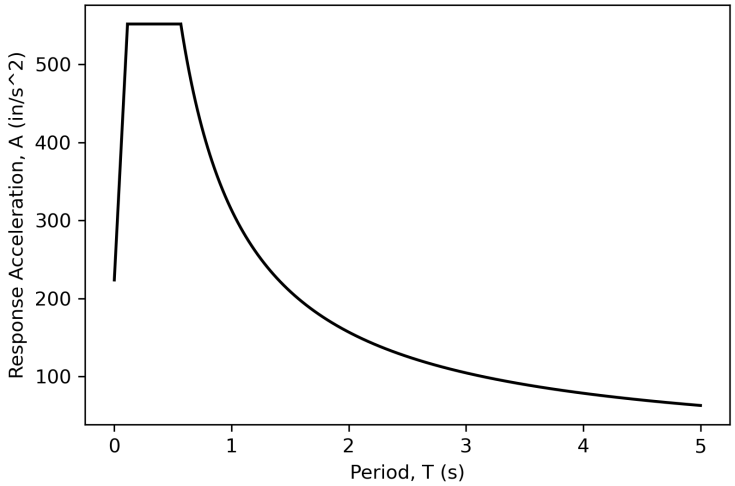

Figure 8: Plot of Response Spectrum

In Etabs, to create the response spectrum the same S_S and S_1 values that were used for the hand calculations were entered as shown in Figure 9. To stay consistent with the hand calculations, the modal case sub type used was Eigen. For the load case, the accelerations were scaled by 386.4 to get the values in the same units as the hand calculations and the modal combination was selected to be SRSS which can be seen in Figure 10.

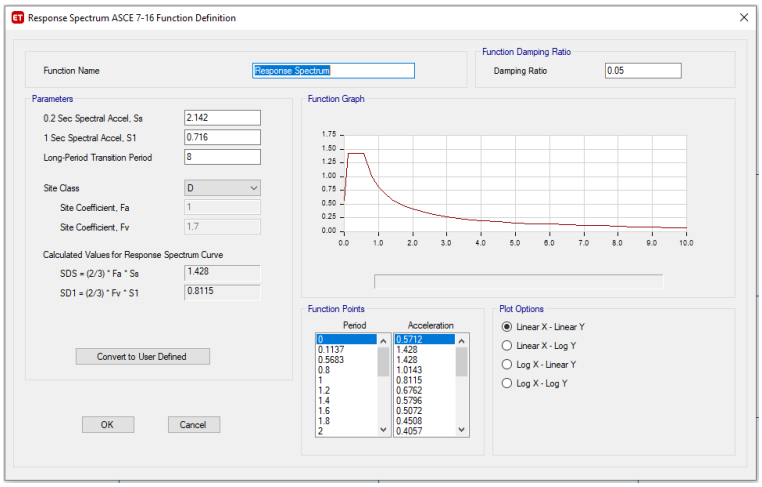

Figure 9: Response Spectrum Input in Etabs

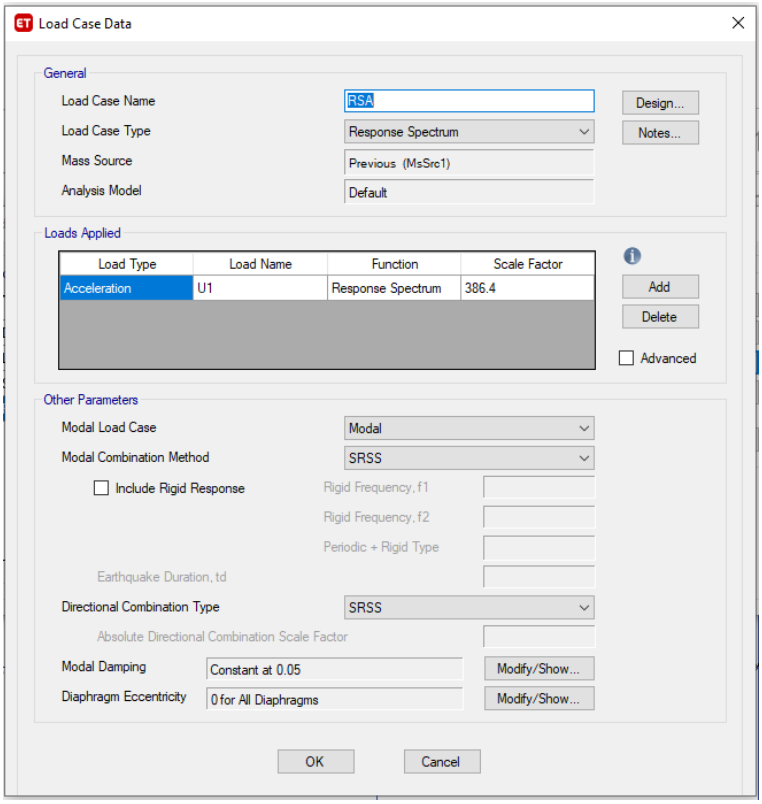

Figure 10: Response Spectrum Load Case Input in Etabs

The max displacements from the response spectrum analysis by hand and from Etabs can be found in Table 2 below. The large percent error is caused by the fact that double bending was assumed for the hand calculations, but this is not the case for Etabs. Etabs does not model the members as perfectly rigid to make the model more realistic. This lower stiffness means that for the same force, the frame will deflect more.

Level	Hand Calculated Displacement	Etabs Displacement	% error
3	6.233 in	7.765 in	24.6%
2	4.881 in	4.8341 in	.964%
1	2.351 in	2.157 in	8.24%

Table 2: Response Spectrum Analysis Results

3.2.2 Linear Modal Time History Analysis

To see how the frame initially performs under earthquake loading, the frame is analyzed using the linear time history analysis (THA) method with the El Centro ground motion. The results from this analysis can be compared to that of the earthquake response spectrum generated by Etabs and the results from this analysis will serve as a baseline for further analysis of the frame. Looking at a time history analysis provides a better view of the overall performance of the frame compared to the response spectrum analysis, and it allows for comparison of performance by looking at the affects from multiple ground motions. Inputting the El Centro ground motion is shown in Figure 11 and the load case created to run the linear time history analysis is shown in Figure 12.

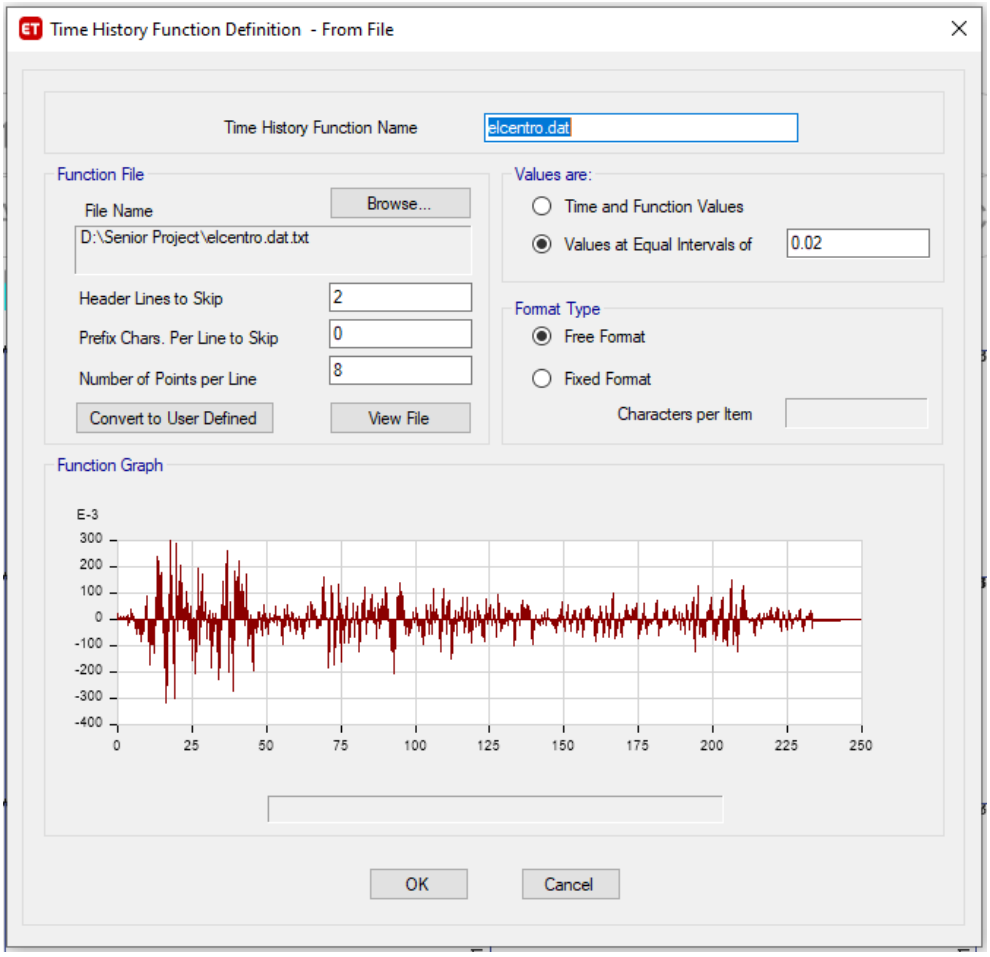

Figure 11: El Centro Ground Acceleration Input in Etabs

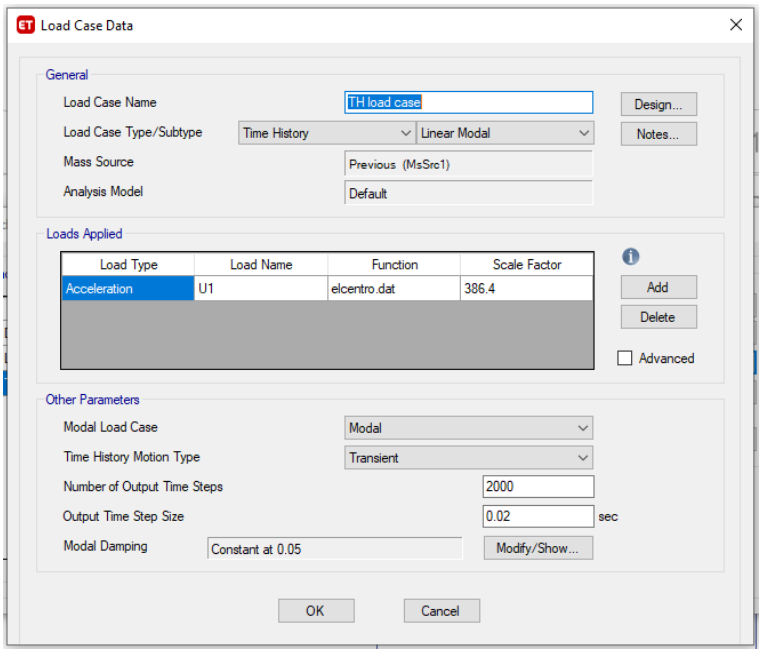

Figure 12: Etabs Input Window for El Centro THA Load Case

Etabs Computer Model Results		
	Max Deflection (in)	Max Acceleration (in/s^2)
EQ Response Spectrum	.6204	48.021
Linear Modal THA	.5909	45.7335

Table 3: El Centro Ground Motion Linear Analysis Results

The acceleration value for the linear modal THA in Table 3 above was found using the relation between the displacement, acceleration, and frequency squared, as well as the relationship between the period and the frequency, as shown by the equations below:

$$\omega = \frac{2\pi}{T} = \frac{2\pi}{.7142} = 8.798\ rad/s$$

$$\text{Displacement, } D = \frac{A}{\omega^2} \longrightarrow A = D\omega^2 = .5909\,in * (8.798\ rad/s)^2 = 45.7335\,in/s^2$$

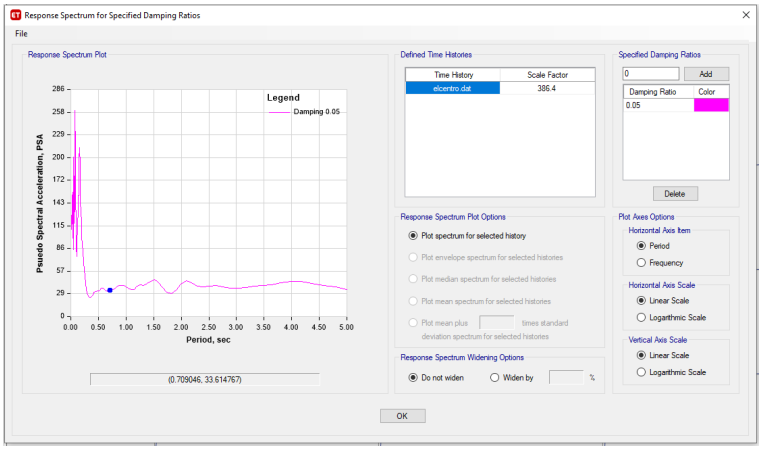

Figure 13: El Centro Acceleration Response Spectrum from Etabs

The acceleration from for the earthquake response spectrum is found from a graph in Etabs shown in Figure 13. The acceleration value is divided by .7 to get a more accurate estimate of what the acceleration would be at the top level of the frame. The same equation used above is used to calculate the displacement based on that acceleration value:

$$A = (33.615\, in/s^2)/.7 = 48.021\, in/s^2 \longrightarrow D = \frac{A}{\omega^2} = \frac{48.021}{8.798^2} = .6204\, in$$

3.3 Nonlinear Dynamic Analysis

3.3.1 Direct Integration Time History Analysis

Nonlinear analysis using direct integration involves solving the equations of motion through integration. The integration takes place at very small time steps compared to how long the structure is being loaded for. The equation of motion is:

$$M\ddot{u}(t) + C\dot{u}(t) + ku(t) = F(t)$$

In the equation above, M, C, and K are the mass, damping, and stiffness matrices, respectively. $\ddot{u}(t)$, $\dot{u}(t)$, and $u(t)$ are the acceleration, velocity and displacement vectors, respectively.

To run direct integration in Etabs, a nonlinear time history load case has to first be created. As with the linear modal time history analysis, the El Centro ground motion is input into Etabs as a time history function. For the direct integration load case, the initial conditions are set to start from zero, and the load type is chosen to be acceleration in the x direction. The scale factor is put in as 386.4 to get the results in the correct units by multiplying by gravity. The number of time steps and the time step size are changed to match the El Centro ground motion data. The input for the direct integration load case is shown in Figure 14. To get the correct damping for this analysis, the settings are changed to specify

damping by period, and for the fundamental period of the structure, .7142, a damping value of .05 is entered. For the second period a value of .1 is entered to create a large enough range between the two periods, and a damping value of .05 is also entered. Doing this forces the damping to be 5% between the first and second period. An in-depth analysis would be required to determine the best value for the second period which is outside the scope of the project. The modal settings for the direct integration load case can be seen in Figure 15. The deflection results from the direct integration time history analysis are shown in table 4 in the next section.

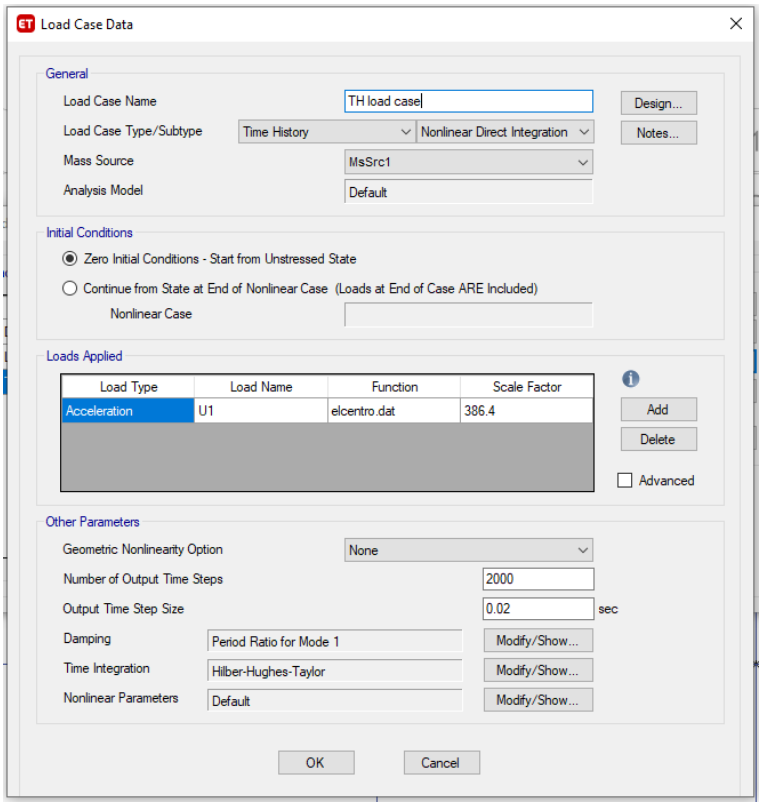

Figure 14: Etabs Input for Direct Integration THA Load Case

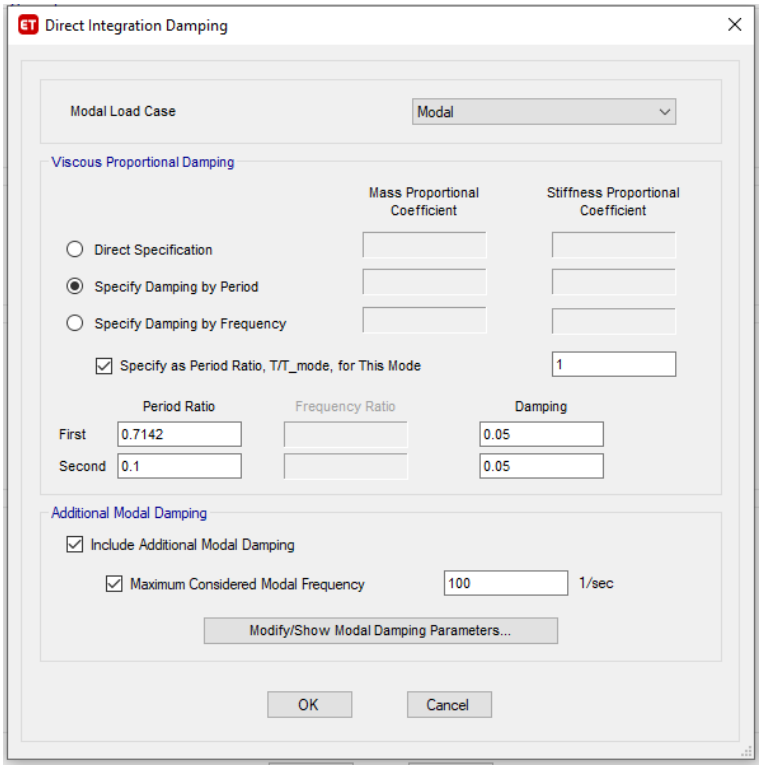

Figure 15: Damping Input for Direct Integration THA Load Case

3.3.2 Fast Nonlinear Analysis (FNA)

FNA is a modal analysis method that is an alternative analysis method that works by separating the nonlinear object force vector $R_{NL}(t)$ from the elastic stiffness matrix and the damped equations of motion [1]. The equation of motion for FNA is:

$$M\ddot{u}(t) + C\dot{u}(t) + ku(t) + R_{NL}(t) = R(t)$$

In the equation above, $R(t)$ is the external applied load vector and $R_{NL}(t)$ is the force vector from all the nonlinear elements. The rest of the variables were defined previously.

FNA works well for structures where specific elements are expected to go nonlinear and the rest of the structure remains elastic. This will be the case when dampers are added to the model. The addition of the dampers allows for the rest of the frame to remain elastic or linear, while the dampers go nonlinear, but FNA does not consider geometric or material nonlinear behavior. FNA is also very efficient, and it is much faster compared to direct integration. FNA is very efficient because it relies on ritz vectors, which are used to determine a sufficient number of structural modes to represent the behavior of the structural response [2]. Only vectors that respond to the particular loading used are sought out.

The ritz vectors represent the equilibrium relationships within the elastic structural system [1]. At every time increment the modal equations are uncoupled and solved, and the forces in the nonlinear degrees of freedom are resolved through an iterative process that will converge to reach equilibrium [1]. As long as FNA has good mode shapes the analysis will produce accurate results, whereas direct integration needs to have small enough time steps to accurately characterize dynamic behavior [1]. FNA also relies on only modal damping and direct integration uses mass and stiffness proportional damping. This is useful since modal damping does not require the formation or storage of a fully populated damping matrix.

To begin to analyze the frame with FNA in Etabs, the modal load case is changed from Eigen to Ritz. For this modal case, the load types are acceleration in the x direction and dead load. The maximum number of modes is set at 100 to ensure that enough modes will be used. The ritz vector modal case input can be seen in Figure 16. Next, in order for FNA to work, there needs to be a load case for dead load. The dead load that is applied to the structure is 100 k at the exterior columns at all levels and 200 k at the interior columns at all levels. To determine if the amount of dead load has any significant effect on the results, the analysis was run with a range of dead load values for the exterior columns: 10 k, 15 k, 20 k, 50 k, 75 k, and 100 k while the interior columns had double the exterior column weight. The results revealed that the dead load applied had a negligible effect on displacement so all results moving forward are based on the 100 k and 200 k dead loads. For this load case the loads applied are just the dead load with the default ramp function used. The modal load case is changed to be the ritz vector modal case that was previously made. For FNA the damping is kept at a constant value of .05. The FNA load case for dead load can be seen in Figure 17.

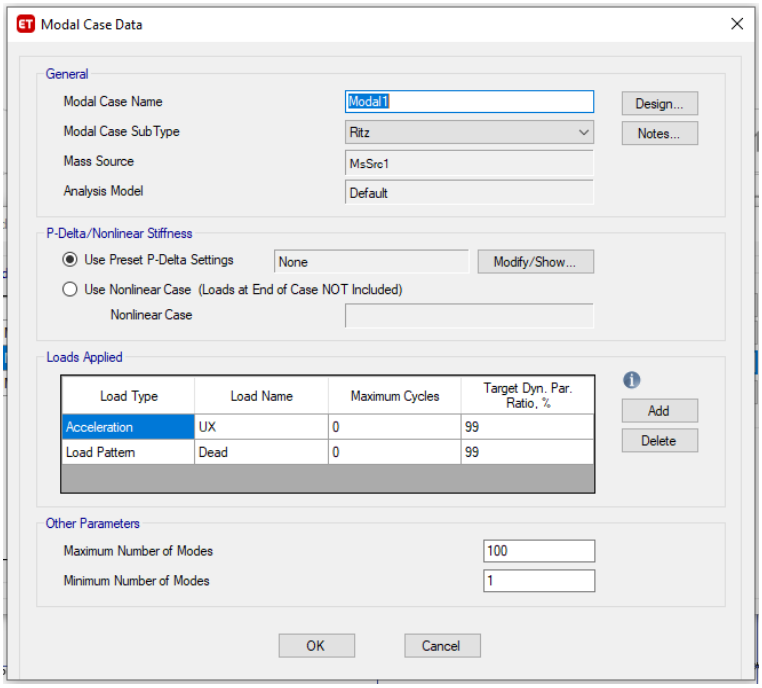

Figure 16: Etabs Input for FNA Modal Case

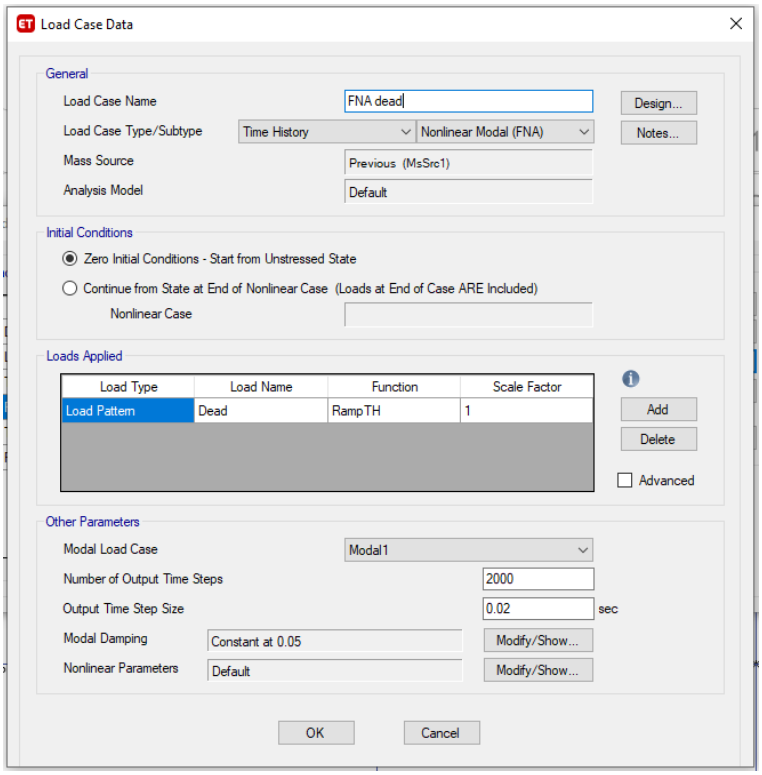

Figure 17: Etabs Input for FNA Dead Load Time History Analysis Load Case

After creating the FNA load case for dead load, a load case needs to be created for the El Centro ground motion. For this load case, instead of starting at zero initial conditions, it is changed to continue from the FNA dead load case. The loads applied is selected as acceleration in the x direction and the function is the El Centro ground motion with the scale factor set as 386.4. The modal case is change to the ritz vector modal case, and as for the dead load case, damping is kept as .05. The input for this load case is shown in Figure 18 below.

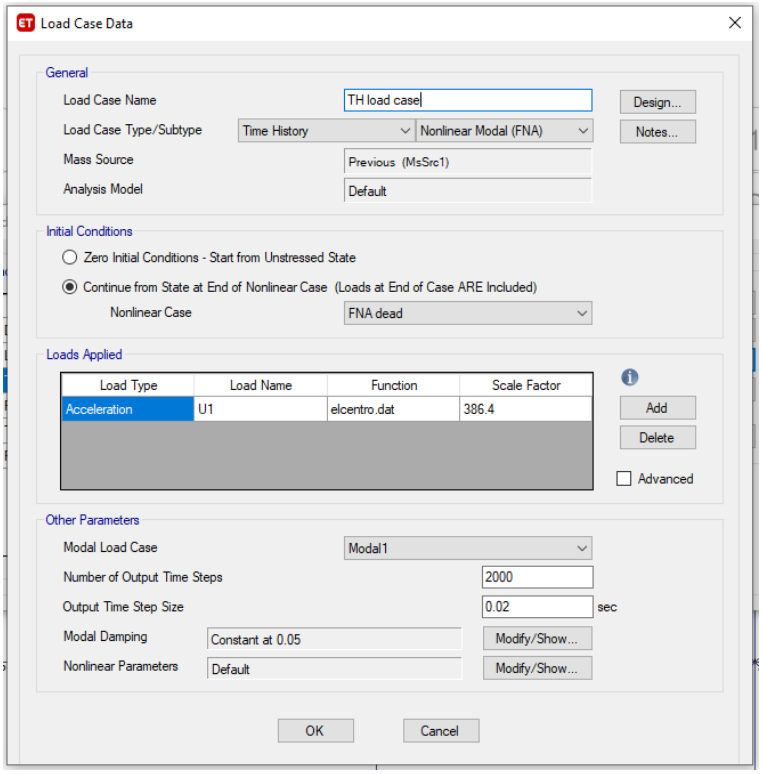

Figure 18: Etabs Input for FNA El Centro Ground Motion Load Case

Etabs Computer Model Results			
	Max Deflection (in)	Min Deflection (in)	Max Acceleration (in/s^2)
Direct Integration THA	.2938	-.5221	40.4086
FNA THA	.3531	-.5909	45.7334
Linear Modal THA	.3531	.5909	45.7335

Table 4: El Centro Ground Motion Nonlinear Analysis Results

The results from FNA and the direct integration analysis are shown in the table above as well as the results from the linear time history analysis to compare to. From these results it is clear there is not a significant difference between the two analysis methods. In fact, for El Centro the results from the linear modal THA and FNA were the same. Because of this, moving forward FNA will be used for all analysis since it tends to be more accurate than direct integration and the analysis takes much less time.

4. PARAMETRIC STUDY

4.1 Ground Motions

For further analysis seven ground motions were chosen. These ground motions are samples of seismic activity from the bay area in California, which is considered to be a high seismic region. The ground motions were acquired from a structural engineering firm and they are maximum considered earthquake (MCE) ground motions. The acceleration plots of the ground motions can be seen in Figure 19 through Figure 25 below. Figures 26 through 32 show the displacement and velocity plots for all of the ground motions.

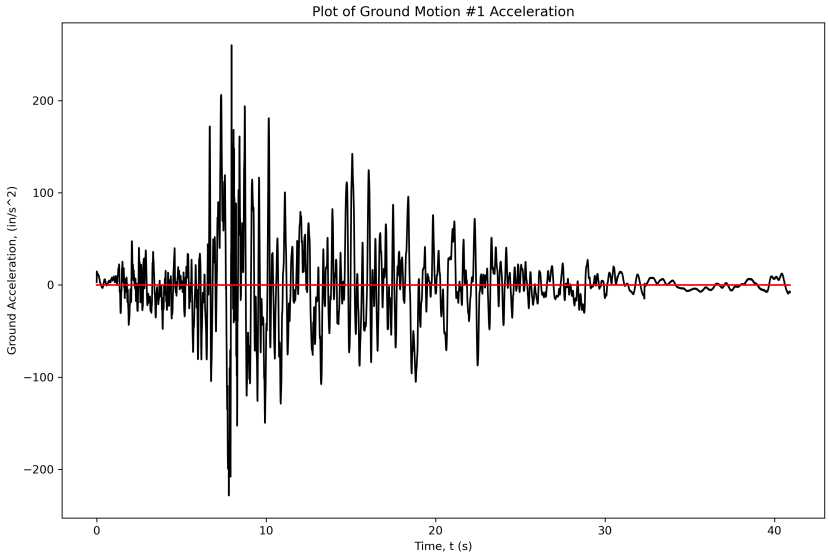

Figure 19: Ground Motion 1 Acceleration Plot

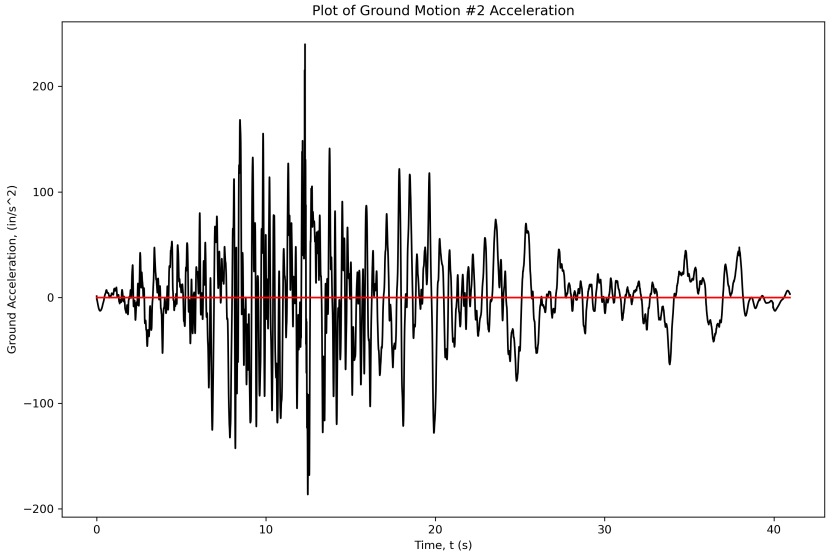

Figure 20: Ground Motion 2 Acceleration Plot

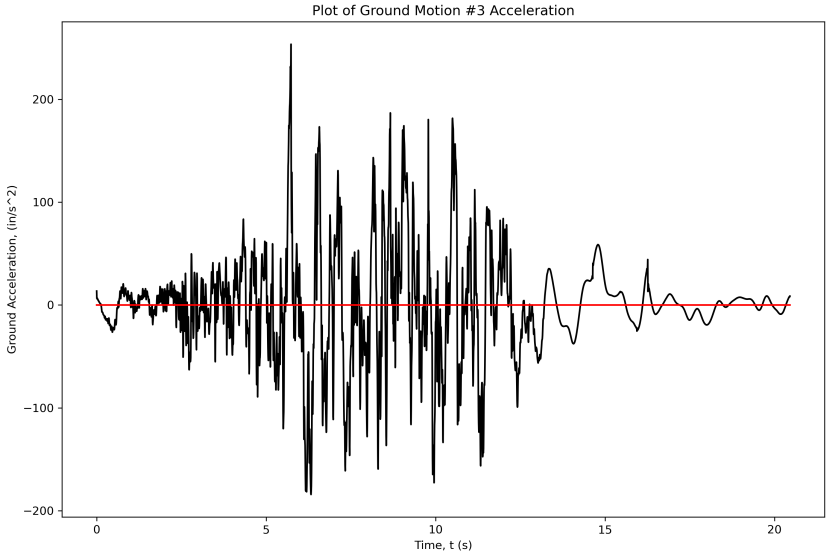

Figure 21: Ground Motion 3 Acceleration Plot

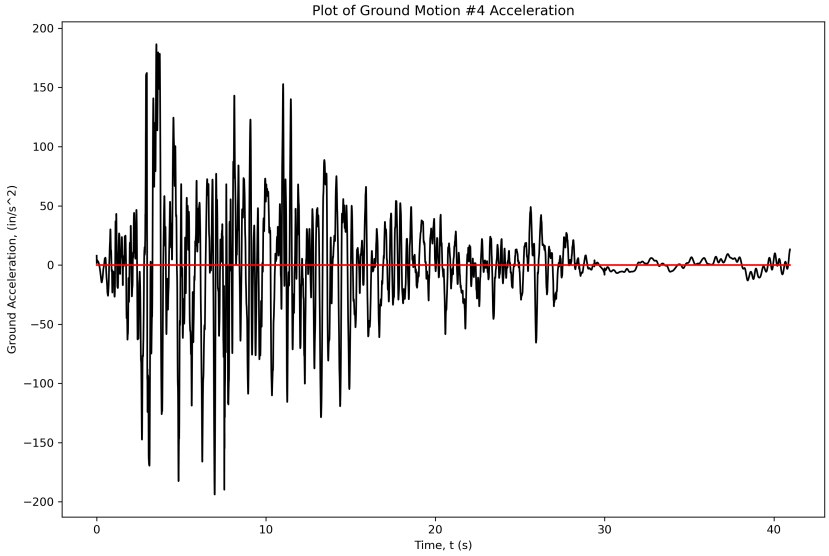

Figure 22: Ground Motion 4 Acceleration Plot

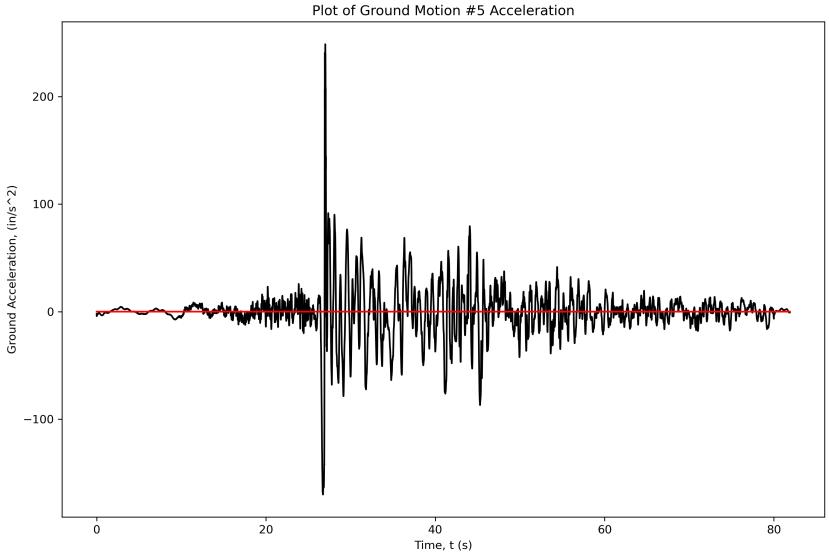

Figure 23: Ground Motion 5 Acceleration Plot

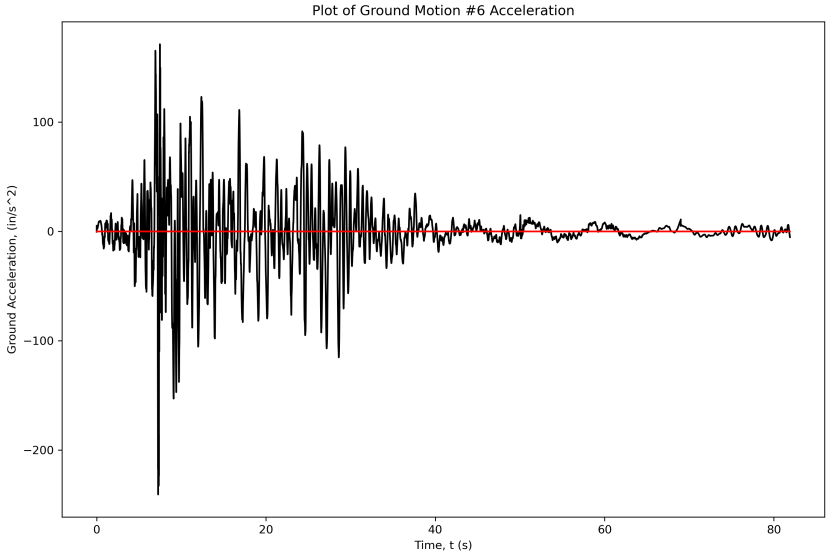

Figure 24: Ground Motion 6 Acceleration Plot

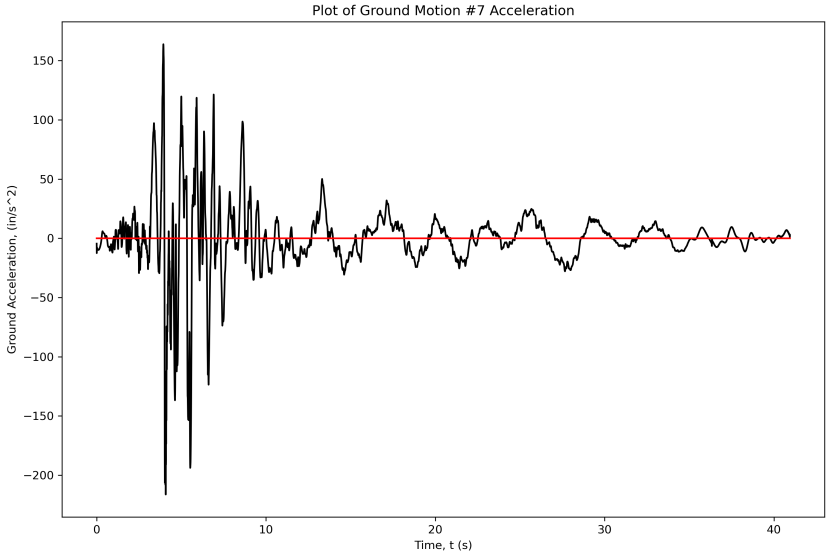

Figure 25: Ground Motion 7 Acceleration Plot

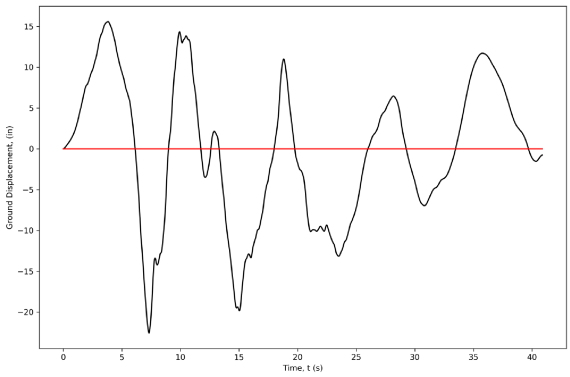

Ground Motion 1 Displacement plot

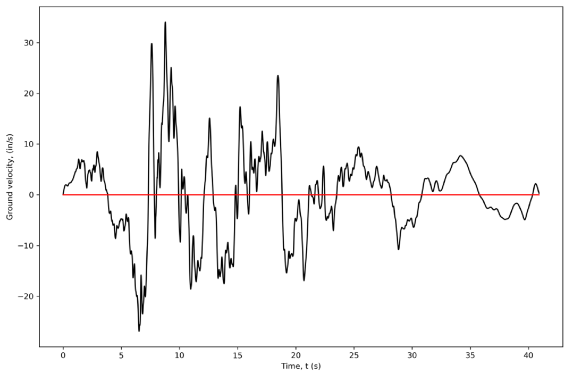

Ground Motion 1 Velocity plot

Figure 26: Plots for Ground Motion 1

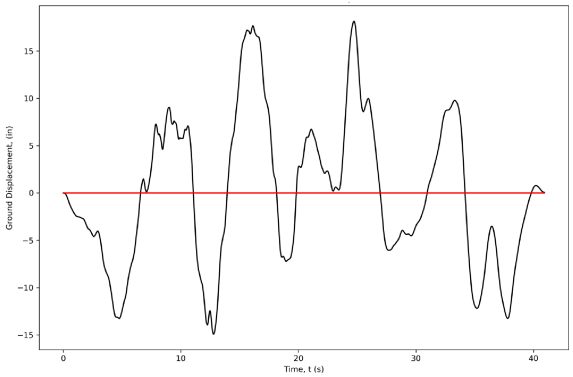

Ground Motion 2 Displacement plot

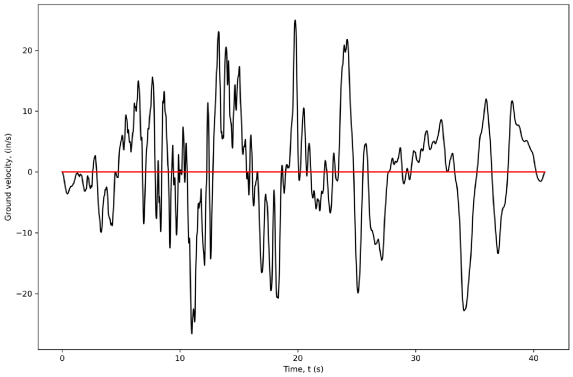

Ground Motion 2 Velocity plot

Figure 27: Plots for Ground Motion 2

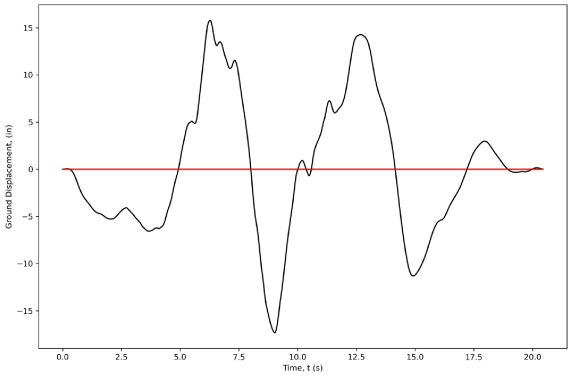

Ground Motion 3 Displacement plot

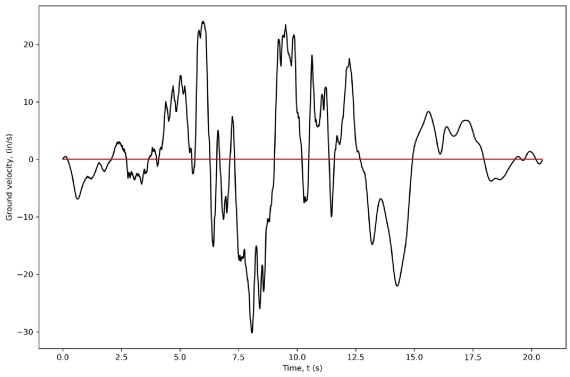

Ground Motion 3 Velocity plot

Figure 28: Plots for Ground Motion 3

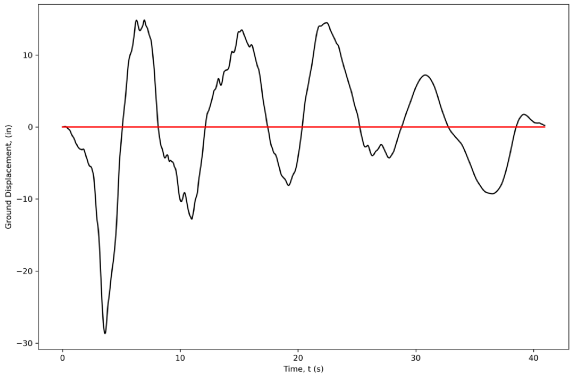

Ground Motion 4 Displacement plot

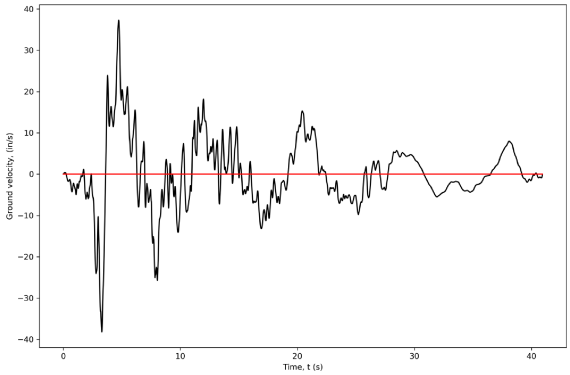

Ground Motion 4 Velocity plot

Figure 29: Plots for Ground Motion 4

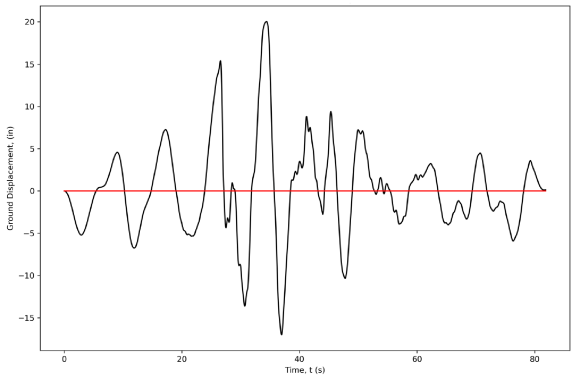

Ground Motion 5 Displacement plot

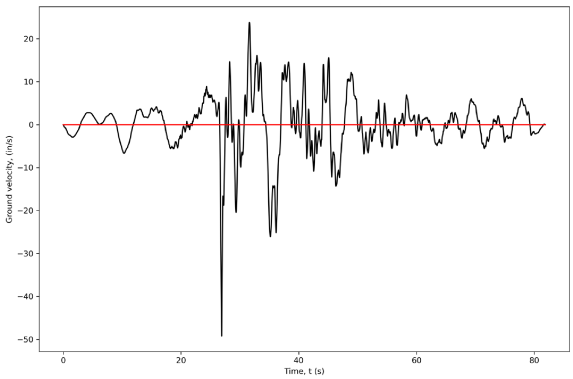

Ground Motion 5 Velocity plot

Figure 30: Plots for Ground Motion 5

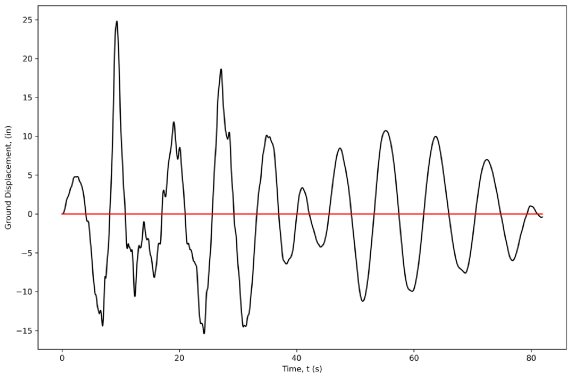

Ground Motion 6 Displacement plot

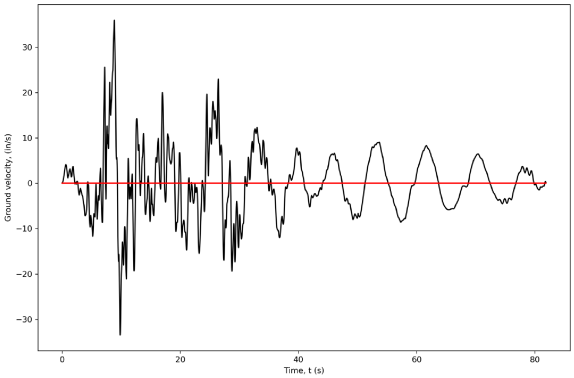

Ground Motion 6 Velocity plot

Figure 31: Plots for Ground Motion 6

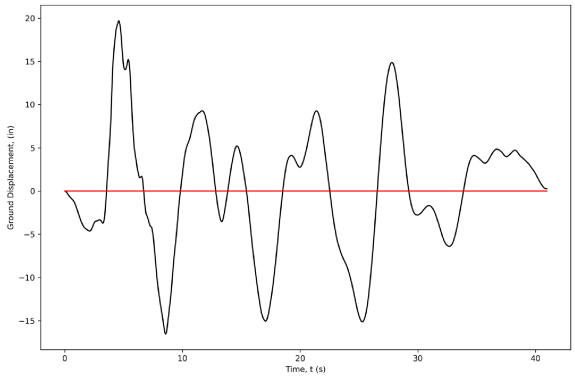

Ground Motion 7 Displacement plot

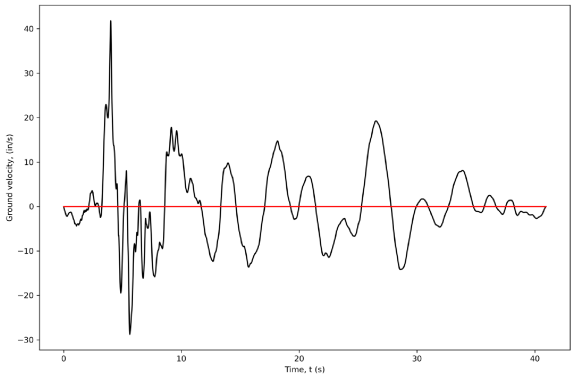

Ground Motion 7 Velocity plot

Figure 32: Plots for Ground Motion 7

4.2 Linear vs Nonlinear Analysis

To begin investigation into the 7 different ground motions, they are each applied to the frame model and analyzed with linear modal THA as well as FNA. This provides a general idea of how the frame will perform when subjected to each ground motion and allows for the results from each to be compared relative to each other. The accuracy of the models can be determined based on how close the results from the 2 analysis methods are. Since the model does not currently have any nonlinear elements, the results from the two analysis methods should be very similar. The input for the two analysis methods is entered into Etabs for each ground motion the same way as for El Centro which is shown in section 3.2.2 and 3.3.2. Note that the time step size and number of time steps are based on the ground motion data that is being input into Etabs. The results from both analysis methods for all seven ground motions are shown in Table 5. In the table GM# represents ground motion and which number ground motion it is.

	FNA THA Results		**Linear Modal THA Results**	
	Max Deflection (in)	Min Deflection (in)	Max Deflection (in)	Min Deflection (in)
GM 1	7.78	-7.86	7.73	-7.91
GM 2	6.72	-7.65	6.70	-7.67
GM 3	7.69	-7.39	7.46	-7.62
GM 4	7.57	-7.59	7.43	-7.72
GM 5	5.30	-8.41	5.33	-8.38
GM 6	8.22	-6.82	8.23	-6.81
GM 7	6.50	-7.75	6.57	-7.67

Table 5: Linear and Nonlinear Analysis Results for 7 Ground Motions

The results in the above table show that the analysis methods, FNA THA and linear modal THA, produce deflection values that are relatively close for all seven ground motions.

4.3 Damper Model

The Damper that is being modeled in Etabs is based on a fluid viscous damper (FVD) made by the company, Taylor Devices Inc. For this damper, Taylor Devices performed experimental tests to determine the hysteretic behavior of the damper. The results from the computer analysis of the damper will be compared to the experimental results acquired from Taylor Devices, to ensure that the model accurately represents the actual performance of the damper.

To create the damper in Etabs, a new link section property was made. To model a fluid viscous

damper, the damper type in Etabs is changed to damper - exponential. Since the frame is modeled along the x-axis, the U1 direction is selected for the direction and the box for nonlinear properties is checked which can be seen in Figure 33. The linear and nonlinear properties of the specific damper are entered, which include the stiffness and effective stiffness, the damping and effective damping, and the damping exponent and are shown in Figure 34. In Etabs, the damper properties are based on the Maxwell model of viscoelasticity where there is an exponential viscous damper in series with a linear spring [7]. The stiffness in the Maxwell model reflects the stiffness of the brace that is often used to connect the damper from one story to another.

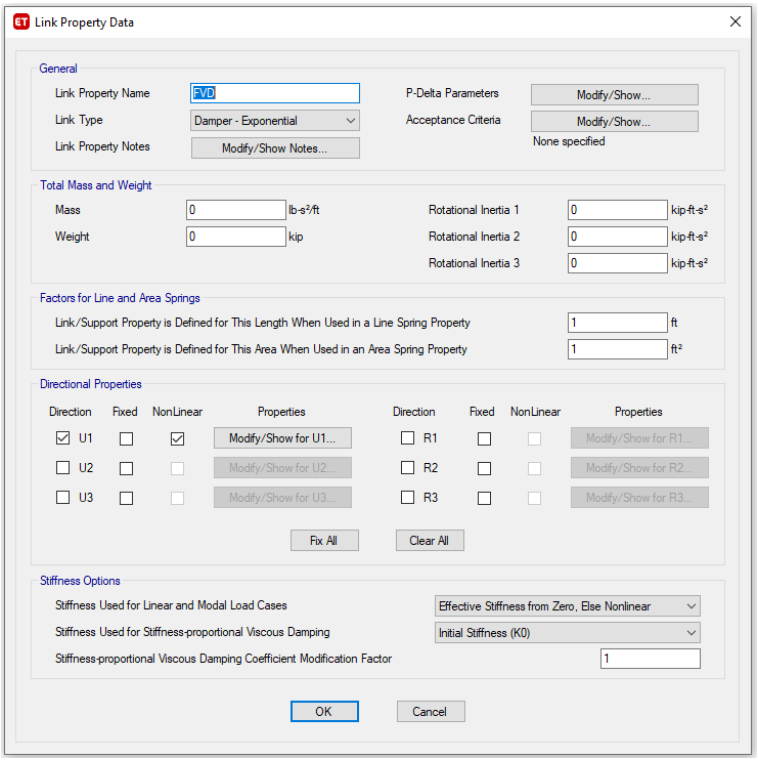

Figure 33: Etabs Input for Fluid Viscous Damper

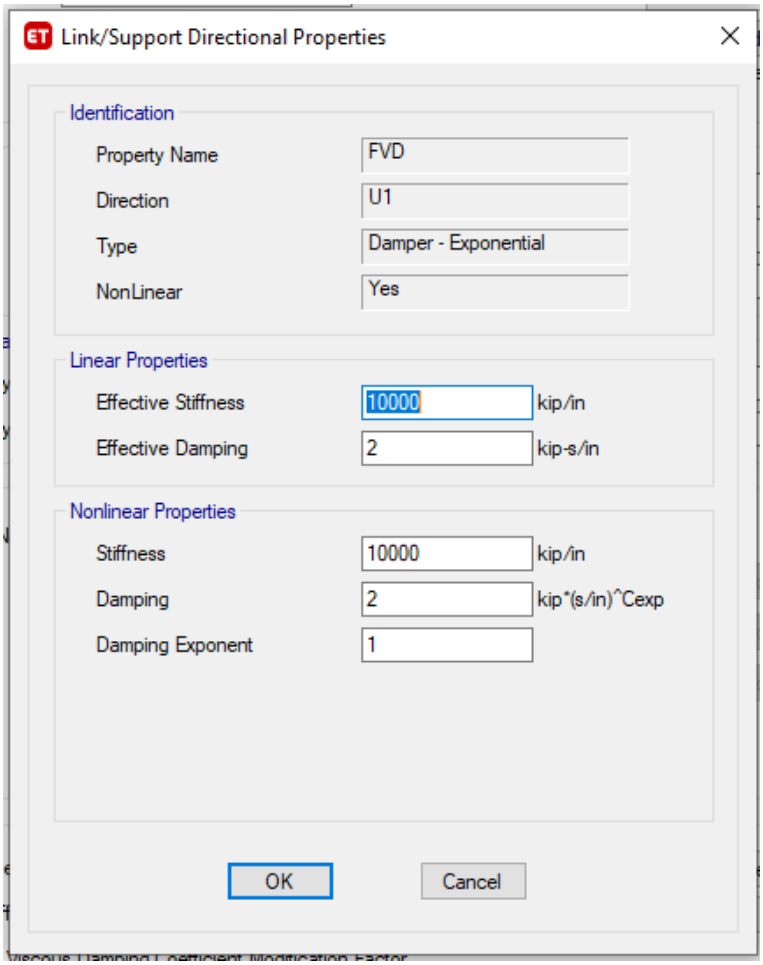

Figure 34: Etabs Input for Damper Properties

For the analysis of this damper, a sine function time history is entered, which is what was used for the experimental testing. The period of the function is 1.88 seconds, the number of steps per cycle is 20, the number of cycles is 5, and the amplitude is 21. The input for the time history function is shown in Figure 35.

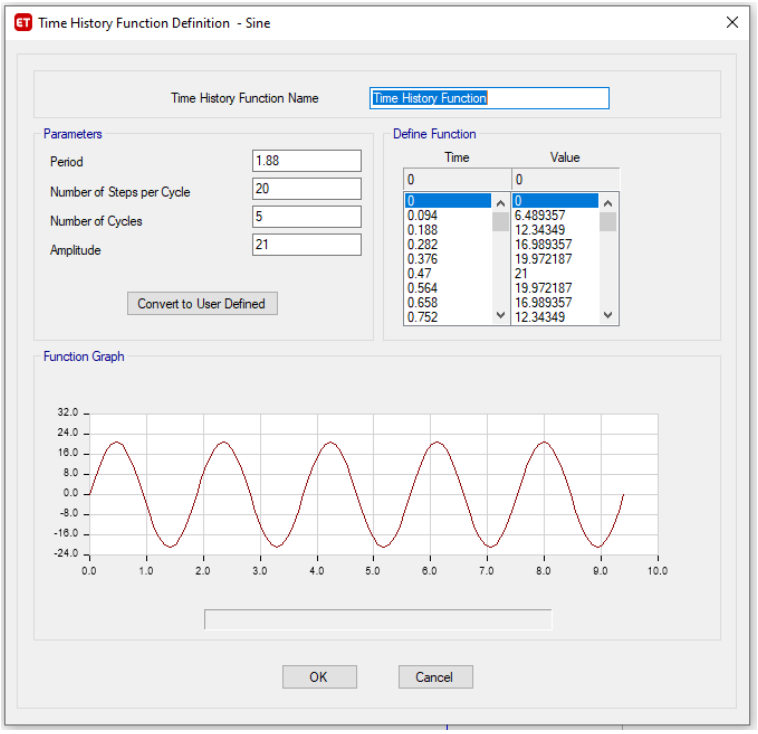

Figure 35: Etabs Input for Sine Function

A load case is created for the analysis of the damper, using nonlinear direct integration. The initial conditions are starting from 0, and the load pattern that is created uses the sine time history function that was previously created. The Number of output steps entered is 200, and the output time step size is .1. When the damper section property is placed in Etabs, it has a pinned support at one end and a roller support at the other end. A one kip load is applied at the roller support pointed toward the other end of the damper. The load case input is shown in Figure 36 and the model of the damper is shown in Figure 37.

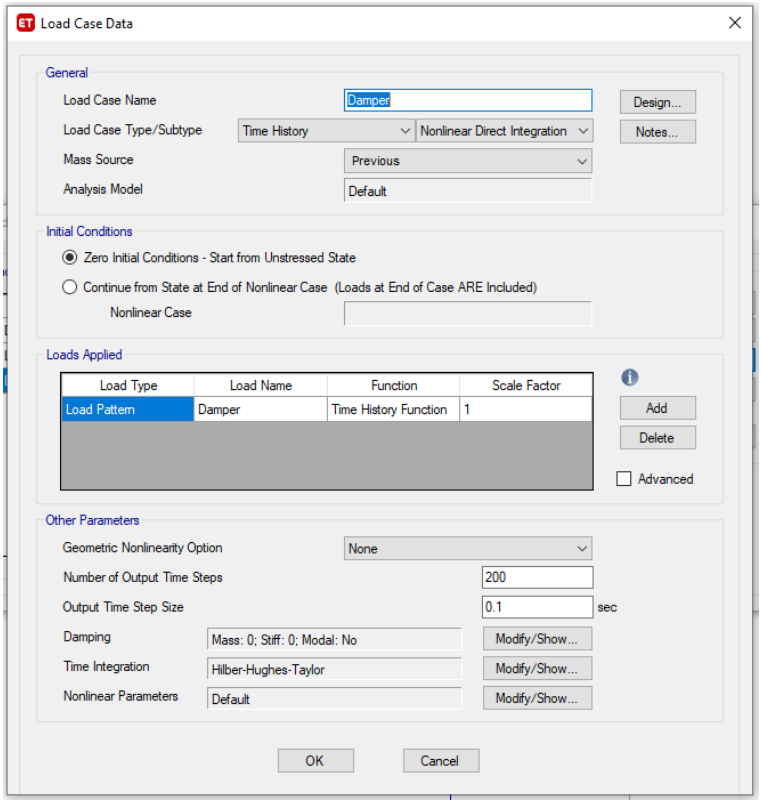

Figure 36: Etabs Input for Damper Load Case

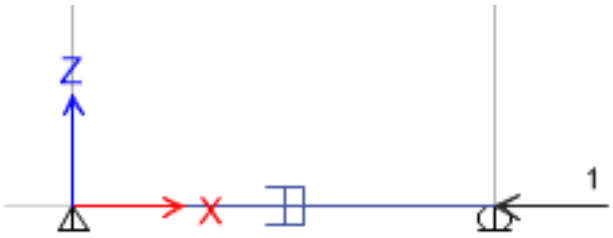

Figure 37a: Damper Model in Etabs

The hysteretic curves from the Etabs model of the damper and from the experimental testing by Taylor Devices are shown in Figures 37b and 37c below. The results show that the hysteretic curves match each other so the damper was modeled correctly in Etabs.

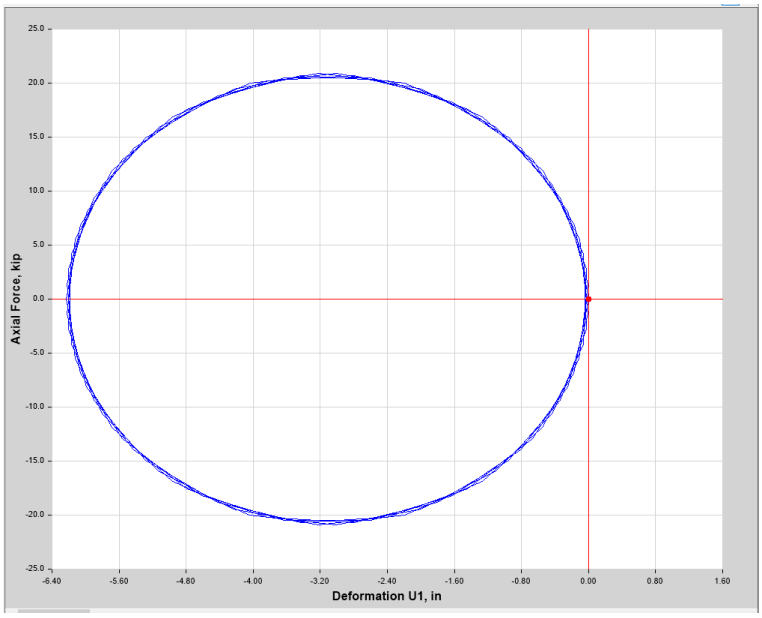

Figure 37b: Hysteretic Curve from Computer Model

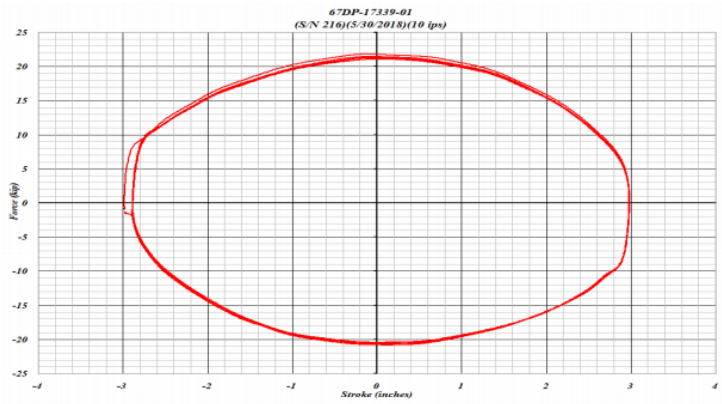

Figure 37c: Hysteretic Curve from Taylor Devices [8]

The damper will now be added to the frame which will be analyzed with FNA for each of the seven ground motions. The orientation of the dampers will be diagonal, going from the lower left corner of a bay in the moment frame to the upper right corner. First a single damper will be added to the top level middle bay. Then a second damper will be added to the bay below, and finally a third damper will be added to the middle bay in the bottom level. The Etabs Models of the three configurations of dampers, and graphs showing the decrease in deflection relative to the frame without any dampers are shown below in Figures 38 through 43. The data for Figures 39, 41 and 43 is shown in Appendix A Tables 8, 9, and 10.

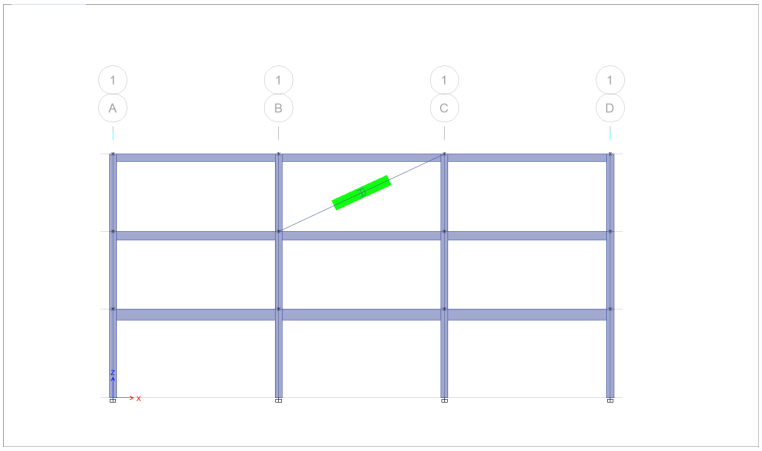

Figure 38: Frame Elevation with 1 Damper

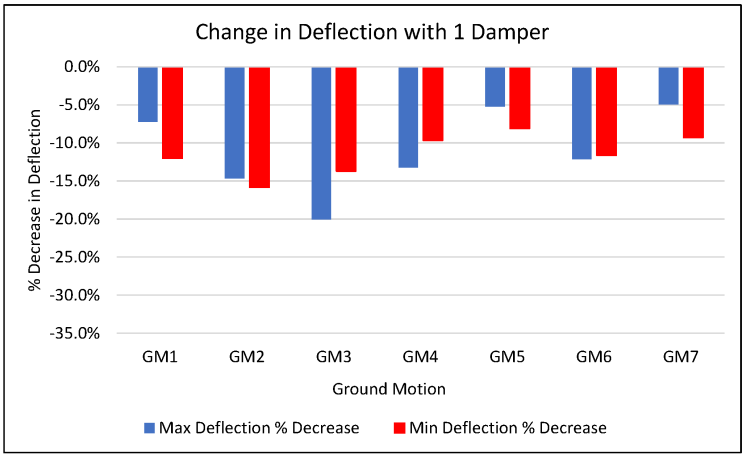

Figure 39: Bar Graph of Deflection Results with 1 Damper

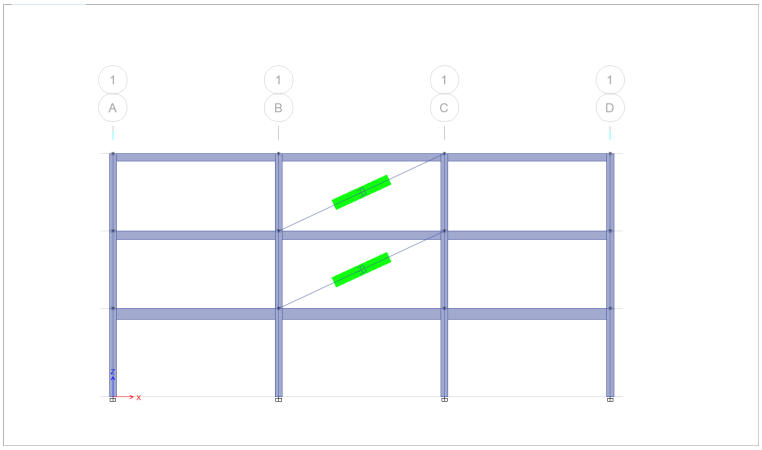

Figure 40: Frame Elevation with 2 Dampers

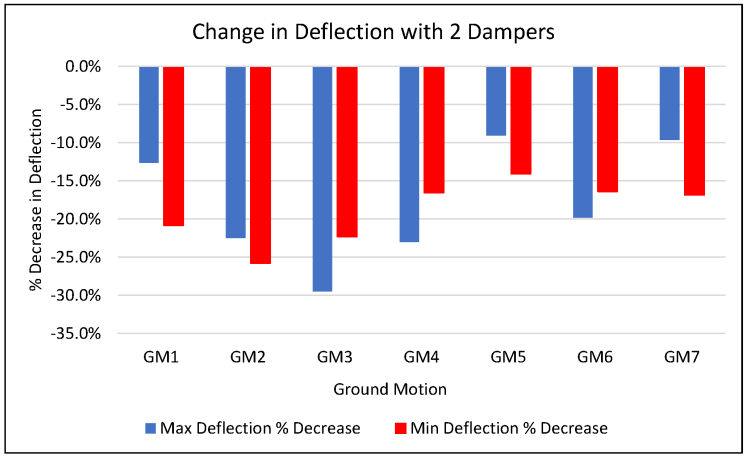

Figure 41: Bar Graph of Deflection Results with 2 Dampers

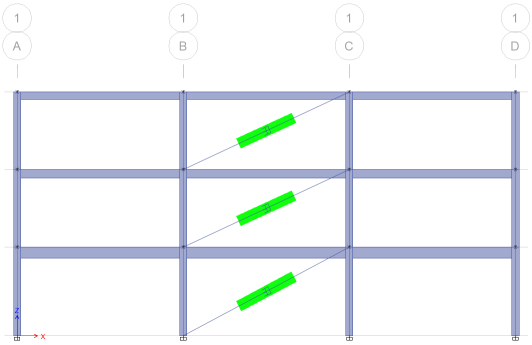

Figure 42: Frame Elevation with 3 Dampers

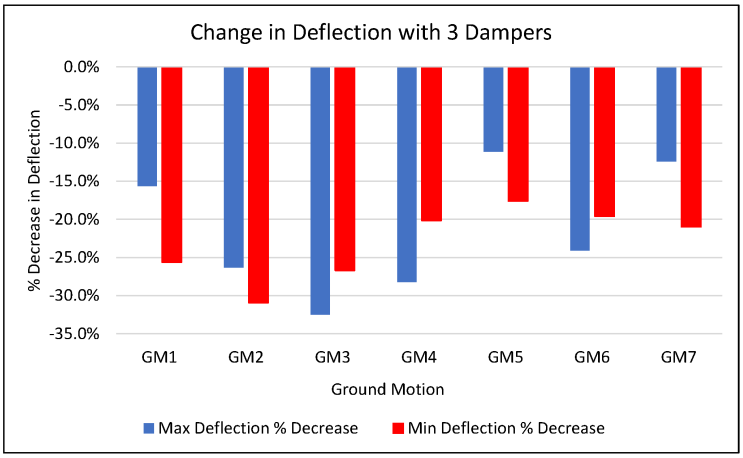

Figure 43: Bar Graph of Deflection Results with 3 Dampers

The graphs above show that as dampers are added to the frame, the deflections for all ground motions decrease both in the positive and negative x direction. The deflection from ground motion 3 decreases by the largest amount and the deflection from ground motion 5 decreases by the smallest amount. The difference in percent decrease in deflection between the maximum and minimum deflection stays consistent as more dampers are added.

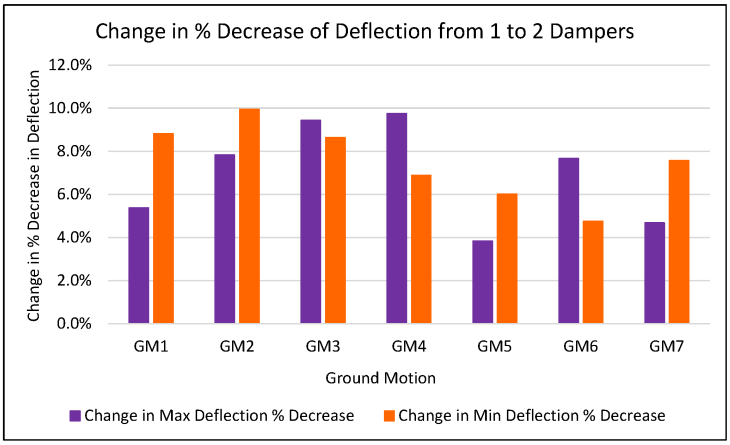

Figure 44: Bar Graph of Change in Results Between 1 to 2 Dampers

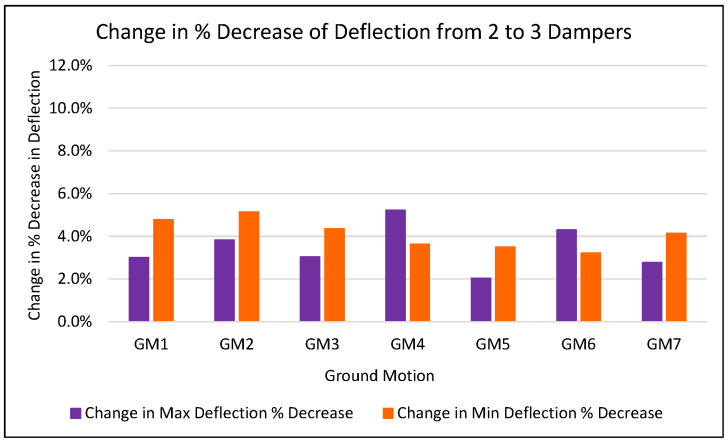

Figure 45: Bar Graph of Change in Results Between 2 to 3 Dampers

Figure 44 and Figure 45 above show how much the percent decrease in deflection changes when going from 1 damper to 2 dampers, and then going from 2 dampers to 3 dampers. The deflection changes by a much larger amount when adding a second damper compared to adding a third. This shows that the there is a limit to the return on investment when adding dampers. The more dampers you add, the smaller the benefit they will provide, meaning that there is a point where it is no longer necessary or helpful to continue to add dampers. Data for Figures 44 and 45 is shown in Appendix A Table 11.

4.4 Damper Location

4.4.1 Damper Configuration

Using only the first ground motion for analysis, a series of different damper configurations in the frame will be modeled and analyzed with FNA to determine which configurations produce the largest decreases in the deflection of the frame. The configurations will fall into 5 categories based on the number of dampers, where they will either have 1 damper, 2 dampers, 3 dampers, 4 dampers, or 6 or more dampers. Figures 46 through 51 below show all the configurations in each of the categories.

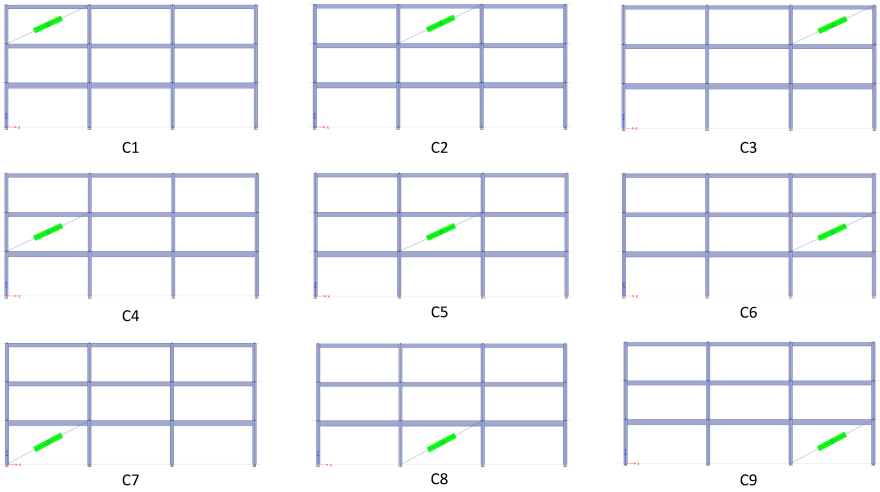

Figure 46: All Damper Configurations with 1 Damper

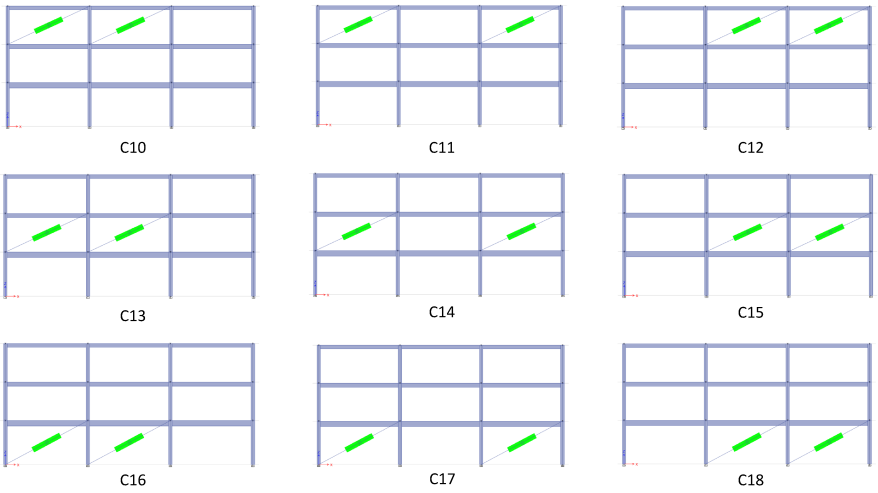

Figure 47: All Damper Configurations with 2 Dampers in a Row of Bays

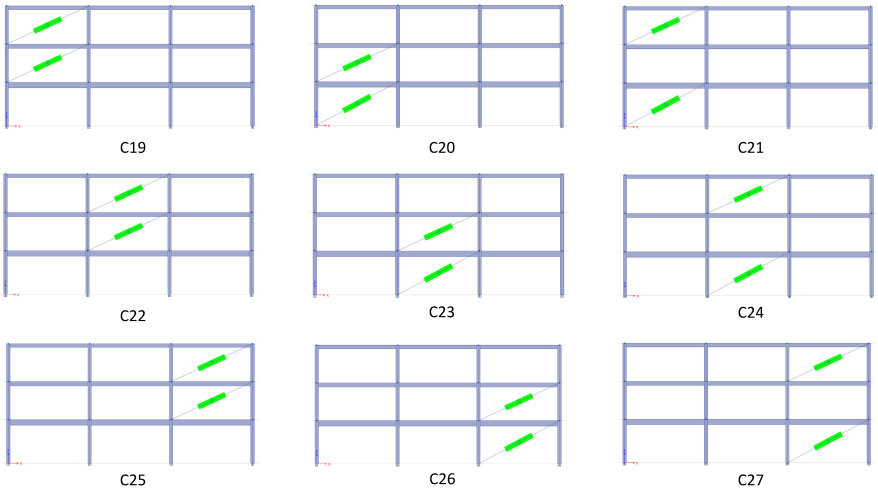

Figure 48: All Damper Configurations with 2 Dampers in a Column of Bays

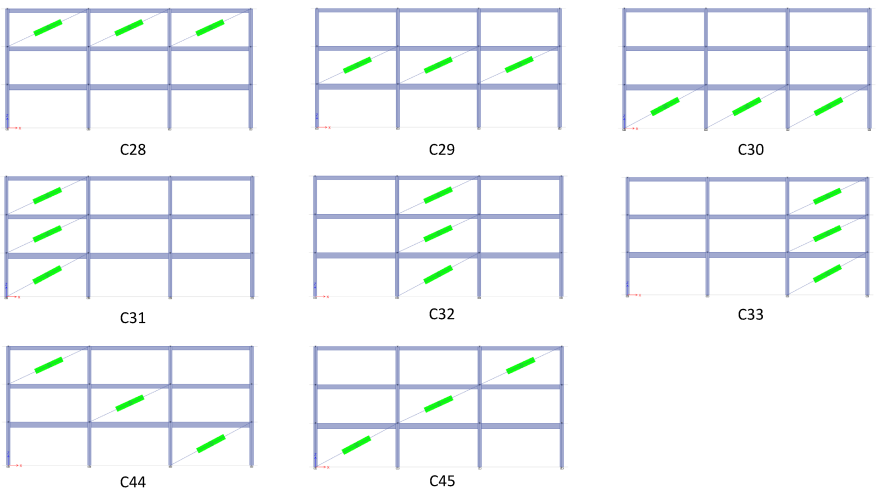

Figure 49: All Damper Configurations with 3 Dampers

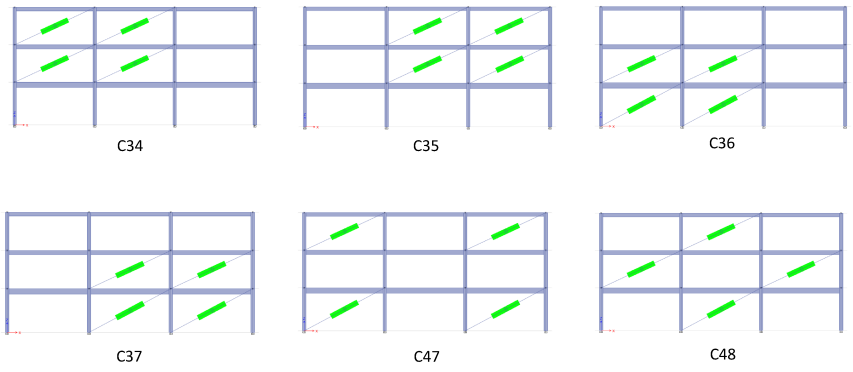

Figure 50: All Damper Configurations with 4 Dampers

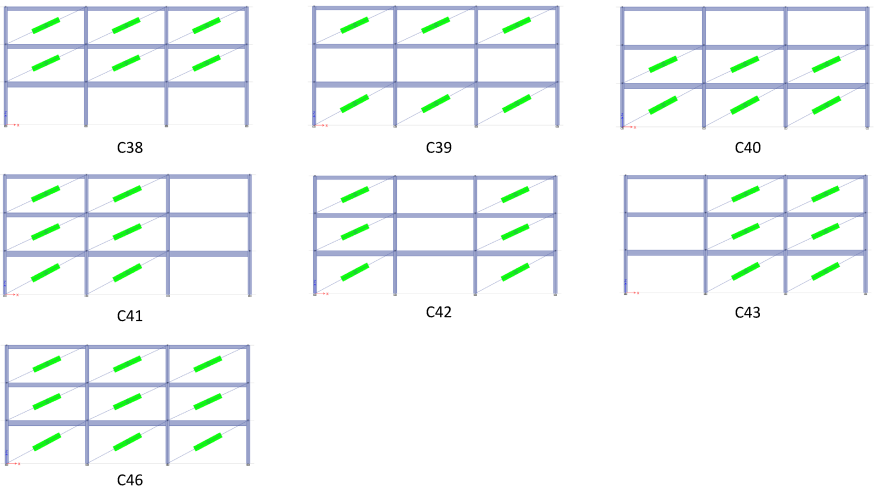

Figure 51: All Damper Configurations with 6 or More Dampers

From the analysis that was carried out, the deflection at the left corner of the top level of the frame was determined for each configuration and the percent decrease from the deflection for the frame without any dampers was determined. The following Figures 52 through 57 show the percent decreases in deflection for each damper configuration category. The data for these graphs is shown in Appendix A Tables 12 through 17, respectively.

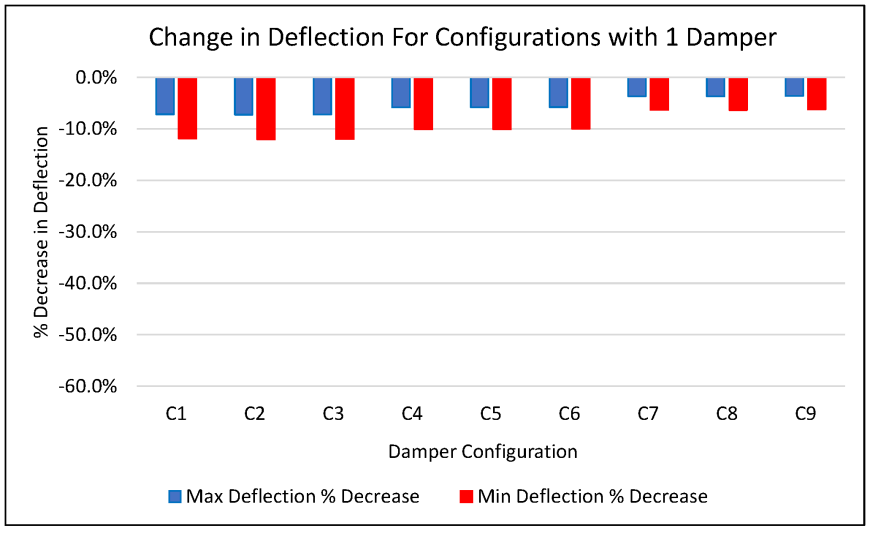

Figure 52: % Decrease in Deflection for Configurations with 1 Damper

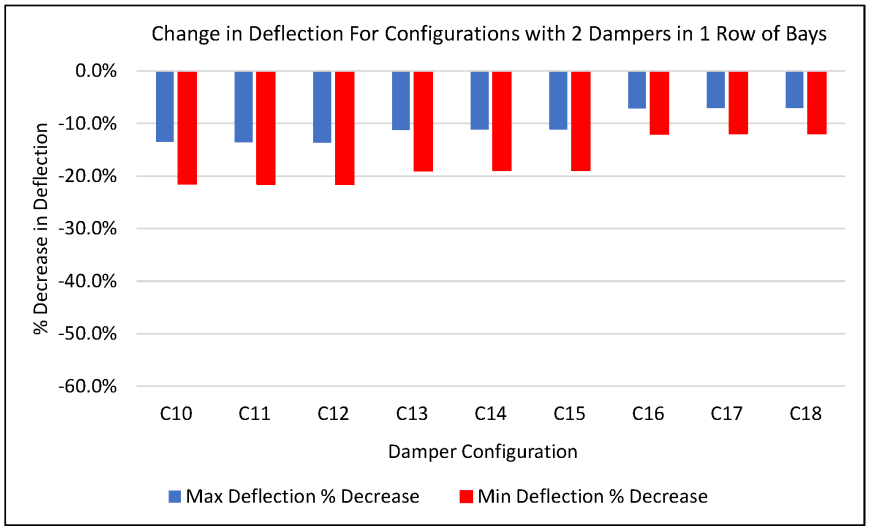

Figure 53: % Decrease in Deflection for Configurations with 2 Dampers in a Row

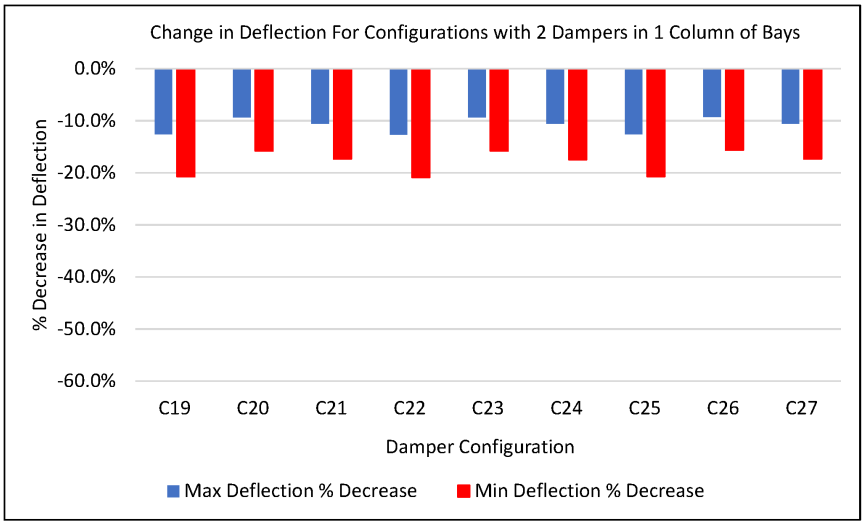

Figure 54: % Decrease in Deflection for Configurations with 2 Dampers in a Column

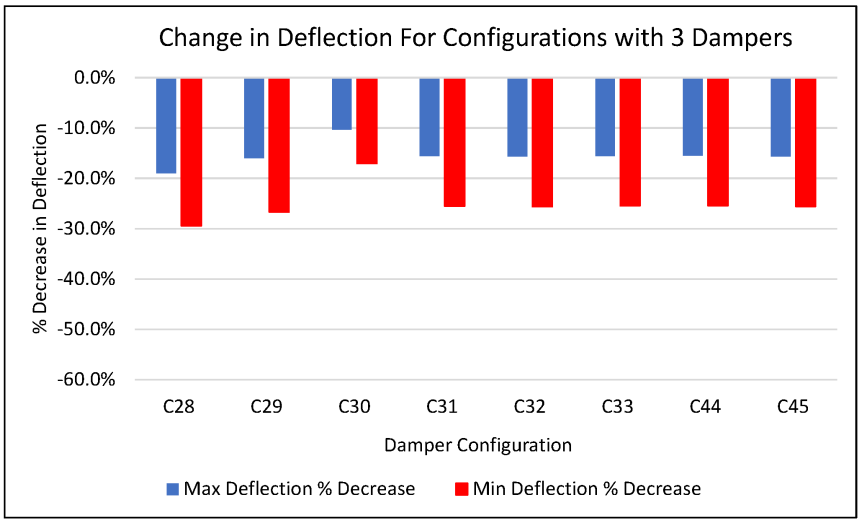

Figure 55: % Decrease in Deflection for Configurations with 3 Dampers

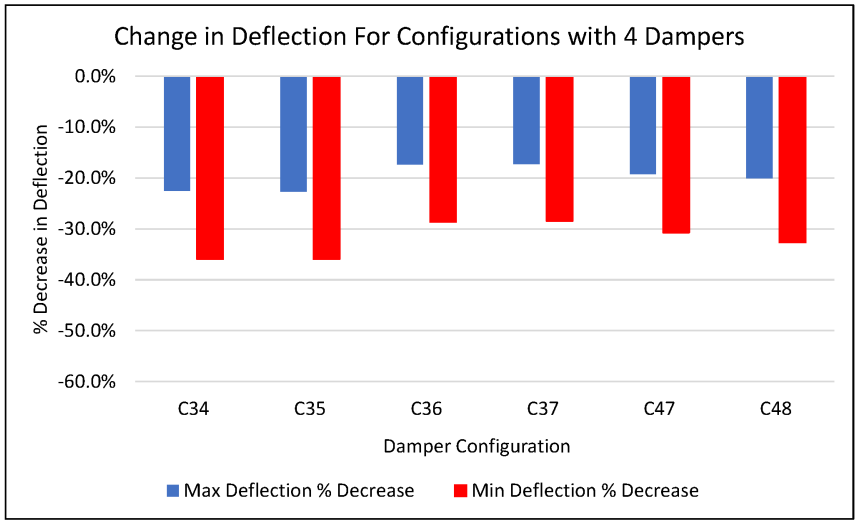

Figure 56: % Decrease in Deflection for Configurations with 4 Dampers

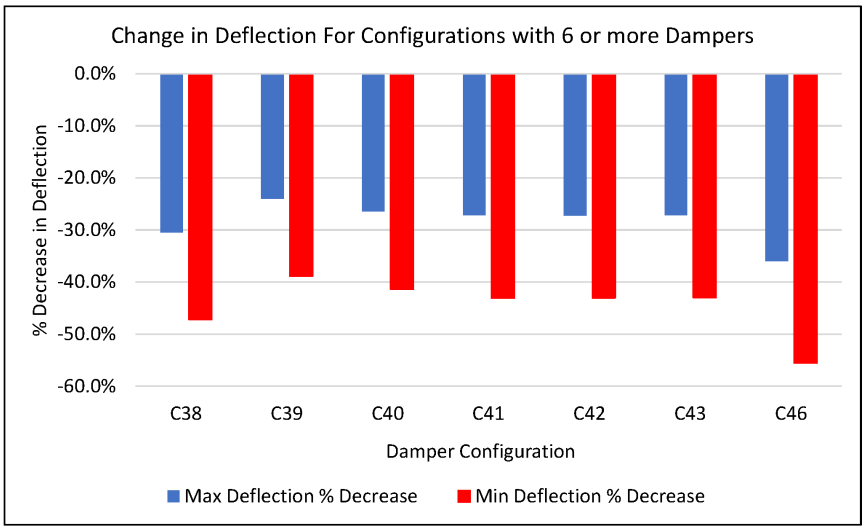

Figure 57: % Decrease in Deflection for Configurations with 6 or More Dampers

The previous graphs show that as more dampers are added to the frame the decrease in deflection increases. Between the different configurations in the same categories, the decrease in deflection does not change significantly. For the configurations with 1 damper, or two dampers in the same row of the bays, the specific bays with the dampers did not impact the results, but when looking at the different levels the values did vary. Based on the results, taking into account the decrease in deflection and the number of dampers, a configuration using three dampers is an optimal choice since it provides a very good return on investment. The decrease in deflection for the 3 damper configurations ranges from 25-30% and those values only increase by approximately 10% when looking at configurations with 4 dampers. When increasing the number of dampers to configurations with 6 or more, the minimal additional decrease in deflection may not be worth the additional cost for those dampers.

When looking at the configurations with 3 dampers, the best performing configuration is number 28, where the 3 dampers are located in all three bays of the top level. The reasoning for this is shown when looking at a plot of the story displacements. The Story displacement between the third and second level is greater than that between the second and first level or between the first level and the base. Adding dampers to the level where the story displacements are greatest results in the largest percent decrease in deflection. A plot of the story displacement for the frame without dampers for the first ground motion is shown in Figure 55b.

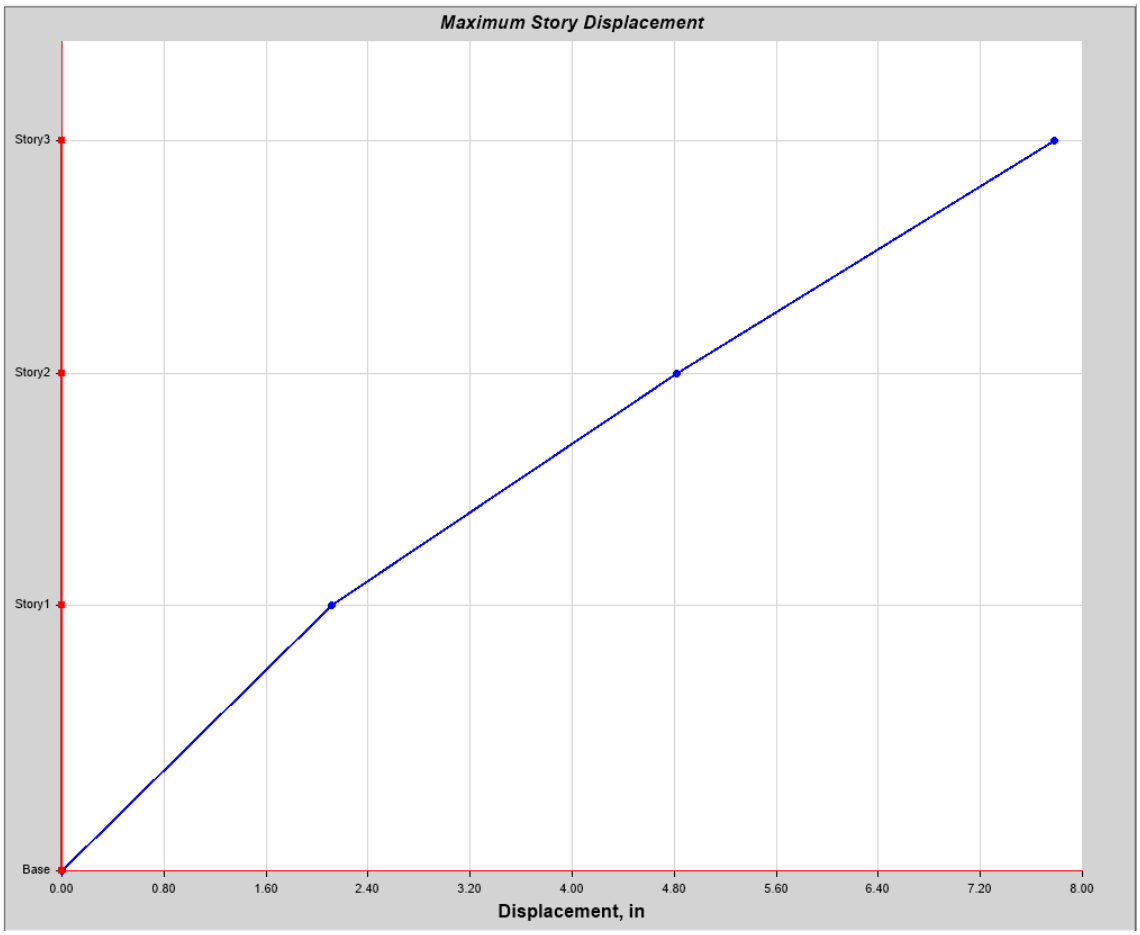

Figure 55b: Story Displacement for Frame without Dampers - GM1

The story displacement plot above shows that the slope is the flattest between the second and third levels, which means the horizontal increase in deflection is the greatest between those 2 levels.

4.4.2 Damper Orientation

Based on the results from looking at the damper configurations, a select number of configurations will now be analyzed to see if the specific orientation of the dampers within the configuration effect the results. The configurations that will be used are: the configuration with dampers in all 3 bays of the top level (C28), the configuration with dampers in all the bays of the middle column of bays (C32), the configuration with dampers in the 4 upper left bays (C34), and the configuration with dampers in all the bays in the top 2 levels (C38). For each configuration, the orientation of the dampers will be changed so that they connect end to end, providing a more direct path for the force through the dampers, that avoids the structural system. Figures 58 through 61 show elevations of the configurations with the new orientations and Figures 62 through 65 show results of the percent change in displacement for both the original and new orientation for all 7 ground motions.

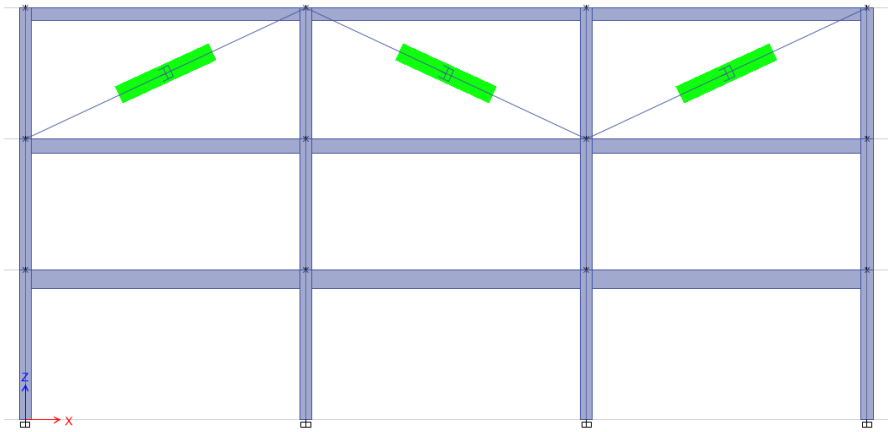

Figure 58: Damper Configuration C28 With New Orientation

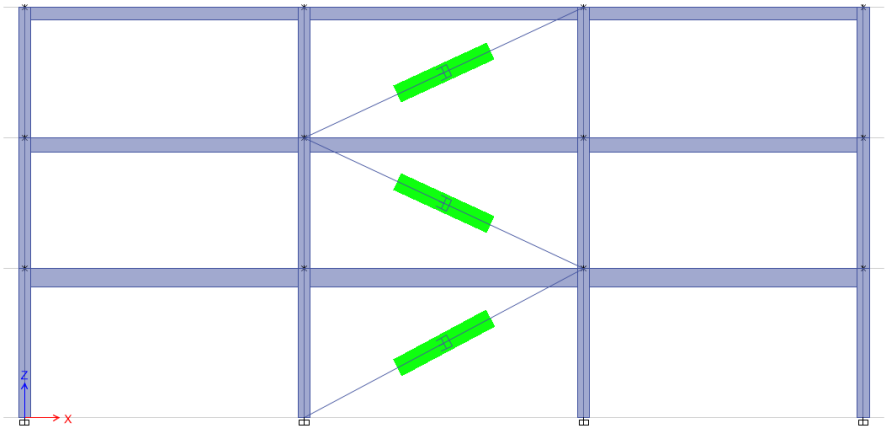

Figure 59: Damper Configuration C32 With New Orientation

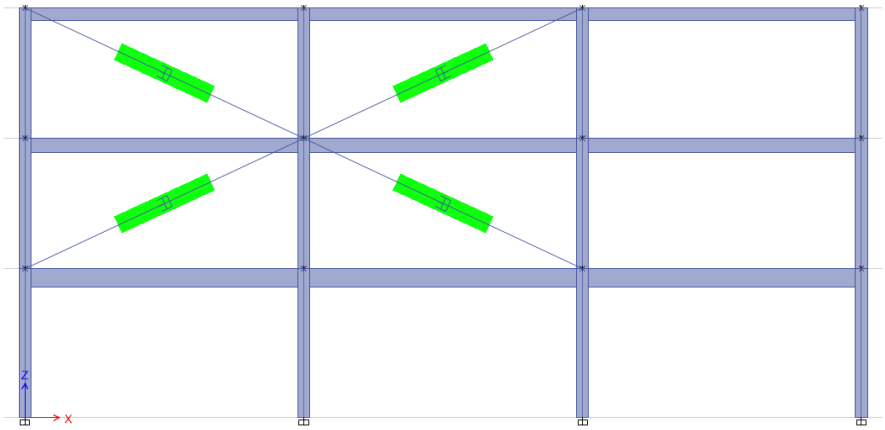

Figure 60: Damper Configuration C34 With New Orientation

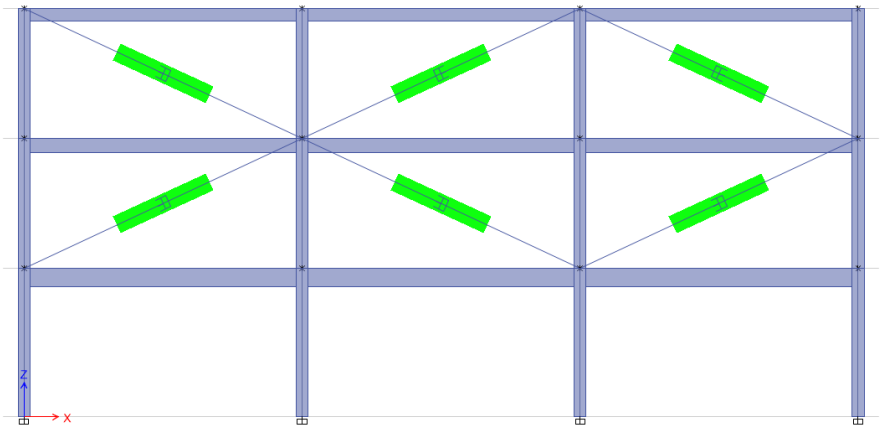

Figure 61: Damper Configuration C38 With New Orientation

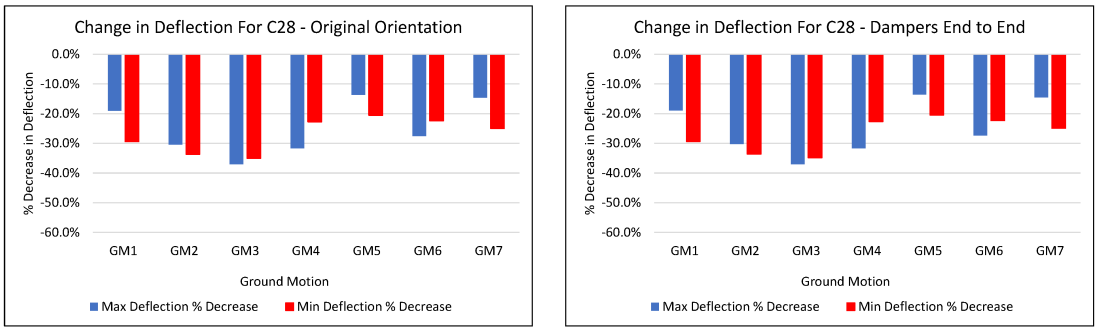

Figure 62: Comparison of Results for Configuration C28 With Original and New Orientation

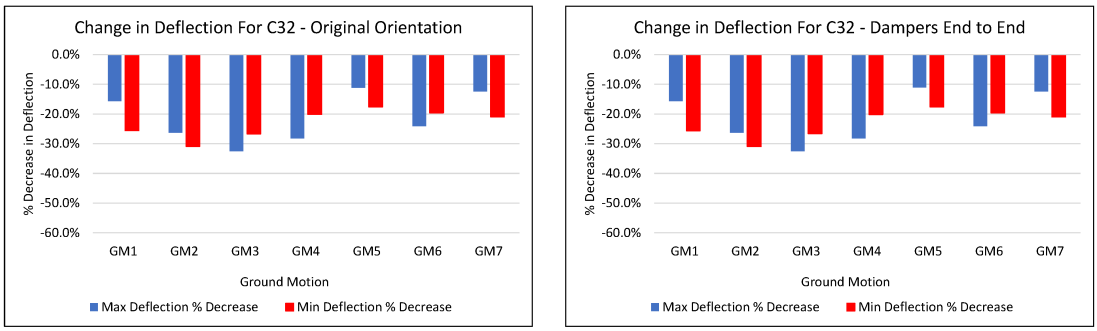

Figure 63: Comparison of Results for Configuration C32 With Original and New Orientation

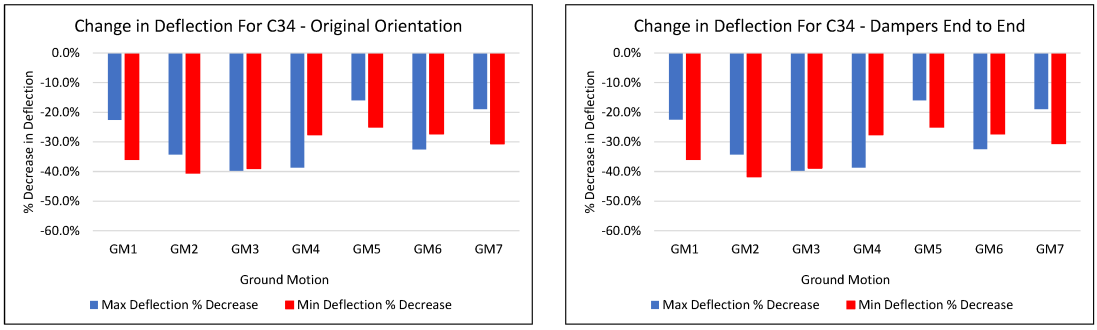

Figure 64: Comparison of Results for Configuration C34 With Original and New Orientation

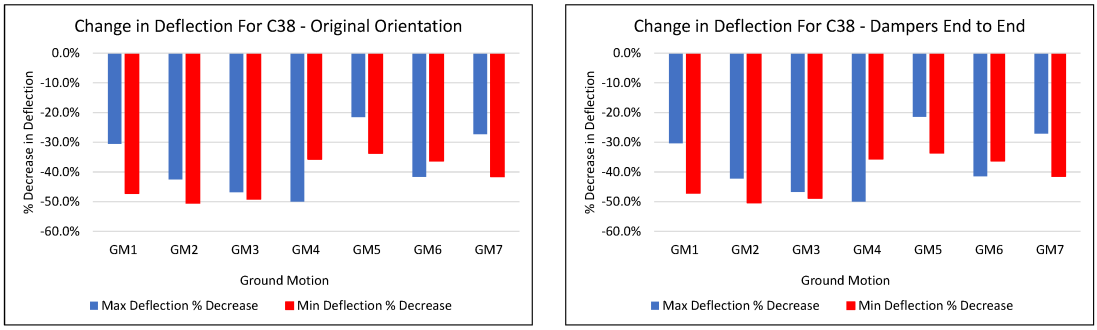

Figure 65: Comparison of Results for Configuration C38 With Original and New Orientation

The Figures above show that for each of the configurations, changing the orientation of the dampers had very little if any impact on the percent decrease in deflection. Moving forward the original orientations will continue to be used for further analysis. Data for Figures 62 through 65 is shown in Appendix A Tables 18 through 25.

4.5 Damper Properties

As discussed previously, the amount of force that a damper can resist is based on the velocity, the damping coefficient C, and the damping exponent, α. In order to determine how the damping coefficient and damping exponent affect performance, both values will be varied to see how the results change. The original value that was used for the coefficient was 2, so for this analysis the value will be both doubled to 4 and cut in half to 1. For all 3 coefficient values, the α value will be varied while C is kept constant. α will be changed from 1 to .75, .5, .2 and .1. Values of α that are less than 1 represent a nonlinear relationship between the force in the damper and the velocity. Two configurations will be used for this analysis. The first is the configuration with dampers in all 3 bays of the top level (C28), and the second is the configuration with dampers in all the bays of the middle column (C32). The results from this analysis are shown in Figures 66 through 71 below, and the data is shown in Appendix A Tables 26 through 31, respectively.

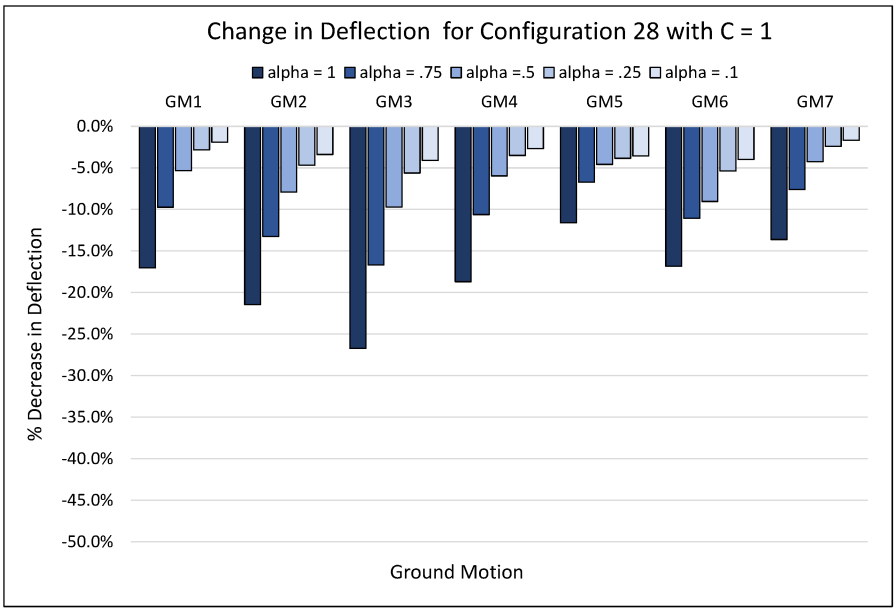

Figure 66: % Decrease in Deflection for Damper Configuration 28 with $C = 1$

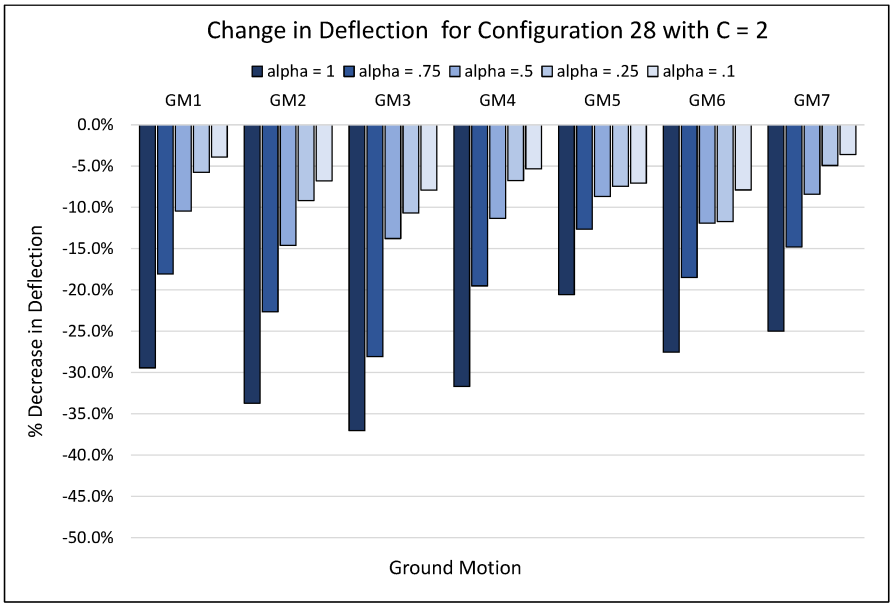

Figure 67: % Decrease in Deflection for Damper Configuration 28 with $C = 2$

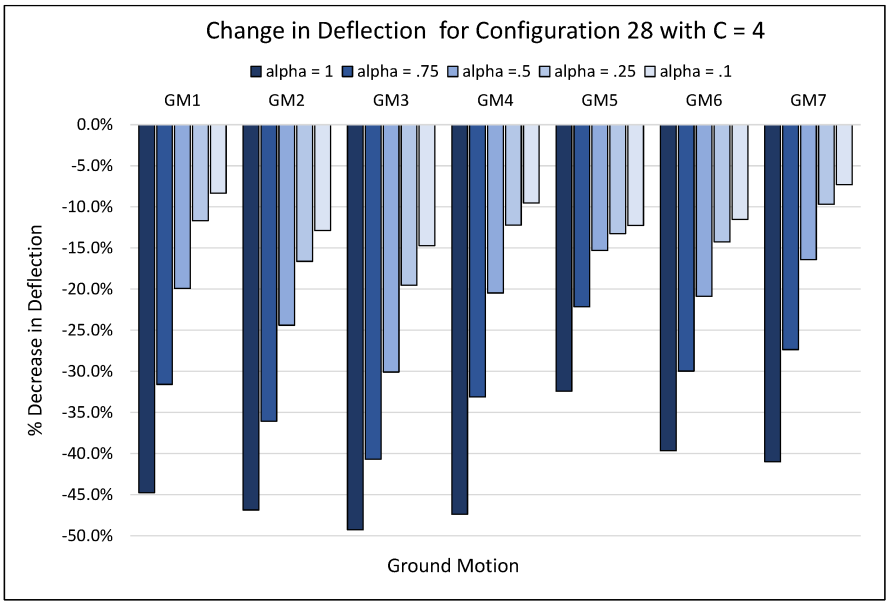

Figure 68: % Decrease in Deflection for Damper Configuration 28 with $C = 4$

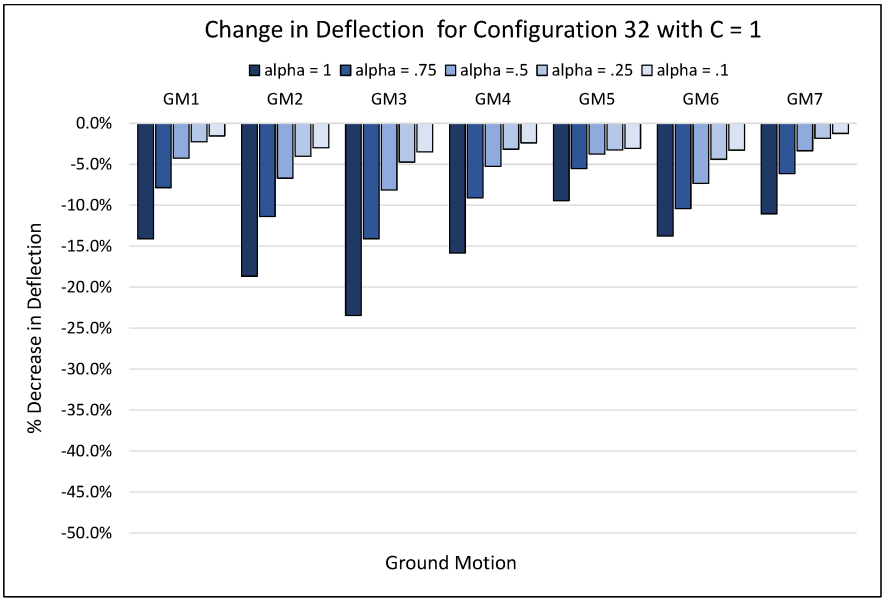

Figure 69: % Decrease in Deflection for Damper Configuration 32 with $C = 1$

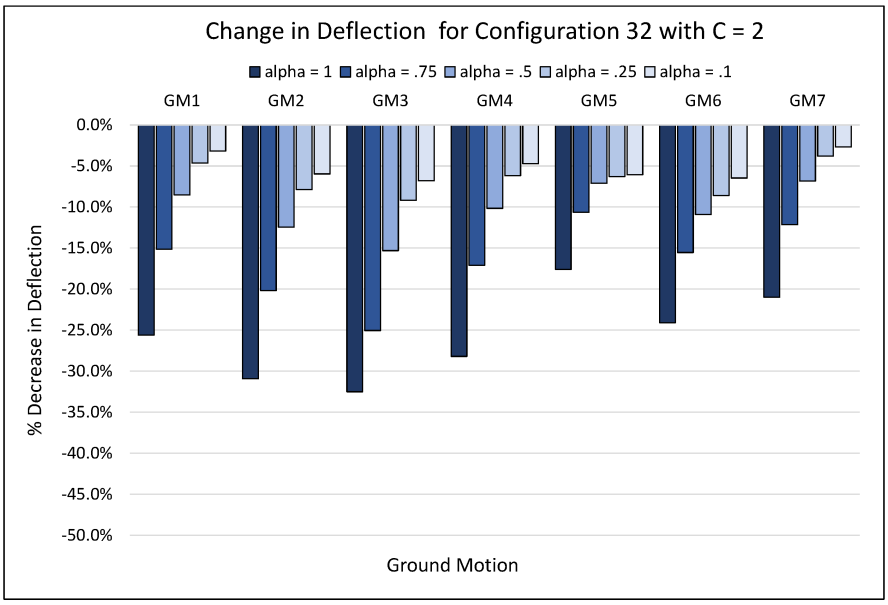

Figure 70: % Decrease in Deflection for Damper Configuration 32 with $C = 2$

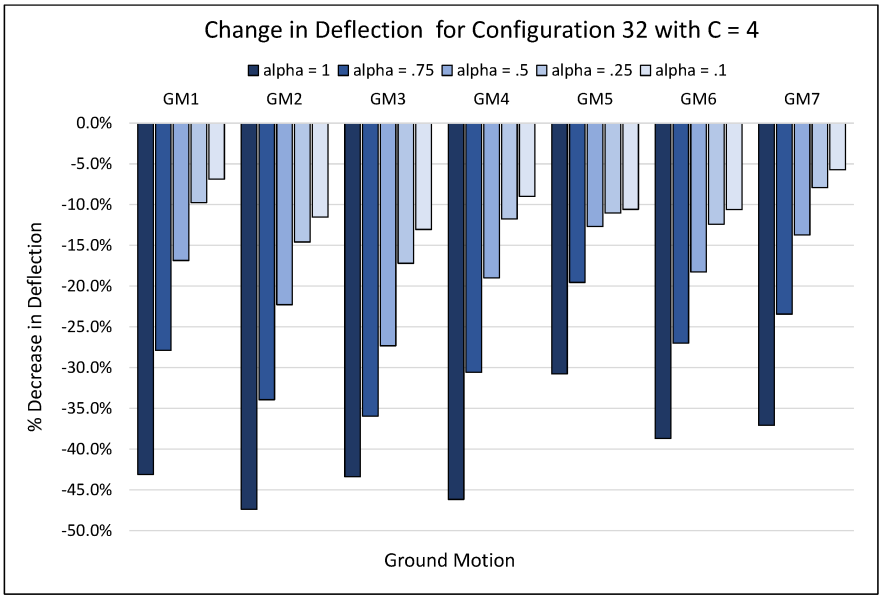

Figure 71: % Decrease in Deflection for Damper Configuration 32 with $C = 4$

In the figures above, it can be seen that as the coefficient increases, the percent decrease in deflection also increases. This is consistent between the two configurations tested and for all seven ground motions. Figure 72 through Figure 75 below provide a visual for how much the percent decrease in deflection increases when the C value changes. The previous figures also show that as the alpha value decreases, the percent decrease in deflection decreases. It is also interesting to note that as alpha decreases, the gap between the percent decrease in deflection for ground motion 5 and the other ground motions gets smaller. This is likely do to the fact that ground motion 5, is a near fault earthquake, which it can be identified as by looking at the pulse on the velocity graph of the ground motion in Figure 30b. Dampers that experience near fault ground motions typically perform better with a smaller alpha value since the damper does not have as much time to dissipate energy, and in order to provide good performance, a damper needs to cycle back and forth. Data for Figures 72 through 75 is shown in Appendix A Tables 32 through 35, respectively.

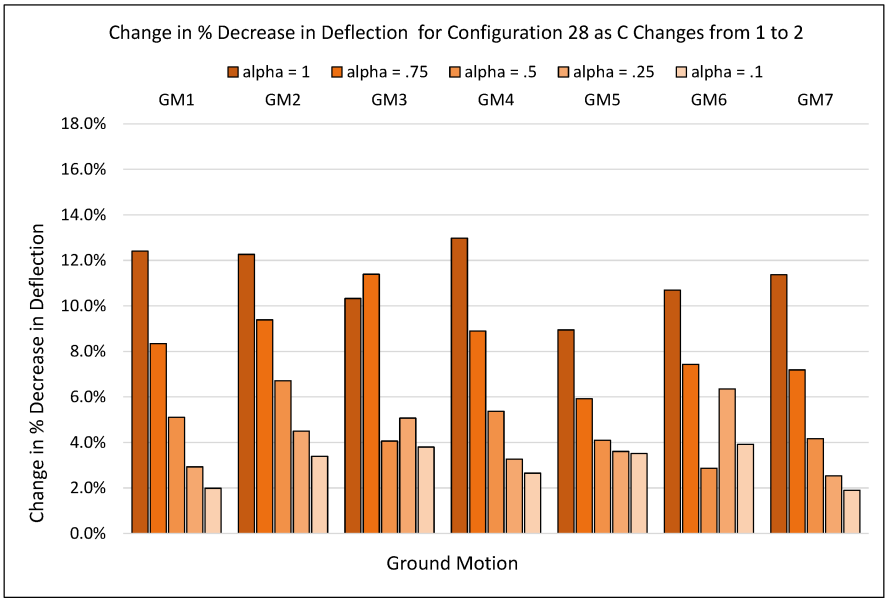

Figure 72: Change in % Decrease in Deflection for Damper Configuration 28 when C goes from 1 to 2

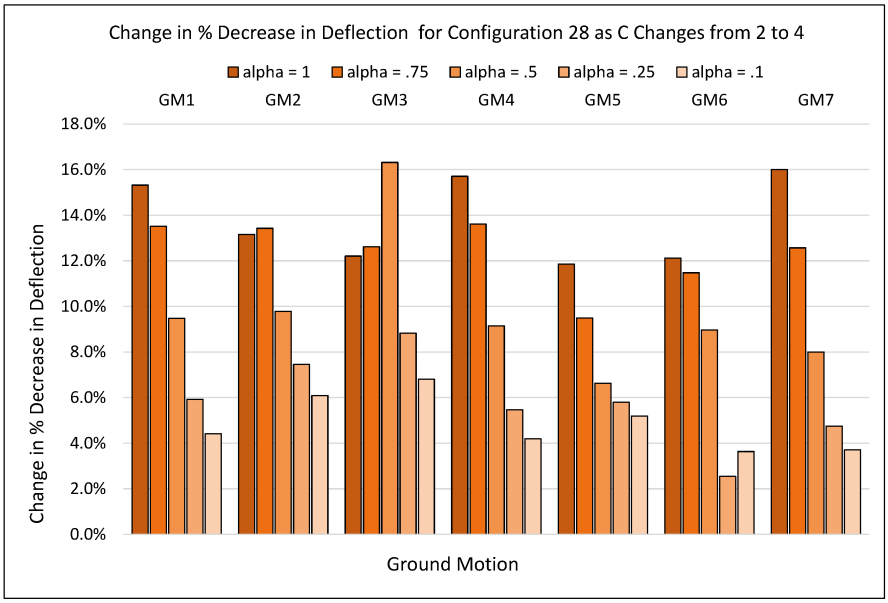

Figure 73: Change in % Decrease in Deflection for Damper Configuration 28 when C goes from 2 to 4

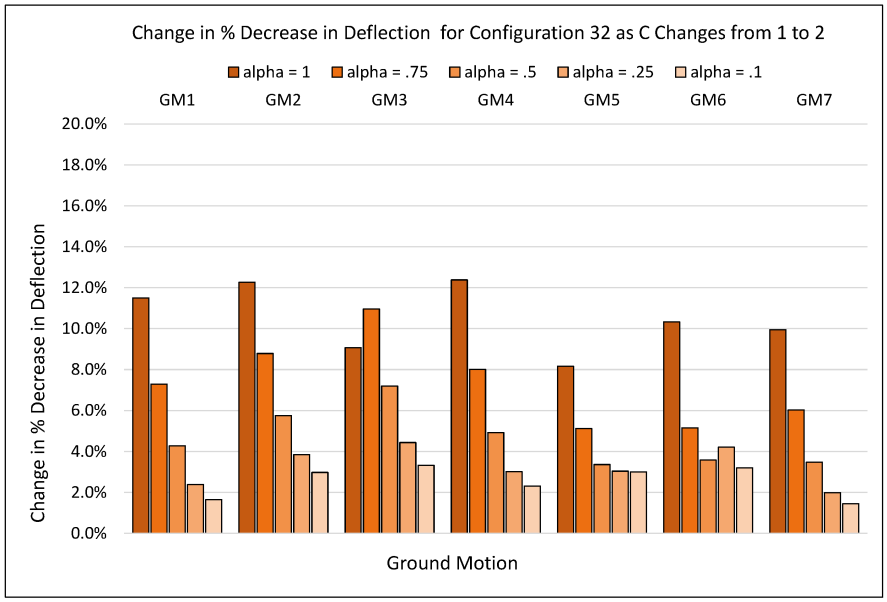

Figure 74: Change in % Decrease in Deflection for Damper Configuration 32 when C goes from 1 to 2

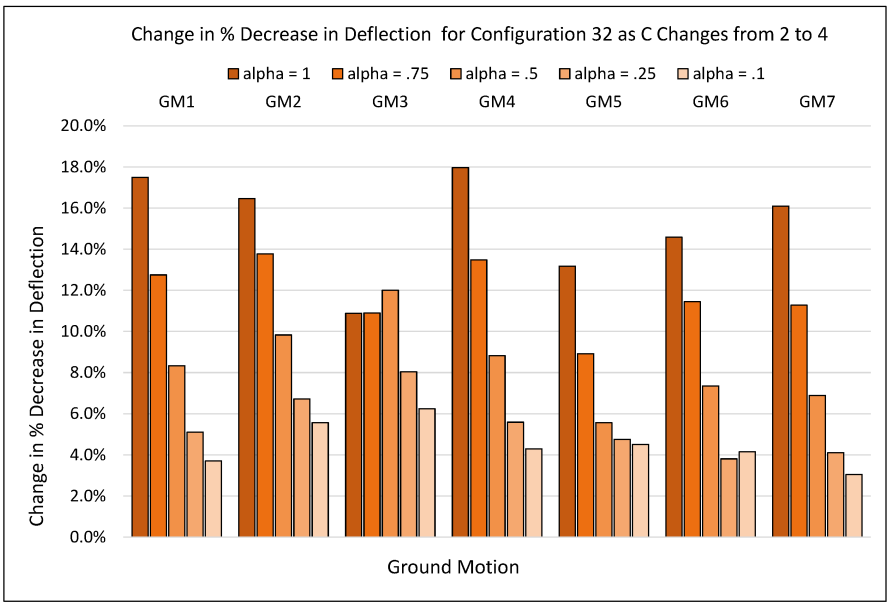

Figure 75: Change in % Decrease in Deflection for Damper Configuration 32 when C goes from 2 to 4

When changing the damper properties, it is important to examine how that affects the hysteretic behavior of the damper. Figure 76 below shows the hysteretic curves for all 5 α values with a constant damping coefficient of 2 for the first ground motion using configuration 28. As α decreases, the hysteretic shape starts to become more uniform, and it turns into more of a vertical oval shape. The very long and straight vertical lines show that as the force in the damper increases or decreases, the deformation stays very constant. This nonlinear relationship also results in the damper being able to resist a significantly smaller amount of force. With an α of 1 the damper experiences a force of around 20 kips but with an α of .1 that decreases down to just under 3 kips. These factors combined cause the area under the hysteretic curve to be smaller with a smaller α value and therefore there is less energy dissipated by the damper. This means the structural members will have to dissipate more of the energy through yielding of the members. Since overall an alpha value of 1 provided the best results, that value will be used for further analysis.

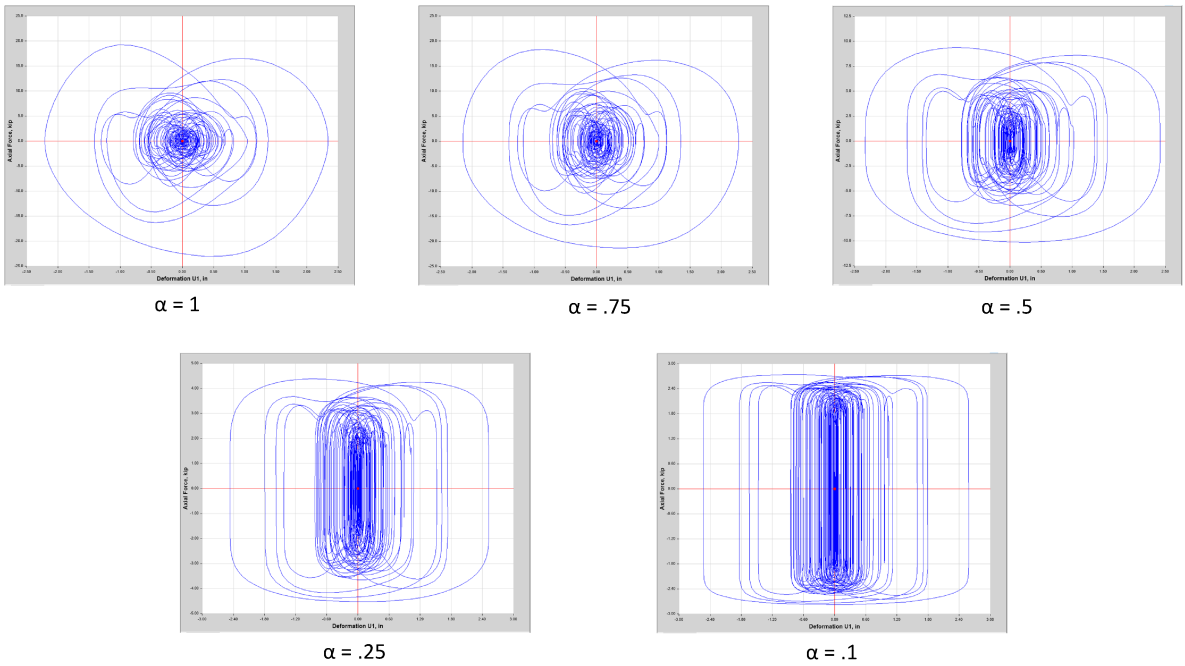

Figure 76: Hysteretic Curves for varying α values with $C = 2$

4.6 Nonlinear Frame with Hinges

In order to determine how the frame will perform when it is allowed to go beyond yield when subjected to the various ground motions, hinges are added to the model at all the beam ends, and at the bases of the columns at the ground. The two damper configurations that will be analyzed with hinges are the configuration with dampers in all bays of the third level (C28) and the configuration with dampers in all bays in the middle column (C32). The plastic rotation angles used as input for the hinge properties in Etabs are found using a python script that is shown in Appendix B. The values are calculated according to Table 9-7.1 in ASCE 41. The Figures 77 through 81 show the input properties for the hinges. There are separate hinge properties for each beam, and for the interior and exterior columns. All of the hinge properties are deformation controlled so the failure will be ductile.

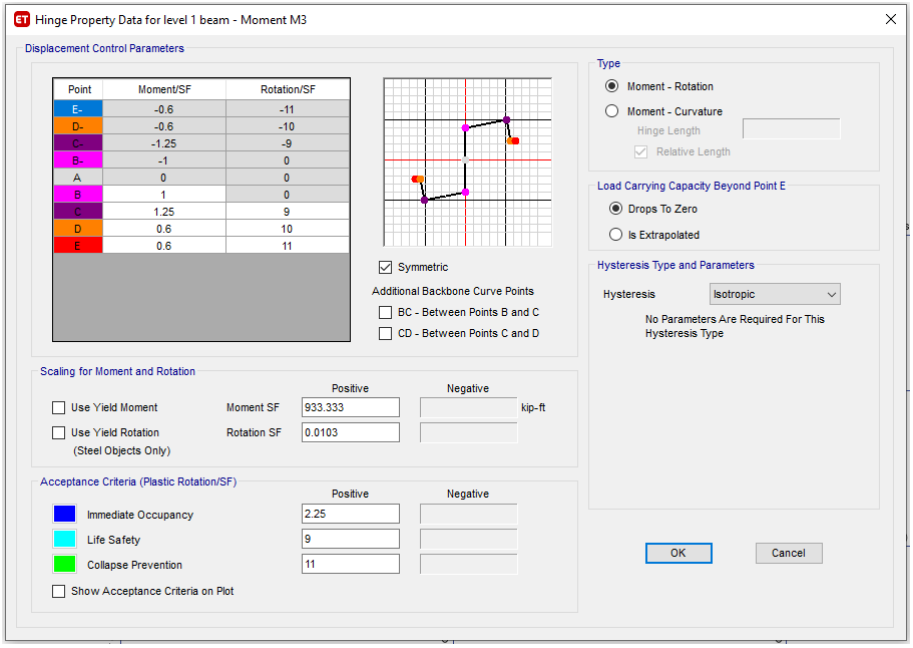

Figure 77: Etabs Input for Level 1 Beam Hinge Property

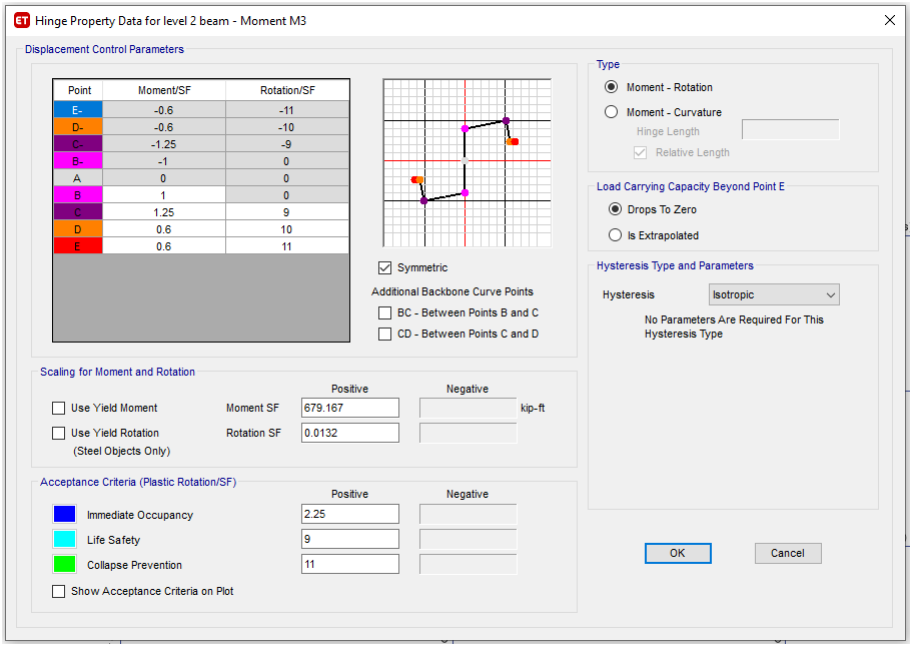

Figure 78: Etabs Input for Level 2 Beam Hinge Property

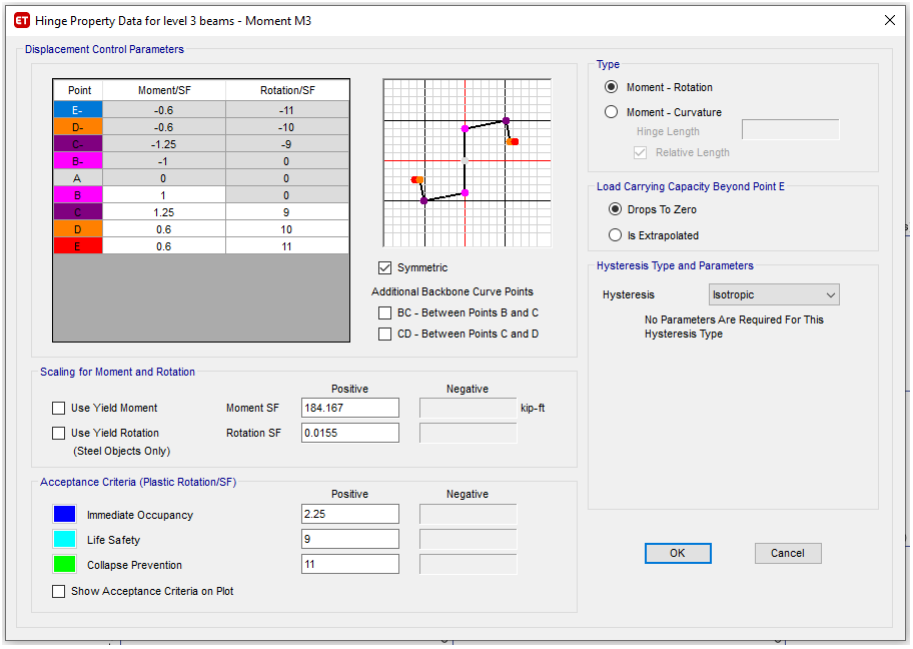

Figure 79: Etabs Input for Level 3 Beam Hinge Property

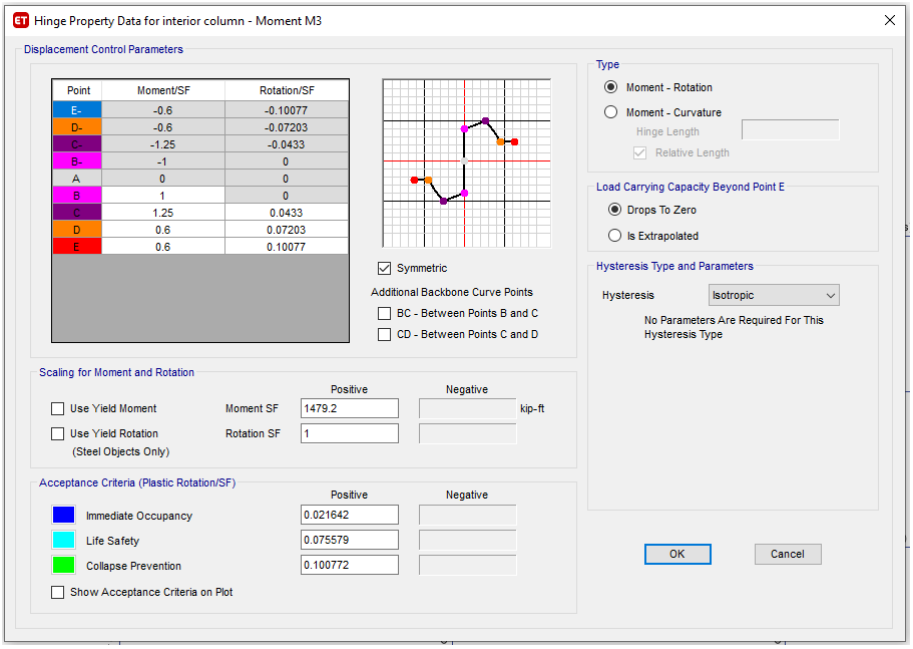

Figure 80: Etabs Input for Interior Column Hinge Property

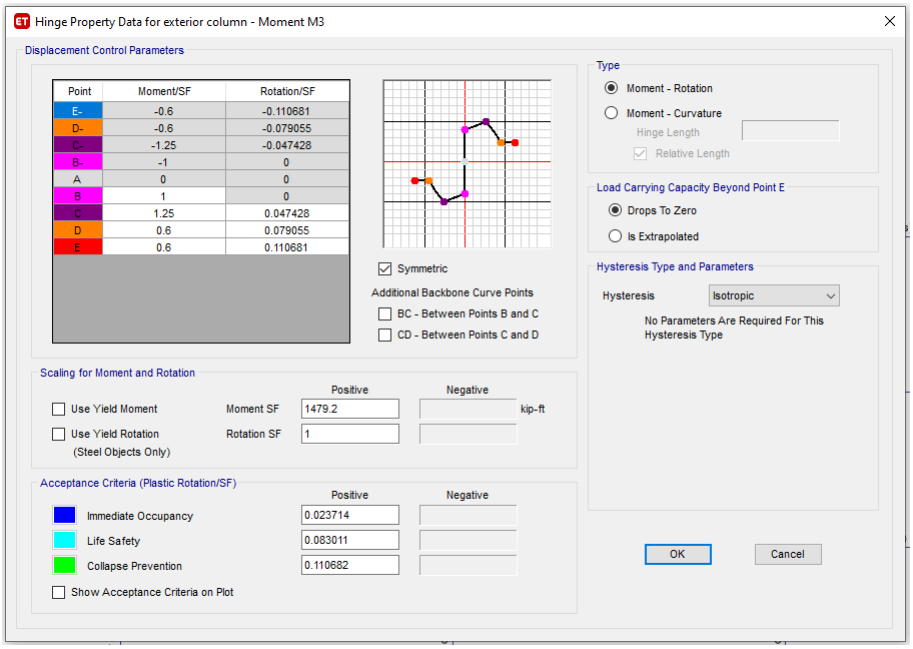

Figure 81: Etabs Input for Exterior Column Hinge Property

The hinges are added to the members at the centroids of the plastic hinges. Table 6 below shows the relative distances of the hinges that are input into Etabs. In addition to adding hinges, rigid end offsets are also added to the model to make the model more realistic. The hinge locations were found by combining half the length of the beam depth and half the length of the column depth at a specific location and dividing by the beam length to get the relative distance along the beam where the hinge is located. The hinge on the other side is in a mirrored position.

Hinge Name	**Hinge Location**
Level 1 Beam Hinge	$.005L$ and $.945L$
Level 2 Beam Hinge	$.047L$ and $.953L$
Level 3 Beam Hinge	$.044L$ and $.966L$
Column Hinge	$.040L$

Table 6: Hinge Locations in Etabs

When the frame is initially analyzed with hinges for all 7 ground motions, the acceleration is not large enough to cause the frame members to go beyond yield. In order to force the frame to yield, the inherent damping value is changed from 5% to 2% and the accelerations for each ground motion are scaled up by 1.5. To allow for an accurate comparison, the 1.5 scale factor and 2% damping are also changed for the models without hinges, and rigid end offsets are added in those models as well. Figures 82 through 84 below show comparisons of deflection for the frame with and without hinges for the same 2 configurations that were previously analyzed, 28 and 32 and for the frame with hinges and no dampers. The data for Figures 82 through 84 can be found in Appendix A Tables 38 through 40, respectively.

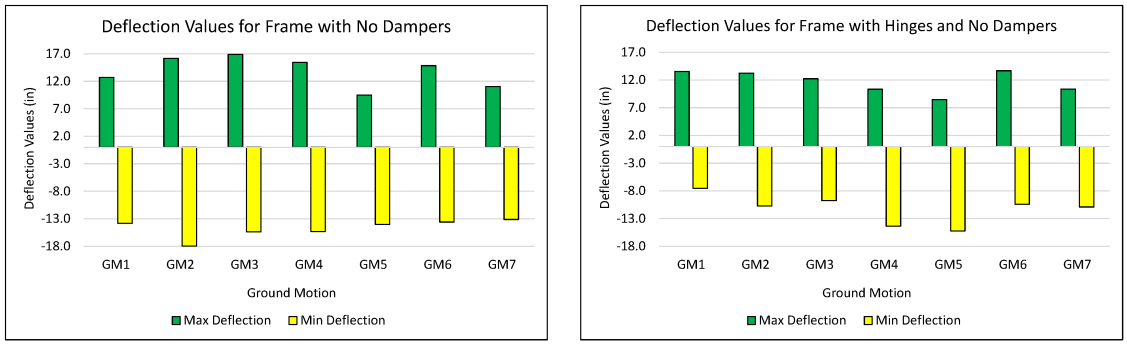

Figure 82: Displacement for the Frame With No Dampers - With and Without Hinges

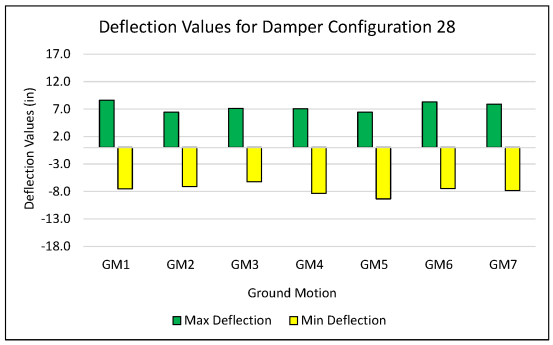

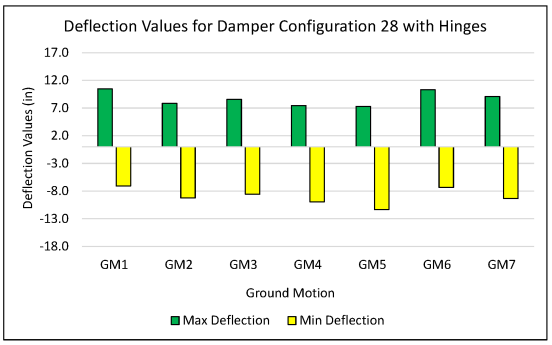

Figure 83: Displacement for Damper Configuration 28 - With and Without Hinges

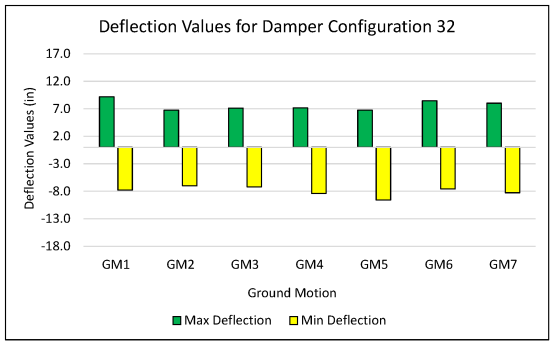

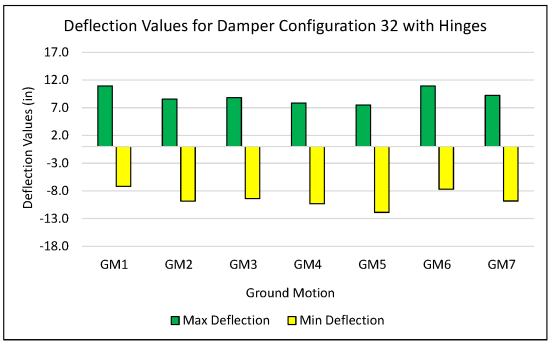

Figure 84: Displacement for Damper Configuration 32 - With and Without Hinges

The graphs above show that when hinges are added to the frame, the displacements at the roof can increase or decrease, depending on the ground motion. When looking at the deflections for the frames with hinges and dampers, some of the deflections are larger than the frame without hinges, but they are still less than the deflection for the frame with hinges and without dampers. This shows that even when the members can yield, the dampers still help to decrease the amount of permanent deflection in the members by dissipating energy. If the right dampers are selected that have appropriate properties for the specific situation, it is possible that they could even entirely eliminate the need for the members to yield. Figures 85 and 86 below show the % decrease in deflection for the two damper configurations, with and without hinges, compared to frames that do not have dampers. The graphs that show the change for frames without hinges have % decreases based on a frame without hinges. The graphs that show the change for frames with hinges have % decreases based on a frame with hinges. The data for Figures 85 and 86 can be found in Appendix A Tables 36 and 37.

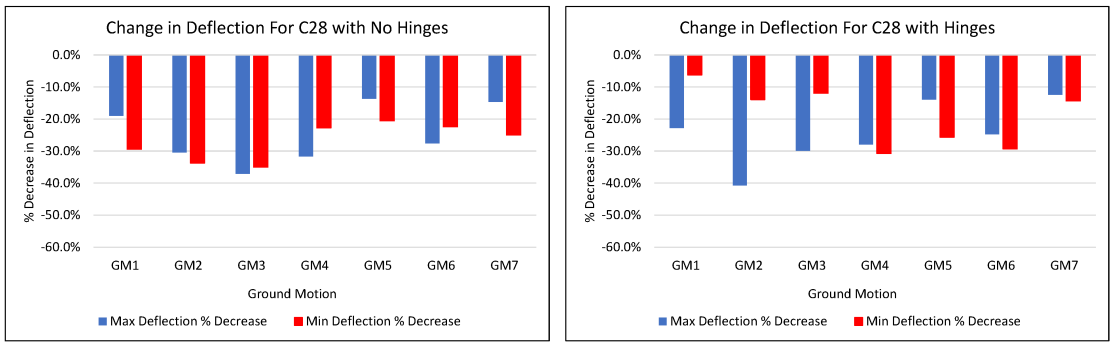

Figure 85: % Decrease in Displacement for Damper Configuration 28 - With and Without Hinges

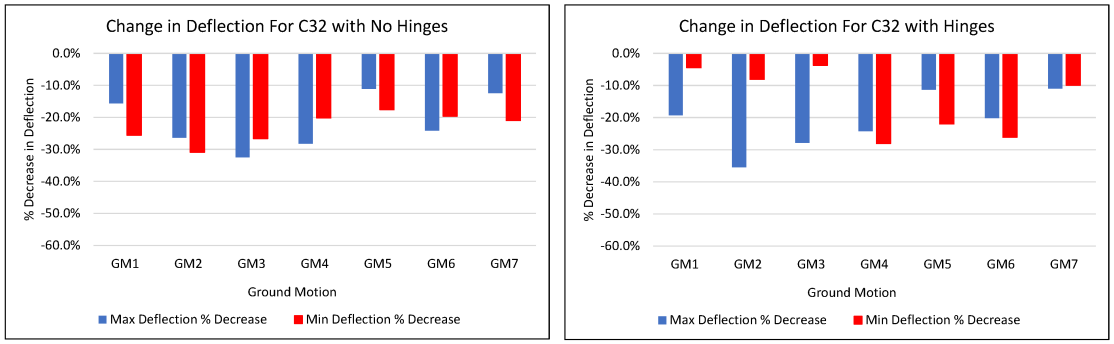

Figure 86: % Decrease in Displacement for Damper Configuration 32 - With and Without Hinges

The graphs showing percent decrease in deflection show that when hinges are added, the variability due to the different ground motions has more of an impact which is a more accurate reflection of reality. There is a larger range in % decrease in deflection, but overall, the performance for each ground motion is much better compared to the frame without dampers. The increased variability means that an in depth look into the specific ground motions for a location would be necessary when deciding the specific dampers to use to get the desired performance.

The 2 configurations were also analyzed with varying coefficient values. As was done previously, values of 1, 2, and 4 were used. The results from this analysis are shown in Figures 87 and 88, and the data can be found in Appendix A Tables 41 and 42, respectively.

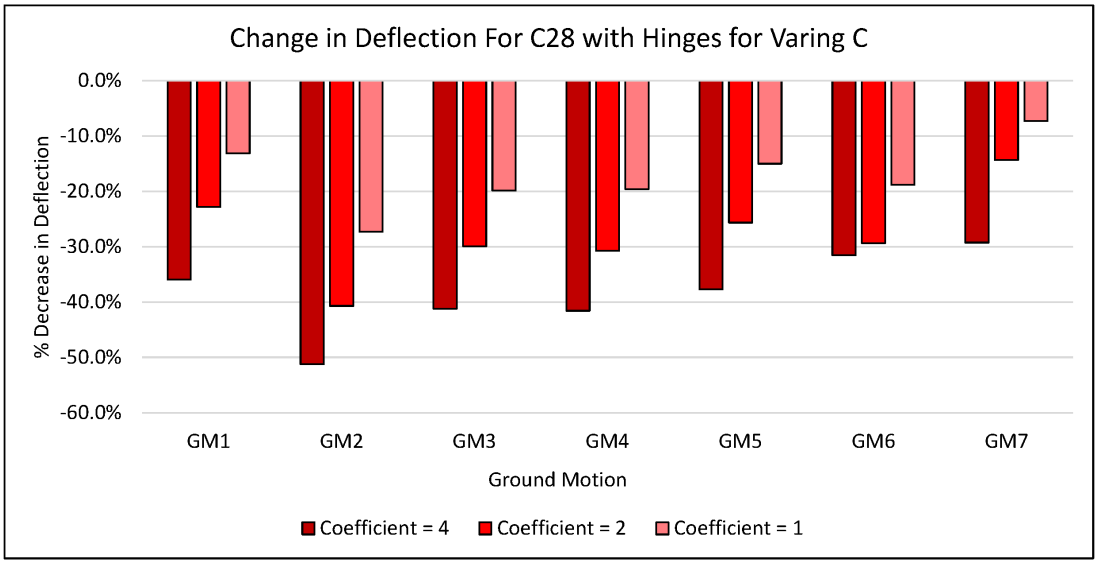

Figure 87: % Decrease in Displacement for Damper Configuration 28 - varying C Values

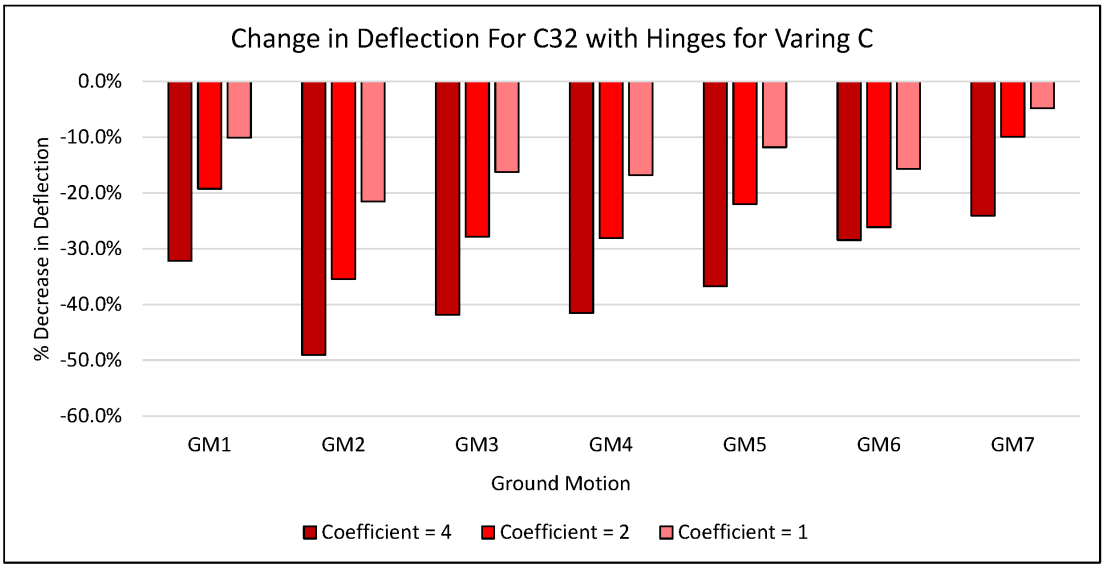

Figure 88: % Decrease in Displacement for Damper Configuration 32 - varying C Values

As C increases, the % decrease in deflection consistently increases, as it did for the frames without hinges. Between the 2 configurations, the increases between the C values are very similar, showing that the specific configuration does not have a significant impact on the effects of changing the value of the coefficient. Overall, the frame performed the best for each C value when experiencing ground motion 2, and the frame performed the worst for each C value when experiencing ground motion 7.

To get a better idea of how the addition of hinges affects the performance, it is necessary to look at the hinge response curves. To provide a consistent comparison, the response curves that are shown in Figures 89 through 91 are all from the left side of the left most beam on the second level. Figure 89 shows the response for the frame without any dampers, Figure 90 shows the response for configuration 28 for ground motions 2 and 7, and Figure 91 shows the response for configuration 32 for ground motions 2 and 7. Both damper configurations were from models that had a damping coefficient of 4.

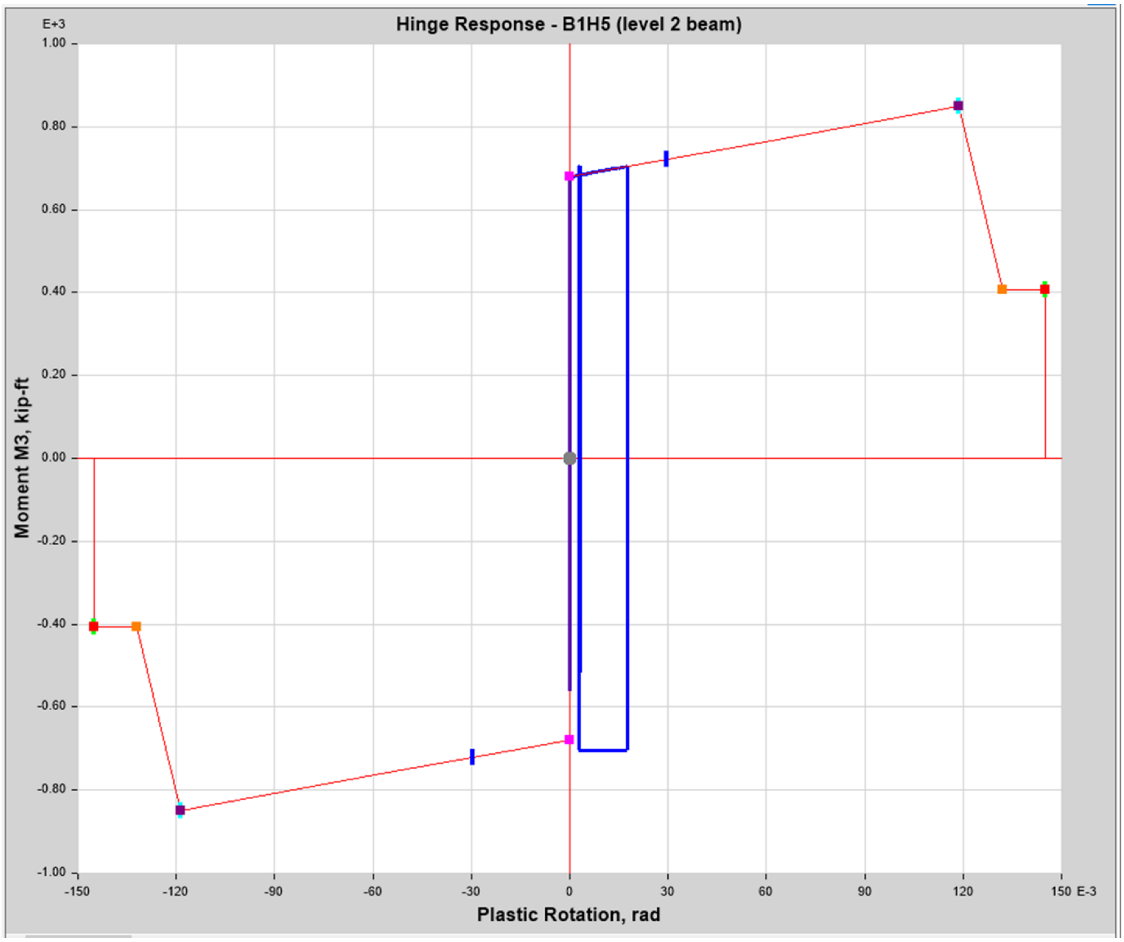

Figure 89: Hinge Response Curve for Frame Without Dampers

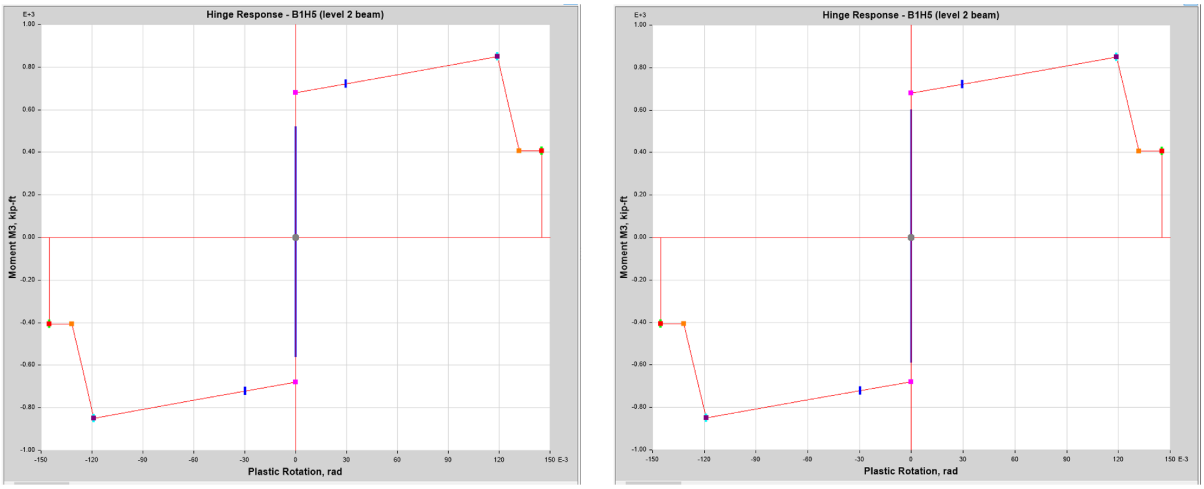

Figure 90: Hinge Response Curves for Frame With Configuration 28 for Ground Motions 2 and 7

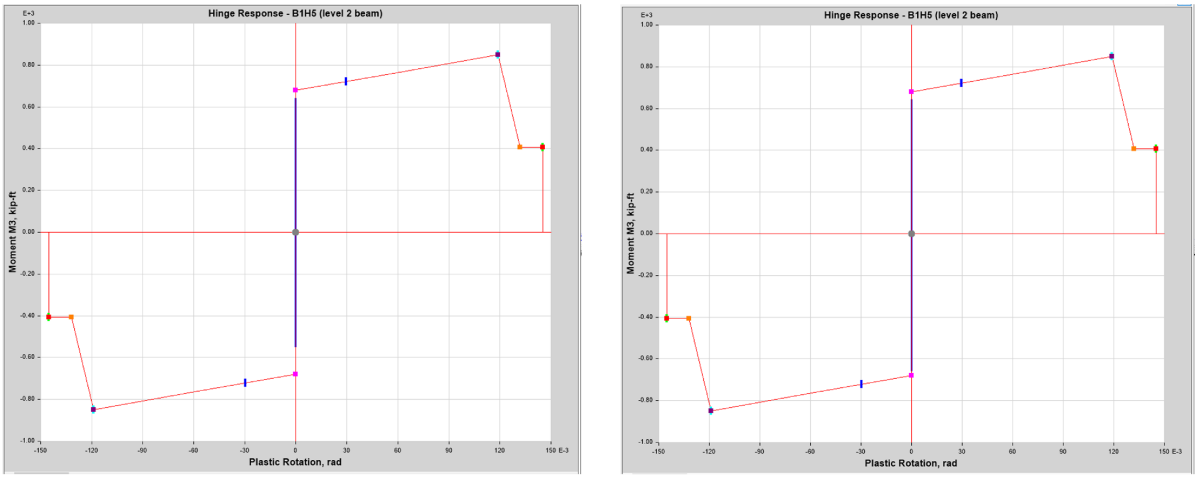

Figure 91: Hinge Response Curves for Frame With Configuration 32 for Ground Motions 2 and 7

The hinge response without any dampers shows that the frame goes beyond the yield point. For both damper configurations 28 and 32, the dampers cause the rotations in the hinges to decrease significantly to the point that the hinges no longer yield. This shows that even when the members are allowed to go inelastic, having dampers prevents that from happening. The difference in performance between the 2 ground motions is relatively insignificant but with ground motions with higher accelerations the improved performance could be even more substantial.

5. RESULTS

5.1 Demand Values

In order to determine how effective the implementation of the dampers are, it is important to look at the impact on the members of the structural frame. The addition of dampers changes the demand that members experience, and if it ends up increasing the demand significantly, this could counteract any benefits provided for the members. For the same 2 ground motions and configurations examined for hinge properties, the axial, shear and moment demands from the Etabs models are shown in Figures 92 through 100. The max demand values for the moments on the members are the most important since the beams are most likely to fail in flexure. Due to this fact, comparisons will be made just for the moment demands. The demands from the frames with dampers will be compared to the demands from the frames without dampers. The % changes in moment demand for the different members are shown in Figure 101 and Figure 102. For all the following figures showing axial, shear and moment diagrams, the title below the diagram indicates which ground motion was used for that model and whether or not the model had hinges. The data for Figures 101 and 102 can be found in Appendix A Tables 43 and 44.

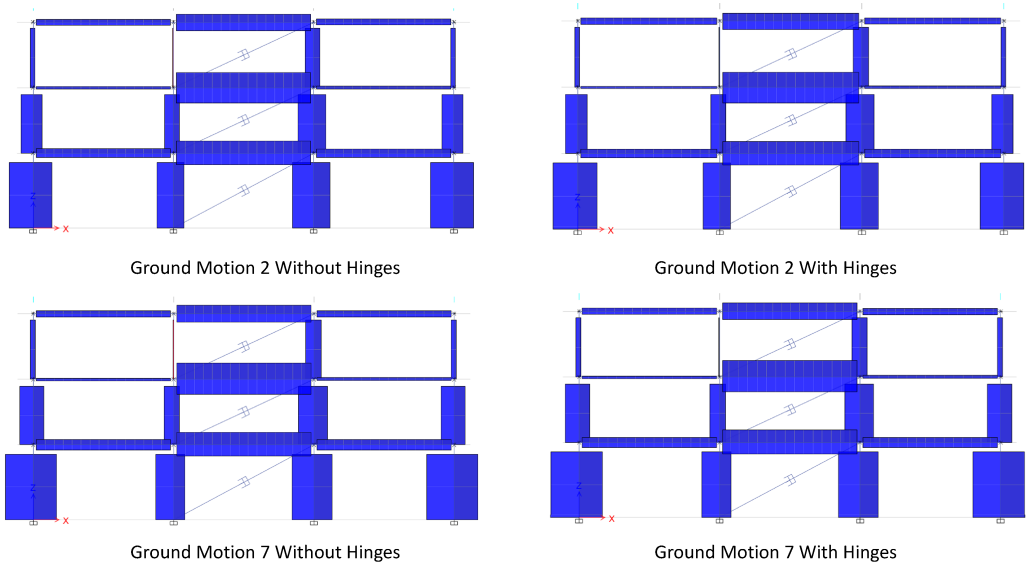

Figure 92: Axial Force Diagrams for Configuration 28

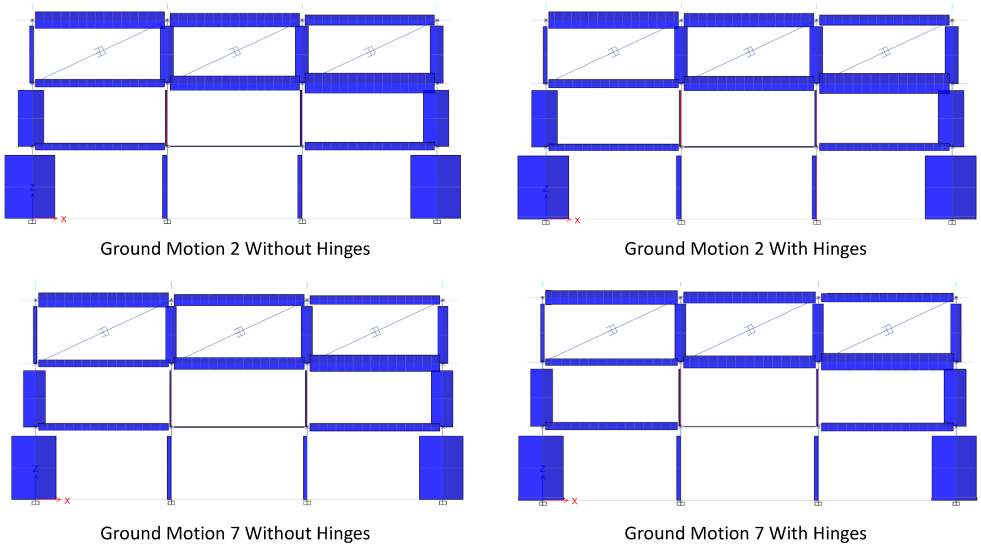

Figure 93: Axial Force Diagrams for Configuration 32

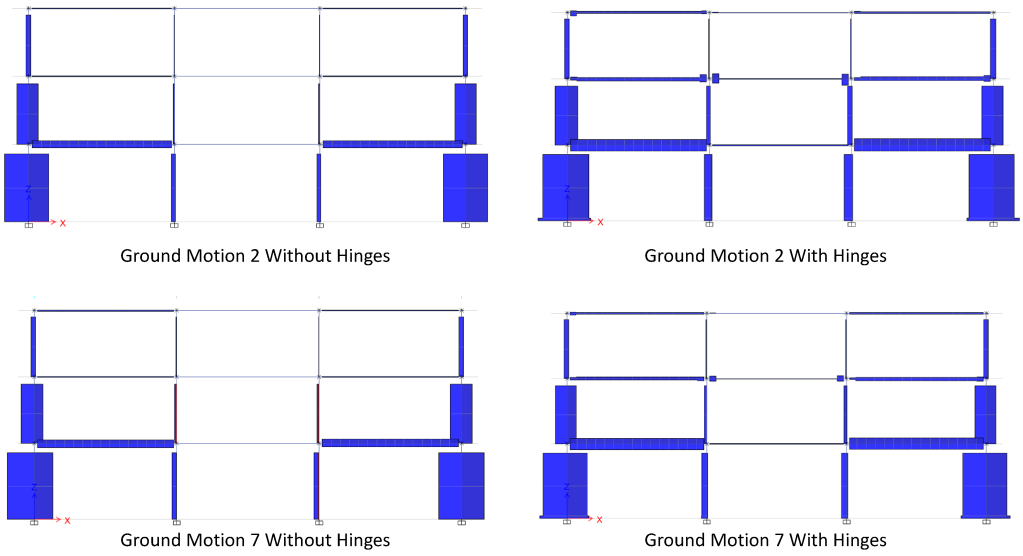

Figure 94: Axial Force Diagrams for Frame with No Dampers

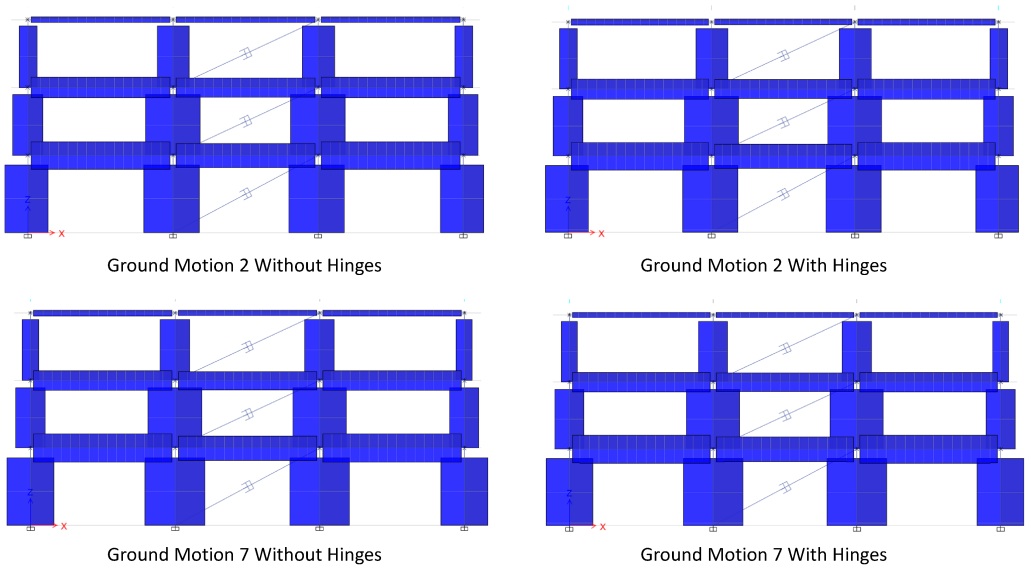

Figure 95: Shear Force Diagrams for Configuration 28

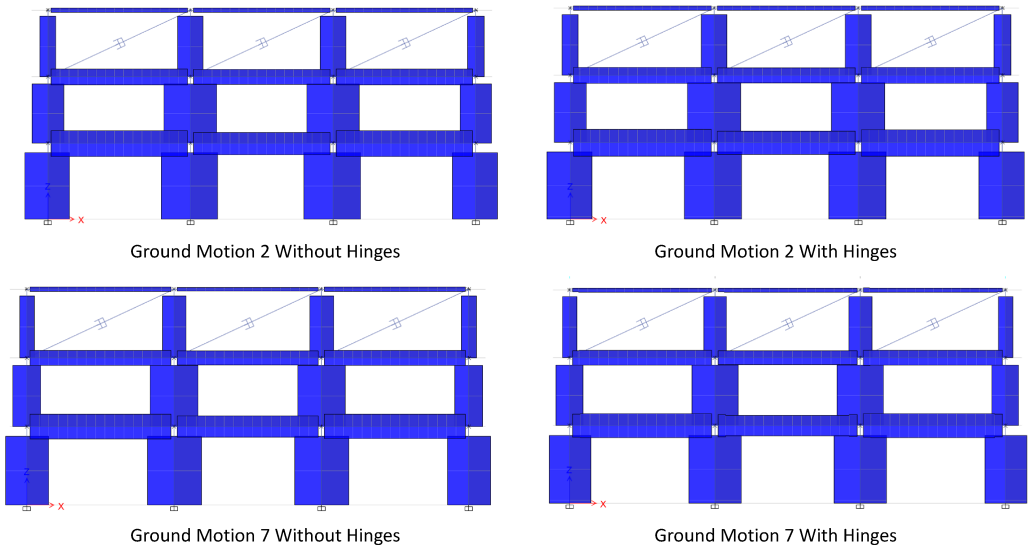

Figure 96: Shear Force Diagrams for Configuration 32

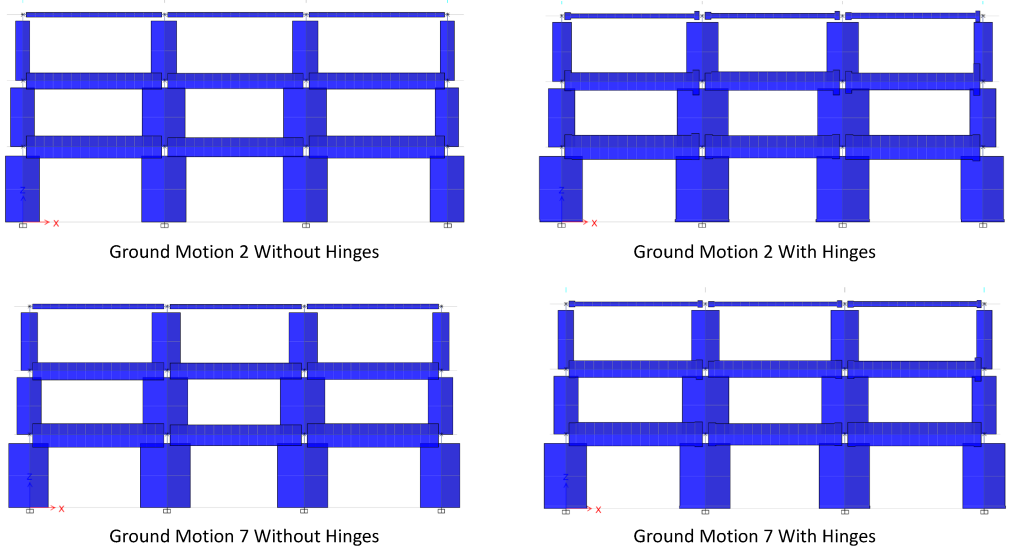

Figure 97: Shear Force Diagrams for Frame with No Dampers

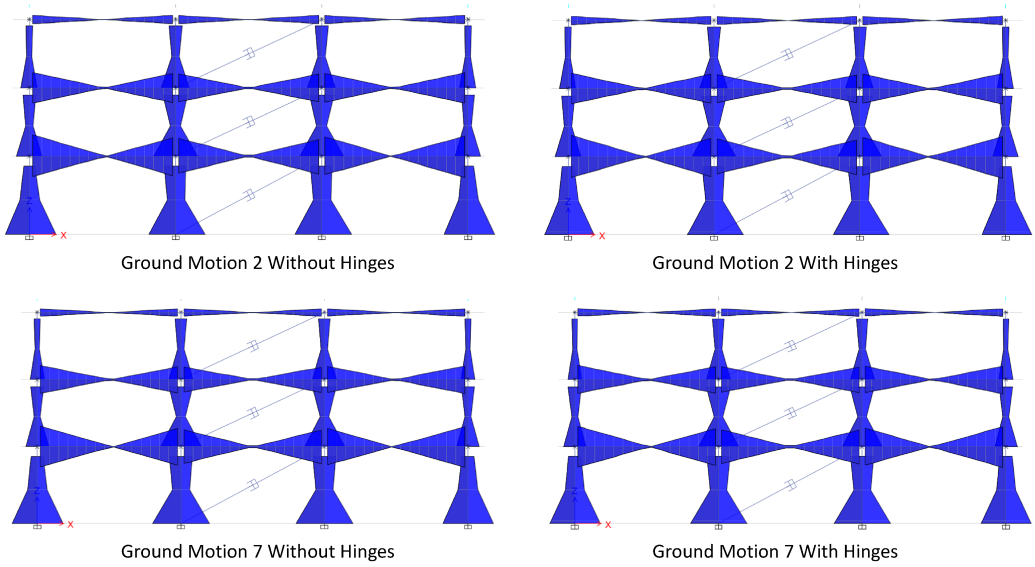

Figure 98: Moment Diagrams for Configuration 28

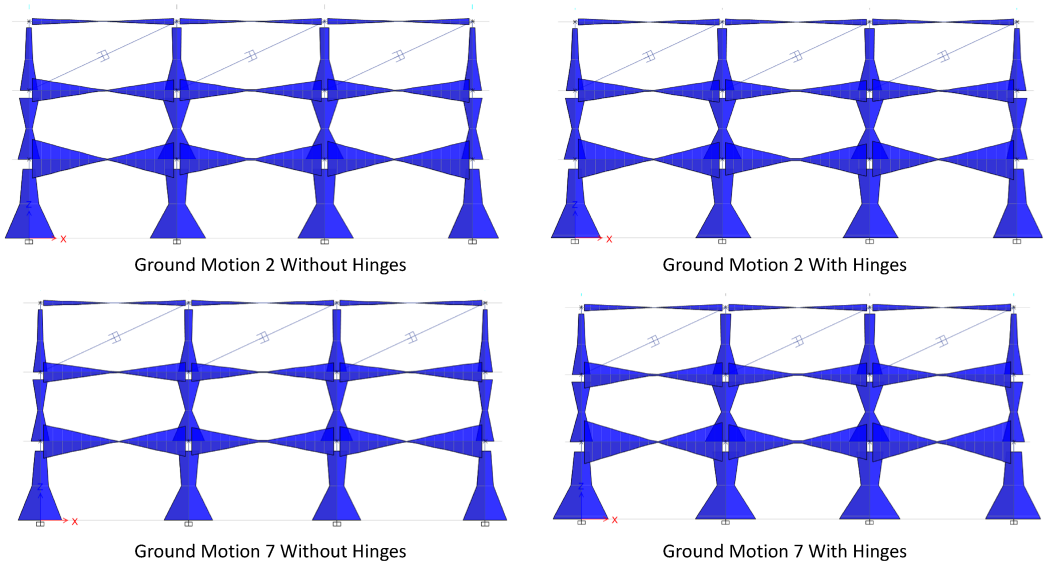

Figure 99: Moment Diagrams for Configuration 32

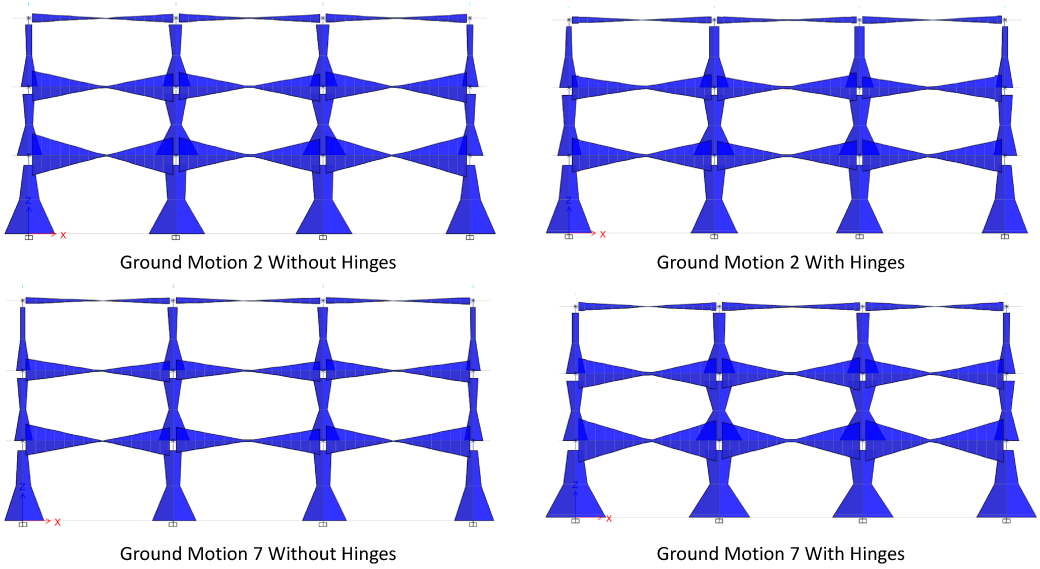

Figure 100: Moment Diagrams for Frame with No Dampers

Table 7 below shows the maximum demand values for the members, for configurations 28 and 32, and ground motions 2 and 7.

Max Moment (k-ft) without Dampers			Max Shear (k) without Dampers			Max Axial Force (k) without Dampers		
	GM2	GM7		GM2	GM7		GM2	GM7
Level 3 Beam	275.35	231.87	Level 3 Beam	38.25	25.52	Level 3 Beam	20.76	10.63
Level 2 Beam	934.31	846.75	Level 2 Beam	112.78	78.19	Level 2 Beam	40.17	19.17
Level 1 Beam	1198.05	1153.23	Level 1 Beam	88.719	80.99	Level 1 Beam	39.99	39.34
Level 1 Column	1612.68	1606.81	Level 1 Column	174.28	167.87	Level 1 Column	186.09	175.83

Max Moment (k-ft) - Configuration 28			Max Shear (k) - Configuration 28			Max Axial Force (k) - Configuration 28		
	GM2	GM7		GM2	GM7		GM2	GM7
Level 3 Beam	161.72	179.62	Level 3 Beam	11.18	13.47	Level 3 Beam	45.92	49.71
Level 2 Beam	618.6	681.88	Level 2 Beam	39.32	47.98	Level 2 Beam	53.83	57.49
Level 1 Beam	1037.82	1076.77	Level 1 Beam	68.87	75.39	Level 1 Beam	20.67	28.69
Level 1 Column	1465.32	1577.62	Level 1 Column	148.91	162.93	Level 1 Column	149.34	160.24

Max Moment (k-ft) - Configuration 32			Max Shear (k) - Configuration 32			Max Axial Force (k) - Configuration 32		
	GM2	GM7		GM2	GM7		GM2	GM7
Level 3 Beam	174.42	197.7	Level 3 Beam	12.05	13.94	Level 3 Beam	43.36	43.68
Level 2 Beam	630.43	735.99	Level 2 Beam	42.48	50.54	Level 2 Beam	79.42	83.64
Level 1 Beam	888.29	1073.44	Level 1 Beam	59.03	71.79	Level 1 Beam	61.52	64.33
Level 1 Column	1211.22	1490.26	Level 1 Column	121.61	150.32	Level 1 Column	124.67	146.64

Table 7: Max Demand Values from Etabs

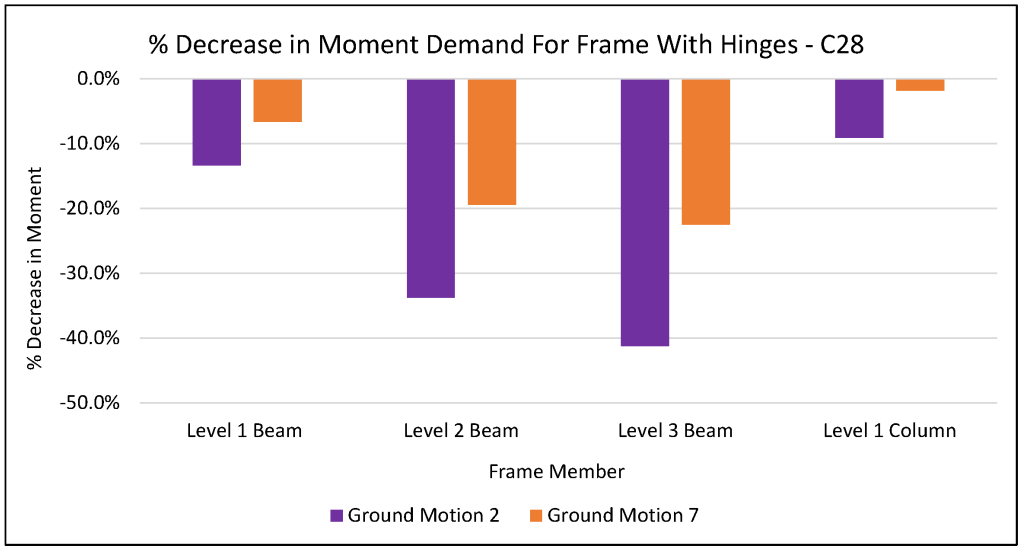

Figure 101: % Change in Moment Demands for Configuration 28

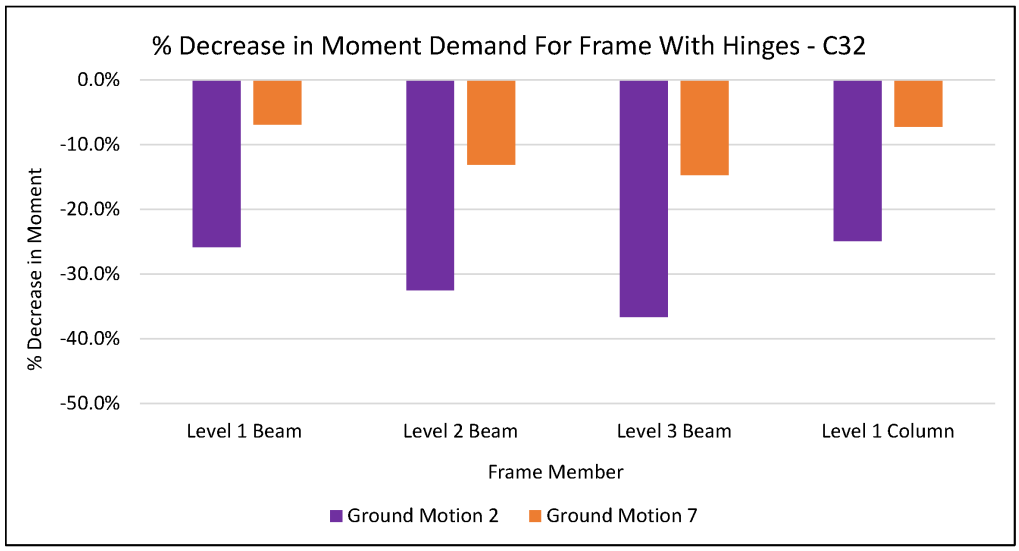

Figure 102: % Change in Moment Demands for Configuration 32

The tables and figures above show that when the model is analyzed without dampers the shear and axial forces can actually be less than after the dampers are added. When looking at the axial force diagrams it is clear the location of the dampers impacts the axial force in the members since the load has to have a path to travel to and from the dampers. The location of the shear forces, on the other hand, does not appear to be impacted by the dampers. That being said, as stated previously, the shear and axial forces are not of major concern. As the figures above show, when dampers are added to the frame the moment demand on certain members can decrease significantly. Although it is important to note that the amount the demand decreases varies significantly depending on both the configuration, the ground motion, and which member is being looked at. With careful analysis, the damper configuration can be chosen to decrease the moment in the most important members, or in members that are most likely to fail.

5.2 Damping Energy

Figures 103b through 106 below show the cumulative energy plots first with dampers and then without. All of the figures are based on ground motion 2. These figures show how energy is dissipated when the frame experiences the ground motion. Figure 103a shows a zoomed in view of the legend for the cumulative energy diagram.

Figure 103a: Legend for the Cumulative Energy Plots

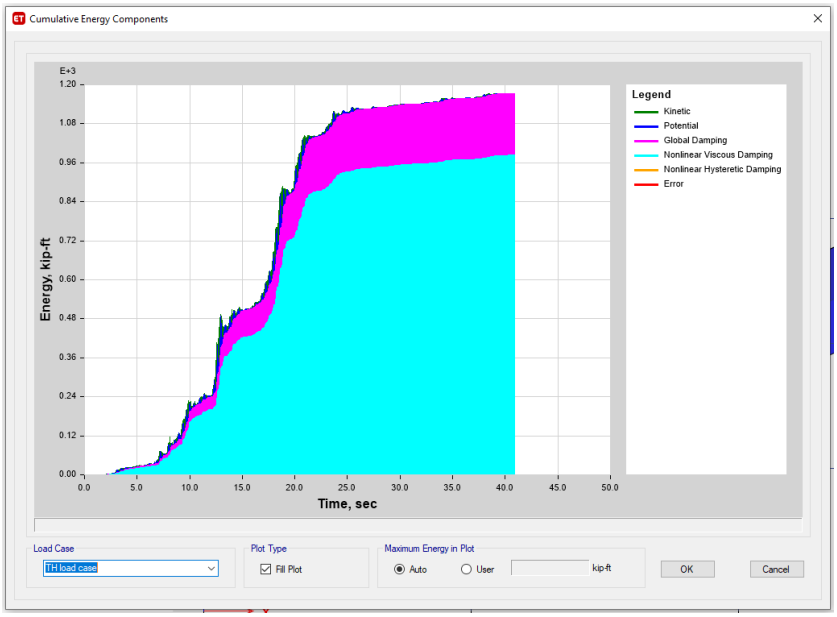

Figure 103b: Cumulative Energy For Damper Configuration 28 - Without Hinges

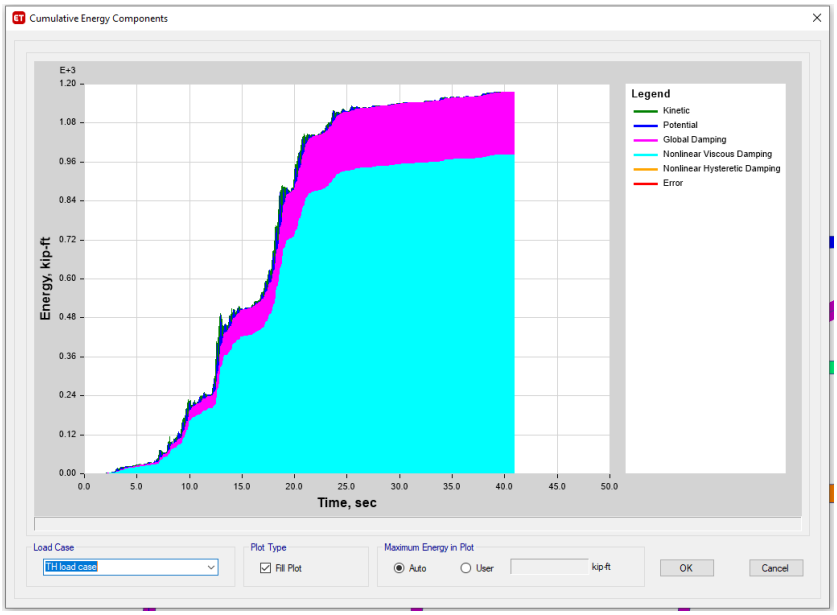

Figure 104: Cumulative Energy For Damper Configuration 28 - With Hinges

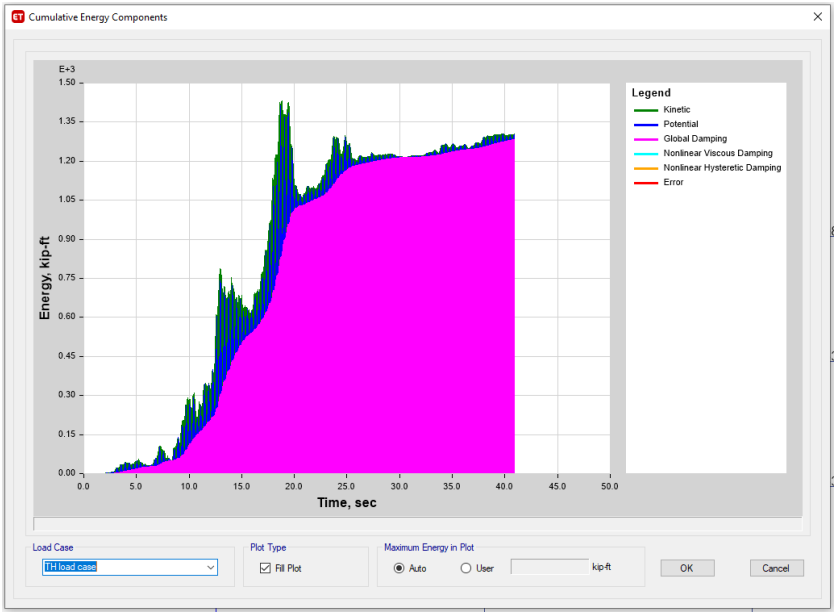

Figure 105: Cumulative Energy For Frame With No Dampers - Without Hinges

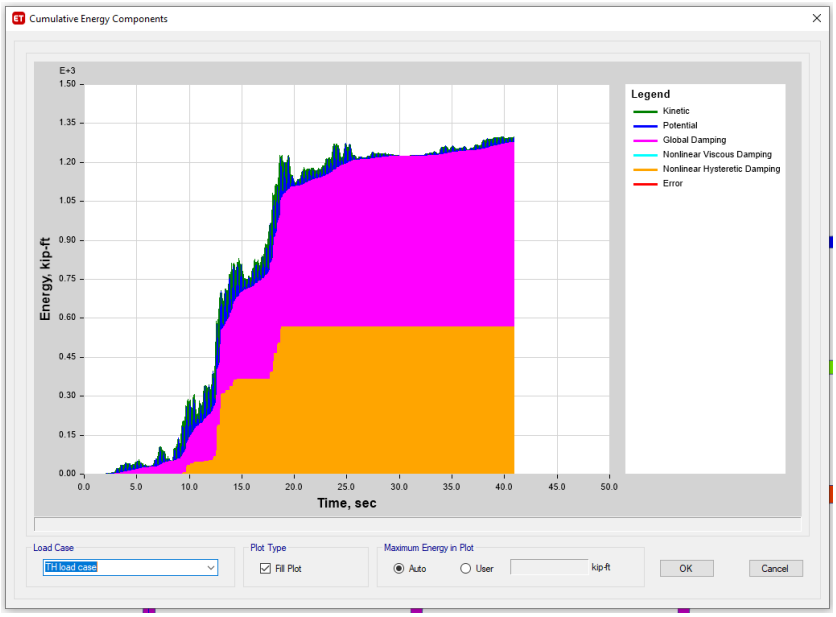

Figure 106: Cumulative Energy For Frame With No Dampers - With Hinges

The first two energy plots show that when there are dampers in the frame, a significant amount of the energy is dissipated through them. The dampers are the dominant source of energy dissipation in the frame and the energy plots show that it takes time for the dampers to dissipate energy. It takes until roughly halfway through for the energy dissipation to reach approximately the max value. When hinges are added to the frame with dampers, the total amount of energy dissipated is even greater, and the dampers dissipate an even larger amount of that energy. This is due to the fact that the increased movement of the frame allows the damper to cycle back and forth even more, dissipating more energy.

When there are no dampers or hinges in the frame, almost all the energy dissipation comes from global damping, which is elastic damping. When hinges are added, a large portion of the dissipated energy comes from nonlinear hysteretic damping which comes from the formation of the plastic hinges in the members. When the members permanently deform, they are dissipating some of the energy from the ground motion.

The energy dissipated from the dampers can also be seen in the hysteretic curves. Figures 107 through 110 below show hysteretic curves for configuration 28, each for ground motion 2 and ground motion 7 with and without hinges.

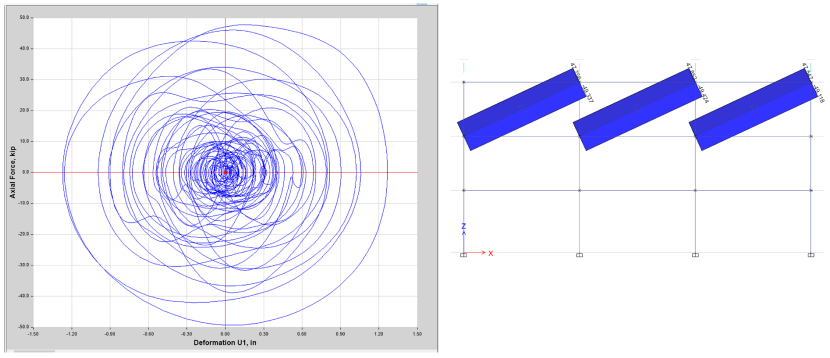

Figure 107: Hysteretic Curve and Damper Axial Force Diagram for Ground Motion 2 - Without Hinges

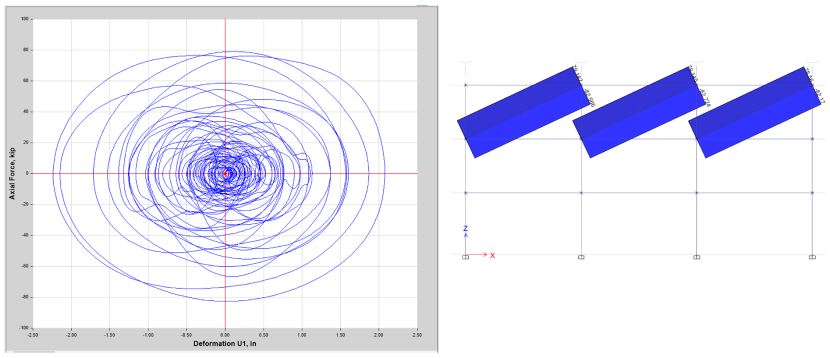

Figure 108: Hysteretic Curve and Damper Axial Force Diagram for Ground Motion 2 - With Hinges

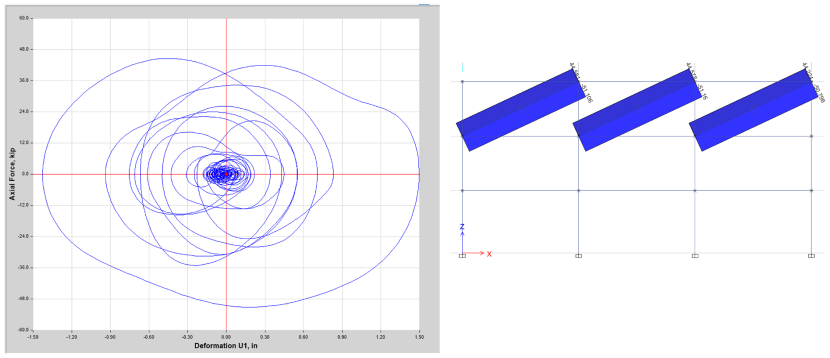

Figure 109: Hysteretic Curve and Damper Axial Force Diagram For Ground Motion 7 - Without Hinges

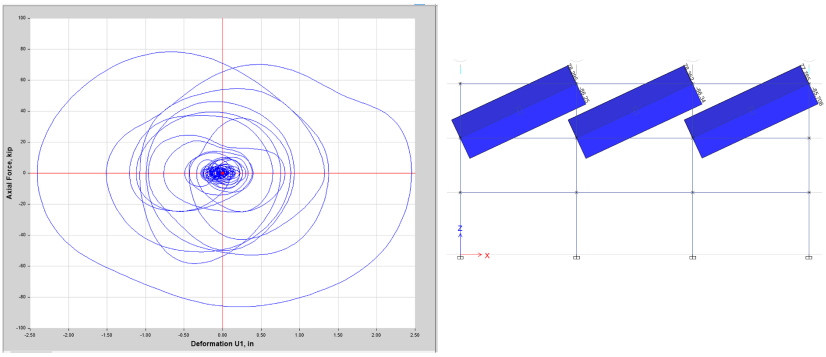

Figure 110: Hysteretic Curve and Damper Axial Force Diagram for Ground Motion 7 - With Hinges

As with the energy plots, these figures show that more energy is dissipated when hinges are added since the dampers experience a greater force and the dampers displace even more, both of which make the area under the force displacement curve greater, which is equal to the amount of energy dissipated. It is also shown that the damper cycles back and forth significantly more for ground motion 2 than for ground motion 7, which aligns with the fact that the frame with dampers performs the best in ground motion 2.

5.3 Base Shear

Figure 111 shows the base shear values for configurations 28 and 32, as well as for the frame without dampers, for ground motions 2 and 7 with and without hinges. Figure 112 shows the frame with damper configurations 28 and 32.

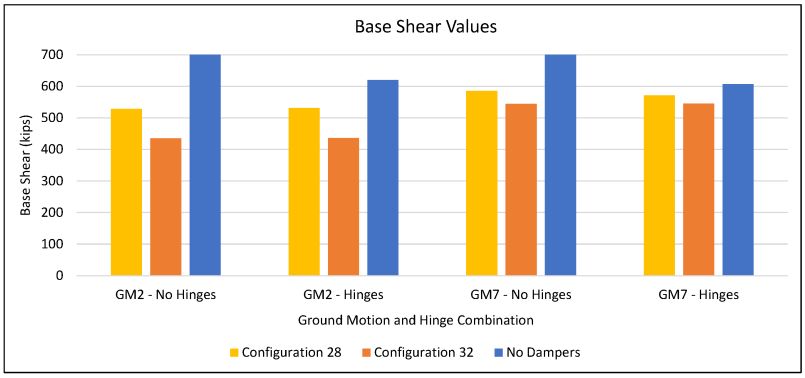

Figure 111: Graph of Base Shear Values

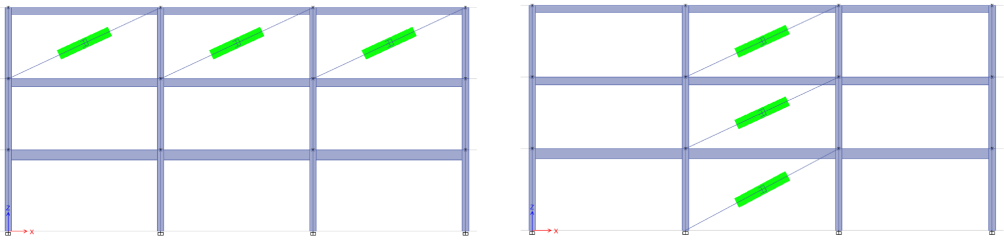

Figure 112: Frame Elevations of Damper Configurations 28 and 32

The base shear is the largest for the frame without dampers regardless of which ground motion is being used or if the frame has hinges in it. Having a smaller base shear shows that the structure is having to resist less of the lateral force from the ground motion since the dampers are absorbing some of that force. The addition of hinges to the model decreases the base shear for the frame without dampers, but it is still not as small as it is for the frame with dampers. Again, this graph shows that the frame performs better for ground motion 2, and for configuration 32, where the dampers are located at all levels in the middle bays of each level.

5.4 Conclusion

From all of the analysis shown in this report, it is clear that adding fluid viscous dampers (FVDs) to a steel special moment frame can provide beneficial effects. FVDs help to reduce the forces the structural frame experiences by redirecting and dissipating energy from a seismic event so that the frame itself does not have to dissipate as much energy. This results in decreased deflection in the frame as well as decreases in the demand forces on the members. It is possible to produce significant improvement in results from the addition of as few as 3 FVDs per frame line. With adequate knowledge of the expected ground motions the frame could experience, the best configuration for dampers can be selected. Careful analysis for specific cases when designing can allow for an exceptional structural system that performs desirably in seismic events.

By using FVDs in a steel special moment frame, not only is the structure much more likely to be safe for occupants during a seismic event, the cost to repair will likely be significantly lower and if included in the initial design, initial construction costs could be lower since the frame does not have to be designed to resist as much force as would be necessary without the dampers. FVDs provide a structural design that goes beyond what is required by code to provide an effective and beneficial option to improve safety and decrease cost. The flexibility with where dampers can be located means their application can be wide spread and tailored to fit any specific project, creating a great way to make sure that structures last through the seismic events they may experience. Thinking about design in terms of overall performance allows for the creation of a resilient building, and fluid viscous dampers are an effective way to implement that idea in the structural system.

APPENDIX A: Data Tables

	FNA THA Analysis for 7 Ground Motions with 1 Damper			
	Max Deflection (in)	% Difference	Min Deflection (in)	% Difference
GM1	7.216	-7.2%	-6.914	-12.0%
GM2	5.734	-14.7%	-6.438	-15.8%
GM3	6.148	-20.1%	-6.377	-13.7%
GM4	6.568	-13.2%	-6.857	-9.7%
GM5	5.022	-5.2%	-7.729	-8.1%
GM6	7.222	-12.1%	-6.026	-11.6%
GM7	6.179	-4.9%	-7.029	-9.3%

Table 8: Data for Figure 39

	FNA THA Analysis for 7 Ground Motions with 2 Dampers			
	Max Deflection (in)	% Difference	Min Deflection (in)	% Difference
GM1	6.798	-12.6%	-6.222	-20.8%
GM2	5.208	-22.5%	-5.677	-25.8%
GM3	5.423	-29.5%	-5.739	-22.3%
GM4	5.83	-23.0%	-6.335	-16.5%
GM5	4.819	-9.1%	-7.224	-14.1%
GM6	6.592	-19.8%	-5.702	-16.4%
GM7	5.875	-9.6%	-6.443	-16.9%

Table 9: Data for Figure 41

	FNA THA Analysis for 7 Ground Motions with 3 Dampers			
	Max Deflection (in)	% Difference	Min Deflection (in)	% Difference
GM1	6.564	-15.6%	-5.847	-25.6%
GM2	4.951	-26.3%	-5.284	-30.9%
GM3	5.19	-32.5%	-5.417	-26.7%
GM4	5.435	-28.2%	-6.06	-20.2%
GM5	4.711	-11.1%	-6.93	-17.6%
GM6	6.239	-24.1%	-5.483	-19.6%
GM7	5.695	-12.4%	-6.123	-21.0%

Table 10: Data for Figure 43

Change in % Decrease in Deflection When Number of Dampers Increases			
1 to 2 Dampers		2 to 3 Dampers	
Max Deflection	Min Deflection	Max Deflection	Min Deflection
5.4%	8.8%	3.0%	4.8%
7.8%	9.9%	3.8%	5.1%
9.4%	8.6%	3.0%	4.4%
9.7%	6.9%	5.2%	3.6%
3.8%	6.0%	2.0%	3.5%
7.7%	4.8%	4.3%	3.2%
4.7%	7.6%	2.8%	4.1%

Table 11: Data for Figure 44 and Figure 45

Damper locations:	Max Deflection (in)	% difference	Min Deflection (in)	% difference	Configuration Number
3rd level					
- left bay only	7.222	-7.2%	-6.925	-11.9%	C1
- middle bay only	7.216	-7.2%	-6.914	-12.0%	C2
- right bay only	7.217	-7.2%	-6.918	-12.0%	C3
2nd level					
- left bay only	7.327	-5.8%	-7.068	-10.1%	C4
- middle bay only	7.327	-5.8%	-7.068	-10.1%	C5
- right bay only	7.331	-5.8%	-7.075	-10.0%	C6
1st level					
- left bay only	7.496	-3.7%	-7.363	-6.3%	C7
- middle bay only	7.496	-3.7%	-7.362	-6.3%	C8
- right bay only	7.500	-3.6%	-7.371	-6.2%	C9

Table 12: Data for Figure 52

Damper locations:	Max Deflection (in)	% difference	Min Deflection (in)	% difference	Configuration Number
3rd level					
- left and middle bays	6.732	-13.5%	-6.170	-21.5%	C10
- left and right bays	6.729	-13.5%	-6.169	-21.5%	C11
- right and middle bays	6.722	-13.6%	-6.164	-21.6%	C12
2nd level					
- left and middle bays	6.909	-11.2%	-6.369	-19.0%	C13
- left and right bays	6.912	-11.2%	-6.374	-18.9%	C14
- right and middle bays	6.913	-11.1%	-6.375	-18.9%	C15
1st level					
- left and middle bays	7.227	-7.1%	-6.916	-12.0%	C16
- left and right bays	7.231	-7.1%	-6.924	-11.9%	C17
- right and middle bays	7.231	-7.1%	-6.924	-11.9%	C18

Table 13: Data for Figure 53

Damper locations:	Max Deflection (in)	% difference	Min Deflection (in)	% difference	Configuration Number
left column					
- top and middle bays	6.803	-12.6%	-6.231	-20.7%	C19
- middle and bottom bays	7.052	-9.4%	-6.618	-15.8%	C20
- top and bottom bays	6.962	-10.5%	-6.498	-17.3%	C21
middle column					
- top and middle bays	6.798	-12.6%	-6.222	-20.8%	C22
- middle and bottom bays	7.052	-9.4%	-6.617	-15.8%	C23
- top and bottom bays	6.956	-10.6%	-6.488	-17.5%	C24
Right Column					
- top and middle bays	6.802	-12.6%	-6.232	-20.7%	C25
- middle and bottom bays	7.060	-9.3%	-6.631	-15.6%	C26
- top and bottom bays	6.961	-10.5%	-6.499	-17.3%	C27

Table 14: Data for Figure 54

Damper locations:	Max Deflection (in)	% difference	Min Deflection (in)	% difference	Configuration Number
3rd level - all 3 bays	6.300	-19.0%	-5.546	-29.4%	C28
2nd level - all 3 bays	6.535	-16.0%	-5.762	-26.7%	C29
1st level all 3 bays	6.980	-10.3%	-6.520	-17.0%	C30
left column - all 3 bays	6.569	-15.6%	-5.855	-25.5%	C31
middle column - all 3 bays	6.564	-15.6%	-5.847	-25.6%	C32
right column - all 3 bays	6.571	-15.5%	-5.862	-25.4%	C33
Diagonal - upper left to lower right	6.573	-15.5%	-5.861	-25.4%	C44
Diagonal - upper right to lower left	6.565	-15.6%	-5.850	-25.6%	C45

Table 15: Data for Figure 55

Damper locations:	Max Deflection (in)	% difference	Min Deflection (in)	% difference	Configuration Number
4 upper left bays	6.026	-22.5%	-5.034	-36.0%	C34
4 upper right bays	6.019	-22.6%	-5.035	-35.9%	C35
4 lower left bays	6.429	-17.4%	-5.611	-28.6%	C36
4 lower right bays	6.437	-17.3%	-5.623	-28.5%	C37
4 corners of Frame	6.282	-19.3%	-5.446	-30.7%	C47
Middle Bay on All Sides	6.218	-20.1%	-5.292	-32.7%	C48

Table 16: Data for Figure 56

Damper locations:	Max Deflection (in)	% difference	Min Deflection (in)	% difference	Configuration Number
3rd & 2nd levels - all bays	5.407	-30.5%	-4.15	-47.2%	C38
3rd and 1st levels - all bays	5.912	-24.0%	-4.806	-38.9%	C39
1st and 2nd levels - all bays	5.722	-26.5%	-4.611	-41.3%	C40
left and middle columns - all bays	5.668	-27.1%	-4.473	-43.1%	C41
right and middle columns - all bays	5.663	-27.2%	-4.478	-43.0%	C42
left and right columns - all bays	5.670	-27.1%	-4.482	-43.0%	C43
all bays in the frame	4.98	-36.0%	-3.493	-55.6%	C46

Table 17: Data for Figure 57

	Dampers in All 3 Bays in 3rd Level (C28) - Original Orientation			
	Max Deflection (in)	% difference	Min Deflection (in)	% difference
GM1	6.300	-19.0%	-5.546	-29.4%
GM2	4.678	-30.4%	-5.071	-33.7%
GM3	4.841	-37.0%	-4.970	-35.0%
GM4	5.172	-31.7%	-5.863	-22.8%
GM5	4.578	-13.6%	-6.681	-20.6%
GM6	5.956	-27.5%	-5.291	-22.4%
GM7	5.550	-14.6%	-5.813	-25.0%

Table 18: Data for Figure 62 (Original Orientation)

	Dampers in All 3 Bays in 3rd Level (C28) - Connected End to End			
	Max Deflection (in)	% difference	Min Deflection (in)	% difference
GM1	6.306	-18.9%	-5.552	-29.4%
GM2	4.688	-30.2%	-5.077	-33.6%
GM3	4.846	-37.0%	-4.982	-34.9%
GM4	5.176	-31.6%	-5.866	-22.7%
GM5	4.581	-13.6%	-6.689	-20.5%
GM6	5.969	-27.4%	-5.296	-22.3%
GM7	5.558	-14.5%	-5.820	-24.9%

Table 19: Data for Figure 62 (New Orientation)

	Dampers in All 3 Bays in Middle Column (C32) - Original Orientation			
	Max Deflection (in)	% difference	Min Deflection (in)	% difference
GM1	6.564	-15.6%	-5.847	-25.6%
GM2	4.951	-26.3%	-5.284	-30.9%
GM3	5.190	-32.5%	-5.417	-26.7%
GM4	5.435	-28.2%	-6.060	-20.2%
GM5	4.711	-11.1%	-6.930	-17.6%
GM6	6.239	-24.1%	-5.483	-19.6%
GM7	5.695	-12.4%	-6.123	-21.0%

Table 20: Data for Figure 63 (Original Orientation)

	Dampers in All 3 Bays in Middle Column (C32) - Connected End to End			
	Max Deflection (in)	% difference	Min Deflection (in)	% difference
GM1	6.564	-15.6%	-5.846	-25.6%
GM2	4.951	-26.3%	-5.280	-31.0%
GM3	5.192	-32.5%	-5.419	-26.7%
GM4	5.432	-28.2%	-6.059	-20.2%
GM5	4.712	-11.1%	-6.929	-17.6%
GM6	6.237	-24.1%	-5.483	-19.6%
GM7	5.694	-12.4%	-6.123	-21.0%

Table 21: Data for Figure 63 (New Orientation)

	Dampers in Upper Left 4 Bays (C34) - Original Orientation			
	Max Deflection (in)	% difference	Min Deflection (in)	% difference
GM1	6.026	-22.5%	-5.034	-36.0%
GM2	4.418	-34.3%	-4.548	-40.5%
GM3	4.635	-39.7%	-4.671	-38.9%
GM4	4.643	-38.7%	-5.493	-27.6%
GM5	4.455	-15.9%	-6.305	-25.0%
GM6	5.549	-32.5%	-4.957	-27.3%
GM7	5.272	-18.9%	-5.378	-30.6%

Table 22: Data for Figure 64 (Original Orientation)

	Dampers in Upper Left 4 Bays (C34) - Connected End to End			
	Max Deflection (in)	% difference	Min Deflection (in)	% difference
GM1	6.029	-22.5%	-5.034	-36.0%
GM2	4.421	-34.2%	-4.455	-41.8%
GM3	4.639	-39.7%	-4.677	-38.9%
GM4	4.641	-38.7%	-5.493	-27.6%
GM5	4.456	-15.9%	-6.305	-25.0%
GM6	5.551	-32.5%	-4.957	-27.3%
GM7	5.273	-18.9%	-5.381	-30.6%

Table 23: Data for Figure 64 (New Orientation)

	Dampers in All Bays of 3rd and 2nd Levels (C38) - Original Orientation			
	Max Deflection (in)	% difference	Min Deflection (in)	% difference
GM1	5.407	-30.5%	-4.150	-47.2%
GM2	3.868	-42.4%	-3.787	-50.5%
GM3	4.092	-46.8%	-3.892	-49.1%
GM4	3.787	-50.0%	-4.881	-35.7%
GM5	4.162	-21.5%	-5.573	-33.7%
GM6	4.796	-41.7%	-4.341	-36.3%
GM7	4.729	-27.2%	-4.528	-41.6%

Table 24: Data for Figure 65 (Original Orientation)

	Dampers in All Bays of 3rd and 2nd Levels (C38) - Connected End to End			
	Max Deflection (in)	% difference	Min Deflection (in)	% difference
GM1	5.418	-30.4%	-4.156	-47.1%
GM2	3.882	-42.2%	-3.793	-50.4%
GM3	4.096	-46.7%	-3.910	-48.9%
GM4	3.790	-49.9%	-4.883	-35.7%
GM5	4.166	-21.4%	-5.584	-33.6%
GM6	4.813	-41.4%	-4.347	-36.3%
GM7	4.739	-27.1%	-4.537	-41.5%

Table 25: Data for Figure 65 (New Orientation)

	Largest Change in Deflection for Configuration 28 (C = 1)						
alpha, α	GM1	GM2	GM3	GM4	GM5	GM6	GM7
1	-17.0%	-21.5%	-26.7%	-18.7%	-11.6%	-16.8%	-13.6%
0.75	-9.7%	-13.3%	-16.7%	-10.6%	-6.7%	-11.1%	-7.6%
0.5	-5.3%	-7.9%	-9.7%	-6.0%	-4.6%	-9.0%	-4.2%
0.25	-2.8%	-4.7%	-5.6%	-3.5%	-3.8%	-5.4%	-2.4%
0.1	-1.9%	-3.4%	-4.1%	-2.7%	-3.6%	-4.0%	-1.7%

Table 26: Data for Figure 66

	Largest Change in Deflection for Configuration 28 (C = 2)						
alpha, α	GM1	GM2	GM3	GM4	GM5	GM6	GM7
1	-29.4%	-33.7%	-37.0%	-31.7%	-20.6%	-27.5%	-25.0%
0.75	-18.1%	-22.6%	-28.1%	-19.5%	-12.7%	-18.5%	-14.8%
0.5	-10.4%	-14.6%	-13.8%	-11.3%	-8.7%	-11.9%	-8.4%
0.25	-5.8%	-9.2%	-10.7%	-6.8%	-7.5%	-11.7%	-4.9%
0.1	-3.9%	-6.8%	-7.9%	-5.3%	-7.1%	-7.9%	-3.6%

Table 27: Data for Figure 67

	Largest Change in Deflection for Configuration 28 (C = 4)						
alpha, α	**GM1**	**GM2**	**GM3**	**GM4**	**GM5**	**GM6**	**GM7**
1	-44.8%	-46.9%	-49.3%	-47.4%	-32.4%	-39.7%	-41.0%
0.75	-31.6%	-36.1%	-40.7%	-33.1%	-22.1%	-30.0%	-27.4%
0.5	-19.9%	-24.4%	-30.1%	-20.5%	-15.3%	-20.9%	-16.4%
0.25	-11.7%	-16.6%	-19.5%	-12.2%	-13.2%	-14.3%	-9.7%
0.1	-8.3%	-12.9%	-14.7%	-9.5%	-12.3%	-11.5%	-7.3%

Table 28: Data for Figure 68

	Largest Change in Deflection for Configuration 32 (C = 1)						
alpha, α	**GM1**	**GM2**	**GM3**	**GM4**	**GM5**	**GM6**	**GM7**
1	-14.1%	-18.7%	-23.4%	-15.8%	-9.4%	-13.8%	-11.0%
0.75	-7.8%	-11.4%	-14.1%	-9.1%	-5.5%	-10.4%	-6.1%
0.5	-4.2%	-6.7%	-8.1%	-5.2%	-3.8%	-7.3%	-3.4%
0.25	-2.3%	-4.0%	-4.7%	-3.2%	-3.2%	-4.4%	-1.8%
0.1	-1.5%	-3.0%	-3.5%	-2.4%	-3.1%	-3.3%	-1.2%

Table 29: Data for Figure 69

	Largest Change in Deflection for Configuration 32 (C = 2)						
alpha, α	**GM1**	**GM2**	**GM3**	**GM4**	**GM5**	**GM6**	**GM7**
1	-25.6%	-30.9%	-32.5%	-28.2%	-17.6%	-24.1%	-21.0%
0.75	-15.1%	-20.2%	-25.0%	-17.1%	-10.6%	-15.5%	-12.2%
0.5	-8.5%	-12.4%	-15.3%	-10.2%	-7.1%	-10.9%	-6.8%
0.25	-4.6%	-7.9%	-9.2%	-6.2%	-6.3%	-8.6%	-3.8%
0.1	-3.2%	-6.0%	-6.8%	-4.7%	-6.1%	-6.5%	-2.7%

Table 30: Data for Figure 70

	Largest Change in Deflection for Configuration 32 (C = 4)						
alpha, α	**GM1**	**GM2**	**GM3**	**GM4**	**GM5**	**GM6**	**GM7**
1	-43.1%	-47.4%	-43.4%	-46.2%	-30.8%	-38.7%	-37.1%
0.75	-27.9%	-33.9%	-35.9%	-30.6%	-19.5%	-27.0%	-23.4%
0.5	-16.9%	-22.3%	-27.3%	-19.0%	-12.7%	-18.3%	-13.7%
0.25	-9.7%	-14.6%	-17.2%	-11.8%	-11.0%	-12.4%	-7.9%
0.1	-6.9%	-11.5%	-13.0%	-9.0%	-10.6%	-10.6%	-5.7%

Table 31: Data for Figure 71

Change in % Decrease in Deflection for Configuration 28 as C goes from 1 to 2							
alpha, α	GM1	GM2	GM3	GM4	GM5	GM6	GM7
1	15.3%	13.2%	12.2%	15.7%	11.9%	12.1%	16.0%
0.75	13.5%	13.4%	12.6%	13.6%	9.5%	11.5%	12.6%
0.5	9.5%	9.8%	16.3%	9.1%	6.6%	9.0%	8.0%
0.25	5.9%	7.5%	8.8%	5.5%	5.8%	2.5%	4.7%
0.1	4.4%	6.1%	6.8%	4.2%	5.2%	3.6%	3.7%

Table 32: Data for Figure 72

Change in % Decrease in Deflection for Configuration 28 as C goes from 2 to 4							
alpha, α	GM1	GM2	GM3	GM4	GM5	GM6	GM7
1	12.4%	12.3%	10.3%	13.0%	8.9%	10.7%	11.4%
0.75	8.3%	9.4%	11.4%	8.9%	5.9%	7.4%	7.2%
0.5	5.1%	6.7%	4.1%	5.4%	4.1%	2.9%	4.2%
0.25	2.9%	4.5%	5.1%	3.3%	3.6%	6.3%	2.5%
0.1	2.0%	3.4%	3.8%	2.6%	3.5%	3.9%	1.9%

Table 33: Data for Figure 73

Change in % Decrease in Deflection for Configuration 32 as C goes from 1 to 2							
alpha, α	GM1	GM2	GM3	GM4	GM5	GM6	GM7
1	17.5%	16.5%	10.9%	18.0%	13.2%	14.6%	16.1%
0.75	12.7%	13.8%	10.9%	13.5%	8.9%	11.4%	11.3%
0.5	8.3%	9.8%	12.0%	8.8%	5.6%	7.4%	6.9%
0.25	5.1%	6.7%	8.0%	5.6%	4.8%	3.8%	4.1%
0.1	3.7%	5.6%	6.2%	4.3%	4.5%	4.1%	3.0%

Table 34: Data for Figure 74

Change in % Decrease in Deflection for Configuration 32 as C goes from 2 to 4							
alpha, α	GM1	GM2	GM3	GM4	GM5	GM6	GM7
1	11.5%	12.3%	9.1%	12.4%	8.2%	10.3%	9.9%
0.75	7.3%	8.8%	11.0%	8.0%	5.1%	5.2%	6.0%
0.5	4.3%	5.8%	7.2%	4.9%	3.4%	3.6%	3.5%
0.25	2.4%	3.8%	4.4%	3.0%	3.0%	4.2%	2.0%
0.1	1.6%	3.0%	3.3%	2.3%	3.0%	3.2%	1.4%

Table 35: Data for Figure 75

Change in Deflection for Configuration 28 with Hinges				
	Max Deflection (in)	% difference	Min Deflection (in)	% difference
GM1	10.458	-22.8%	-7.072	-6.2%
GM2	7.852	-40.7%	-9.247	-13.9%
GM3	8.572	-29.9%	-8.580	-12.0%
GM4	7.452	-27.9%	-9.948	-30.7%
GM5	7.285	-13.9%	-11.330	-25.7%
GM6	10.293	-24.7%	-7.359	-29.4%
GM7	9.080	-12.4%	-9.342	-14.4%

Table 36: Data for Figure 85

Change in Deflection for Configuration 32 with Hinges				
	Max Deflection (in)	% difference	Min Deflection (in)	% difference
GM1	10.941	-19.3%	-7.204	-4.5%
GM2	8.548	-35.5%	-9.872	-8.1%
GM3	8.821	-27.9%	-9.383	-3.7%
GM4	7.830	-24.3%	-10.329	-28.1%
GM5	7.506	-11.3%	-11.886	-22.0%
GM6	10.920	-20.2%	-7.694	-26.1%
GM7	9.236	-10.9%	-9.827	-9.9%

Table 37: Data for Figure 86

	Deflection Values For Frame with No Dampers			
	No Hinges		Hinges	
	Max Deflection (in)	Min Deflection (in)	Max Deflection (in)	Min Deflection (in)
GM1	12.708	-13.846	13.551	-7.543
GM2	16.144	-17.978	13.245	-10.744
GM3	16.898	-15.365	12.232	-9.745
GM4	15.42	-15.33	10.339	-14.363
GM5	9.478	-14.031	8.464	-15.240
GM6	14.837	-13.601	13.678	-10.417
GM7	11.051	-13.125	10.368	-10.909

Table 38: Data for Figure 82

	Deflection Values For Configuration 28			
	No Hinges		Hinges	
	Max Deflection (in)	Min Deflection (in)	Max Deflection (in)	Min Deflection (in)
GM1	8.626	-7.53	10.458	-7.072
GM2	6.445	-7.093	7.852	-9.247
GM3	7.129	-6.232	8.572	-8.580
GM4	7.044	-8.340	7.452	-9.948
GM5	6.442	-9.352	7.285	-11.330
GM6	8.287	-7.473	10.293	-7.359
GM7	7.882	-7.829	9.080	-9.342

Table 39: Data for Figure 83

	Deflection Values For Configuration 32			
	No Hinges		Hinges	
	Max Deflection (in)	Min Deflection (in)	Max Deflection (in)	Min Deflection (in)
GM1	9.175	-7.769	10.941	-7.204
GM2	6.741	-6.988	8.548	-9.872
GM3	7.106	-7.192	8.821	-9.383
GM4	7.153	-8.385	7.830	-10.329
GM5	6.752	-9.593	7.506	-11.886
GM6	8.455	-7.572	10.920	-7.694
GM7	8.02	-8.275	9.236	-9.827

Table 40: Data for Figure 84

Percent Change in Deflection for Configuration 28 with Hinges with Varying C Values							
Coefficient, C	GM1	GM2	GM3	GM4	GM5	GM6	GM7
1	-13.1%	-27.3%	-19.9%	-19.6%	-15.0%	-18.8%	-7.3%
2	-22.8%	-40.7%	-29.9%	-30.7%	-25.7%	-29.4%	-14.4%
4	-35.9%	-51.2%	-41.2%	-41.6%	-37.7%	-31.6%	-29.3%

Table 41: Data for Figure 87

Percent Change in Deflection for Configuration 32 with Hinges with Varying C Values							
Coefficient, C	GM1	GM2	GM3	GM4	GM5	GM6	GM7
1	-10.1%	-21.5%	-16.3%	-16.8%	-11.8%	-15.7%	-4.8%
2	-19.3%	-35.5%	-27.9%	-28.1%	-22.0%	-26.1%	-9.9%
4	-32.2%	-49.1%	-41.9%	-41.6%	-36.7%	-28.5%	-24.1%

Table 42: Data for Figure 88

% Decrease in Moment Demand For Frame With Hinges - Configuration 28				
	Level 1 Beam	Level 2 Beam	Level 3 Beam	Level 1 Column
Ground Motion 2	-13.4%	-33.8%	-41.3%	-9.1%
Ground Motion 7	-6.6%	-19.5%	-22.5%	-1.8%

Table 43: Data for Figure 101

% Decrease in Moment Demand For Frame With Hinges - Configuration 32				
	Level 1 Beam	Level 2 Beam	Level 3 Beam	Level 1 Column
Ground Motion 2	-25.9%	-32.5%	-36.7%	-24.9%
Ground Motion 7	-6.9%	-13.1%	-14.7%	-7.3%

Table 44: Data for Figure 102

APPENDIX B: Python Scripts

Python Script for Eigen Analysis Function

```python
import numpy as np

# Eigen Analysis, finds natural frequencies and mode shapes
def genEig(K,M):

    # K is the stiffness matrix
    # M is the mass matrix
    # omega2 is the frequency matrix with the omegas on the diagonal
    # m is mass normalized mode shape matrix

    [n,m] = K.shape
    Minv = np.linalg.inv(M)
    d,v = np.linalg.eig(K@Minv) # solve the converted K-lambdaM
    v = Minv@v # unconvert the eigenvectors
    flag = 1
    while flag > 0: #sort the eigen values and vectors
        flag = 0
        for i in range(0,n-1):
            if d[i+1]<d[i]: # swap
                d[[i, i+1]] = d[[i+1,i]]
                v[:,[i,i+1]] = v[:,[i+1,i]]
                flag = 1
    for i in range(0,n): # normalize v
        v[:,i] *= (1/np.sqrt(v[:,i].T@M@v[:,i]))
    omega2 = v.T@K@v
    omega2 = np.round(omega2,6)
    v = np.round(v,6)
    print('\nOmega2 =\n ', omega2)
    print('\nPhi =\n ', v)
    return omega2, v
```

Python Script for Response Spectrum Analysis - Part 1

```python
## Linear Dynamic Analysis - Response Spectrum Analysis ##

import numpy as np
import matplotlib.pyplot as plt
import math

# create the stiffness and mass matrices
E = 29000 #ksi
I = 2400 #in^4
H1 = 168 # in ( 14 ft)
H2 = 192 # in (16 ft)
k3 = (12*E*I)/(H1**3)
k2 = (12*E*I)/(H1**3)
k1 = (24*E*I)/(H2**3)
K = np.array([[k3,-k3,0],[-k3,k3+k2,-k2],[0,-k2,k2+k1]],dtype = float)
M = np.array([[.3814,0,0],[0,.4316,0],[0,0,.4375]],dtype = float)

# solve for and check the omega sqaured matrix and mode shape matrix
from Eigen_Analysis_file import genEig
W2, Phi = genEig(K,M)

check1 = Phi.T@M@Phi
check1 = np.round(check1,4)
check2 = Phi.T@K@Phi
check2 = np.round(check2,4)

# create and plot the response spectrum
def Response_Accel(T):
    # T is the largest value for the period that you want to plot
    g = 386.4
    A_SDS = 1.428*g
    A_SD1 = .8115*g
    To = .2*(A_SD1/A_SDS)
    Ts = A_SD1/A_SDS
    T1 = np.linspace(.001,To,1000)
    A1 = A_SDS*(.4 + (.6*(T1/To)))
    T2 = np.linspace(To,Ts,1000)
    A2 = np.repeat(A_SDS,len(T2))
    T3 = np.linspace(Ts,T,1000)
    A3 = A_SD1/T3
    return T1, T2, T3, A1, A2, A3
```

Python Script for Response Spectrum Analysis - Part 2

```python
T = 5
T1, T2, T3, A1, A2, A3 = Response_Accel(T)
fig2 = plt.figure()
plt.plot(T1,A1,'k',T2,A2,'k',T3,A3,'k')
plt.title('Design Response Acceleration')
plt.xlabel('Period, T (s)')
plt.ylabel('Response Acceleration, A (in/s^2)')
plt.show
fig2.savefig('RS_acceleration', dpi = 300)

# calculate period, acceleration, and displacement for each mode
Mode_periods = []
Mode_accel = []
Mode_disp = []
for i in range(0,len(W2)):
    T_mode_i = (2*math.pi)/math.sqrt(W2[i][i])
    if T_mode_i <= T1[-1]:
        T_range = T1
        A_range = A1
    elif T_mode_i > T2[-1]:
        T_range = T3
        A_range = A3
    else:
        T_range = T2
        A_range = A2
    A_mode_i = np.interp(T_mode_i,T_range,A_range)
    D_mode_i = A_mode_i/W2[i][i]
    Mode_periods.append(T_mode_i)
    Mode_accel.append(A_mode_i)
    Mode_disp.append(D_mode_i)

# define the influence vector and the modal participation vector
L = np.array([[1],[1],[1]])
gamma = -Phi.T@M@L

# find the max q for each mode and convert back to u
qmax_values = []
Mode_u_values = []
for i in range(0,len(Mode_disp)):
    qmax_i = Mode_disp[i]*gamma[i]
    qmax_values.append(qmax_i)
    phi_vector = Phi[:,i]
    u_mode_i = phi_vector*qmax_i
    u_mode_i = np.reshape(u_mode_i,(3,1))
    Mode_u_values.append(u_mode_i)
```

Python Script for Response Spectrum Analysis - Part 3

```python
# find max displacment at each DOF using SRSS to combine modal values
umax_DOF_values = []
for i in range(0,len(Mode_u_values)):
    DOF = i
    u_sum = 0
    for j in range(0,len(Mode_u_values)):
        u_value = (Mode_u_values[j][DOF])**2
        u_sum += u_value
    umax_DOF_i = math.sqrt(u_sum)
    umax_DOF_values.append(umax_DOF_i)

print('\n max displacement at DOFs: \n',umax_DOF_values)

Etabs_displacements = np.array([7.764604,4.834071,2.15689])
differences = []
for i in range(0,len(umax_DOF_values)):
    percent_dif = ((umax_DOF_values[i] - Etabs_displacements[i])/umax_DOF_values[i])*100
    differences.append(percent_dif)
print('\n percent differences between Python and Etabs',differences)
```

Python Script for Ground Motion Plots - Part 1

```python
# plots of displacement, velocity and acceleration for different ground motions

import pandas as pd
import numpy as np
import matplotlib.pyplot as plt
import new_avg_file as NA
import math
from scipy import integrate

# plotting acceleration from the ground motion
GM = 1 #Note: 7 possible ground motions
delta_t = .01 #Note: .01 for GM1, .005 for all others
path = 'D:\Senior Project\ground_motions\GM' + str(GM) + ' Data.csv'
data_frame = pd.read_csv(path,header=None)
array = data_frame.to_numpy()
shape = array.shape
length = shape[0]*shape[1]
GM_list = np.reshape(array,(length,1))*386.4
T_values = np.arange(.02,3,delta_t)
t_step = np.arange(0,delta_t*len(GM_list),delta_t)
fig1 = plt.figure(figsize=(12,8))
y_values = [0]*len(t_step)
plt.plot(t_step,GM_list,'k',t_step,y_values,'r')
title = 'Plot of Ground Motion #' + str(GM) + ' Acceleration'
plt.title(title)
plt.xlabel('Time, t (s)')
plt.ylabel('Ground Acceleration, (in/s^2)')
fig_name = 'GM' + str(GM) + '_plot'
fig1.savefig(fig_name, dpi = 300)
```

Python Script for Ground Motion Plots - Part 2

```python
# plotting velocity from the ground motion
GM_acceleration = np.array(GM_list).flatten()
GM_velocity = integrate.cumtrapz(GM_acceleration,t_step)
fig3 = plt.figure(figsize=(12,8))
t_step2 = np.delete(t_step,[-1])
y_values2 = [0]*len(t_step2)
plt.plot(t_step2,GM_velocity,'k',t_step2,y_values2,'r')
title = 'Plot of Ground Motion #' + str(GM) + ' Velocity'
plt.title(title)
plt.xlabel('Time, t (s)')
plt.ylabel('Ground velocity, (in/s)')
fig_name = 'GMV' + str(GM) + '_plot'
fig3.savefig(fig_name, dpi = 300)

# plotting displacement from the ground motion
GM_displacement = integrate.cumtrapz(GM_velocity,t_step2)
fig4 = plt.figure(figsize=(12,8))
t_step3 = np.delete(t_step2,[-1])
y_values3 = [0]*len(t_step3)
plt.plot(t_step3,GM_displacement,'k',t_step3,y_values3,'r')
title = 'Plot of Ground Motion #' + str(GM) + ' Displacement'
plt.title(title)
plt.xlabel('Time, t (s)')
plt.ylabel('Ground Displacement, (in)')
fig_name = 'GMD' + str(GM) + '_plot'
fig4.savefig(fig_name, dpi = 300)
plt.show()
```

Python Script for Hinge Properties - Part 1

```python
## Nonlinear Static Analysis - Pushover Analysis ##

import math
import numpy as np

# modeling parameters a, and b for steel beams
E = 29000 #ksi
G = 11500 #ksi
Fy = 50 #ksi
Fye = 50 #ksi
W24x84_properties = {'Z':224,'I':2370,'d':24.1,'tf':.770,'tw':.470}
W18x76_properties = {'Z':163,'I':1330,'d':18.21,'tf':.68,'tw':.425}
W16x26_properties = {'Z':44.2,'I':301,'d':15.69,'tf':.345,'tw':.25}
Beam_properties =[W24x84_properties, W18x76_properties, W16x26_properties]
L_beam = 30*12 #in

theta_y_list = []
a_beam_list = []
b_beam_list = []
for i in range(0,len(Beam_properties)):
    properties = Beam_properties[i]
    As = (properties['d'] - 2*properties['tf'])*properties['tw']
    eta = (12*E*properties['I'])/(L_beam**2*G*As)
    theta_y = (properties['Z']*Fy*L_beam*(1+eta))/(6*E*properties['I'])
    theta_y_list.append(theta_y)
    a_beam = 9*theta_y
    b_beam = 11*theta_y
    a_beam_list.append(a_beam)
    b_beam_list.append(b_beam)
print('beam a values:\n',a_beam_list)
print('\nbeam b values:\n', b_beam_list)
```

Python Script for Hinge Properties - Part 2

```python
# modeling parameters, a and b, for steel column in compression
W14x193_properties = {'Ag':56.8,'bf_over_2tf':5.45,'h_over_tw':12.8,'ry':4.05}

PG_list = [103.1,203.49,106.95,208.48,111.31,214.6] #kips
L = 167.9 #unbraced length, in inches
    # PG_list goes from top to bottom levels and
    # for each level the values go exterior then interior columns

a_value_list = []
b_value_list = []
IO_list = []
LS_list =[]
CP_list = []
for i in range(0,len(PG_list)):
    check_list = []
    check1_limit = .30*math.sqrt(E/Fye)
    if W14x193_properties['bf_over_2tf'] <= check1_limit:
        Check1 = True
    else:
        Check1 = False
    check_list.append(Check1)
    Pye = W14x193_properties['Ag']*Fye
    PG_over_Pye = PG_list[i]/Pye
    if PG_over_Pye < (.2*W14x193_properties['h_over_tw']):
        check2_limit = 2.45*math.sqrt(E/Fye)*(1 - (.71*PG_over_Pye))
        if (.2*W14x193_properties['h_over_tw']) <= check2_limit:
            Check2 = True
        else:
            Check2 = False
    elif PG_over_Pye >= (.2*W14x193_properties['h_over_tw']):
        check2_limit1 = .77*math.sqrt(E/Fye)*(2.93 - PG_over_Pye)
        check2_limit2 = 1.49*math.sqrt(E/Fye)
        if (.2*W14x193_properties['h_over_tw']) <= check2_limit1 and check2_limit1 <= check2_limit2:
            Check2 = True
        else:
            Check2 = False
    check_list.append(Check2)
    check_array = np.asarray(check_list)
    if np.all(check_array) == True:
        a = (.8*(1 - PG_over_Pye)**2.2)*((.1*(L/W14x193_properties['ry']))+(.8*W14x193_properties['h_over_tw']))**-1 - .0035
        b =  (7.4*(1 - PG_over_Pye)**2.3)*((.5*(L/W14x193_properties['ry']))+(2.9*W14x193_properties['h_over_tw']))**-1 - .006
        IO = .5*a
        LS = .75*b
        CP = b
        a_value_list.append(a)
        b_value_list.append(b)
        IO_list.append(IO)
        LS_list.append(LS)
        CP_list.append(CP)

print('\n a values: \n',a_value_list)
print('\n b values: \n',b_value_list)
print('\n IO values: \n',IO_list)
print('\n LS values: \n',LS_list)
print('\n CP values: \n',CP_list)
```

REFERENCES

[1] “Fast Nonlinear Analysis (FNA) - Technical Knowledge Base.” *Computers and Structures, Inc. - Technical Knowledge Base*, 6 June 2016, wiki.csiamerica.com/pages/viewpage.action?pageId=9536464.

[2] Lu, Y., and G. R. Morris. “ASSESSMENT OF THREE VISCOUS DAMPING METHODS FOR NONLINEAR HISTORY ANALYSIS: RAYLEIGH WITH INITIAL STIFFNESS, RAYLEIGH WITH TANGENT STIFFNESS, AND MODAL.” *16WCEE 2017*, World Conference on Earthquake Engineering, 13 Jan. 2017, www.wcee.nicee.org/wcee/article/16WCEE/WCEE2017-1170.pdf.

[3] “Our Story.” *Taylor Devices Inc*, www.taylordevices.com/about-us/.

[4] “Damping Solutions for Structural Applications.” *Taylor Devices Inc*, www.taylordevices.com/structural/.

[5] W., Taylor. “The History of Taylor Devices.” *Blog*, 13 Jan. 2020, blog.taylordevices.com/the-history-of-taylor-devices.

[6] “What Is a Direct Acting Damper System?” *Taylor Devices Inc*, www.taylordevices.com/direct-acting-damping/.

[7] Taylor Devices, Inc. *Damper Manual LP*, go.taylordevices.com/damper-manual.

[8] Richard DePasquale. “Final Production Damper Test Report For FFHE School.” Taylor Devices Inc., 6 Sept. 2018.